Studies on Guest-responsive Luminescence Properties of Coordination Polymers Based on Nitridotetracyanorhenate(V) Ion

三浦, 大樹

https://doi.org/10.15017/2534377

出版情報：九州大学, 2019, 博士（理学）, 課程博士
バージョン：
権利関係：

Studies on Guest-responsive Luminescence Properties of Coordination Polymers Based on Nitridotetracyanorhenate(V) Ion

Hiroki Miura
July 2019
Department of Chemistry
Graduate School of Science
Kyushu University

Contents

General Introduction

1. Porous Coordination Polymers (PCPs) and Metal-Organic Frameworks (MOFs)

Porous coordination polymers (PCPs) and metal-organic frameworks (MOFs) have attracted significant attention as new classes of porous materials due to their scientific, social, and economic importance. This field was developed in the 1990s and the corresponding research has grown exponentially over the past decades. Several pioneering studies were performed by Kitagawa, Yaghi, and Férey, who comprehensively introduced the concept of PCPs and have extensively discussed their future applications.[1] PCPs and MOFs consist of metal ions or metal clusters as nodes and organic-, inorganic-, or metallo-ligands as bridging linkers (**Figure 1**). Linkages based on coordination bonds extend endlessly to form one, two, or three-dimensional framework structures. The initial studies focused on highly regular and designable framework structures as basic studies of the porous materials and their crystal engineering. Until the mid-1990s, two other types of porous materials, inorganic and carbon-based materials, dominated the field. Zeolites consist of hydrated alkaline or alkaline-earth aluminosilicates with a general formula of $M^{n+}_{x/n}[(AlO_2)_x(SiO_2)_y]^{x-}\cdot wH_2O$ and have highly crystalline and regular channels or cavities. However, strategic synthesis with a designed structure is difficult and their frameworks are extremely rigid.[3] Therefore, extensive screening of synthesis conditions is required for preparation of the products having desired structures. These materials can be used as containers for composite materials or as molecular sieves with controlled pore size, channel direction, and surface area. Activated carbons also exhibit high porosity with high surface area, but their porous structures contain many irregular channel structures with a broad pore size distribution because of the disordered networks of defective hexagonal carbon layers. Therefore, their disordered porous structures are often unsuitable for functions such as storage, separation, or sensing of specific guest molecules.[4]

In contrast, PCPs and MOFs have more developed features. As described above, PCPs and MOFs are formed based on coordination bonds which give rise to versatile unique characteristics. Their crystalline compounds can be easily prepared by self-assembly methods and with appropriate choice of components (i.e. nodes as well as bridging- and co-ligands), their structures are designable, highly regular, and rigid or

flexible. Intra- and inner-framework interactions, such as hydrogen/metal-metal bonds, π-π, CH-π, electrostatic, and van der Waals interactions, enable the generation of either rigid or flexible structures. Subsequently, various chemical and physical properties can be imparted to the frameworks by introducing building components and functionalization.[2] These keys features are not exhibited by the above-mentioned conventional porous materials (i.e., zeolites and activated carbon).

In the framework of PCPs, nano-size cavities with open channels for access of guest molecules are formed. In addition, the affinities between the framework and guest molecules (host-guest interactions) can be tuned by changing the nature of their components.[5] Well-designed frameworks make PCPs extremely attractive for applications including gas storage[6] and separation,[7] heterogeneous catalysis,[8] and drug delivery.[9] In addition, PCPs can exhibit useful physical properties such as luminescence,[10] magnetism,[11] and electrical conductivity[12] because the coordination units reflect their basic properties in the PCP framework. Moreover, these features can be switched depending on the encapsulated guest molecules. In a large number of flexible PCPs, their frameworks exhibit structure conversions, including framework expansion, shrinkage, and transformation, accompanied by guest ad-/de-sorption and exchange due to modified host-guest interactions, unlike in other porous materials. Most physical properties are sensitive to these structural changes and the emission properties are susceptible to structural changes and the rigidity/flexibility of the luminescent center. To combine porosity-related functions and desired physical properties, we investigated the luminescent properties of PCPs.

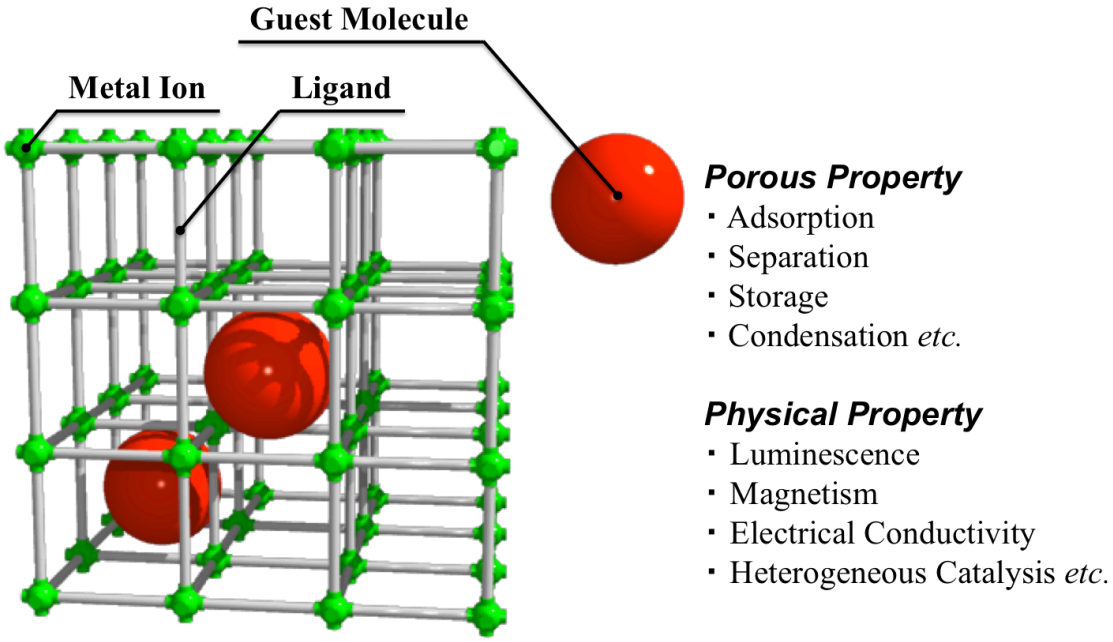

Figure 1. Schematic structure of PCPs or MOFs

2. Luminescent PCPs

2.1. Luminescence concepts in PCPs

PCPs are promising as a luminescent platform because their frameworks are composed of inorganic and the organic moieties that can provide luminescent properties. Various luminogenic moieties can be embedded in the proper position in the frameworks. Organic linkers and framework metal ions have been used as luminogens, whereas typically used luminescent metal ions are lanthanides. Linker-based luminescence includes the ligand-to-metal charge transfer (LMCT) and metal-to-ligand charge transfer (MLCT) as well as ligand-centered emission.

The photophysical properties of π-conjugated organic compounds in the solid state have been extensively studied.[13] Luminescent properties in the solid state are often different from the solution state due to the degree of conjugation among the luminophores as the π-conjugation system is strongly involved in absorbance, emission, and electronic transition. For the same reason, the luminophore structure affects its photophysical properties, which are similar in PCPs. The π-conjugated luminophores as linkers in PCPs are rigidified, causing spectral shifts, increased emission quantum yields, and increased emission lifetime due to the decreased nonradiative decay caused

by the restricted molecular vibration.[14] Zhou *et. al*. reported the enhanced quantum yields PCPs $[Zr_6(ETTC)_6]_n$ (PCN-94, H_2ETTC = 4',4''',4''''',4'''''''''-(ethene-1,1,2,2-tetrayl)tetrakis(([1,1'-biphenyl]-4-carboxylic acid))) (**Figure 2**).[14b] PCN-94 showed a blue emission at 470 nm with 76.2% emission quantum yield, while the free ligand molecule exhibited a yellow color emission at 545 nm with 30.0% emission quantum yield at room temperature under aerobic condition. The quantum yield enhancement and blue-shift of the $ETTC^{4-}$-based luminescence in PCN-94 was attributed to the formation of the framework structure. The rigidifying aromatic back-bones restricted nonradiative decay, and fixed to the structure in a state of lost flatness, resulting in destabilization of the LUMO of the $ETTC^{4-}$ unit.

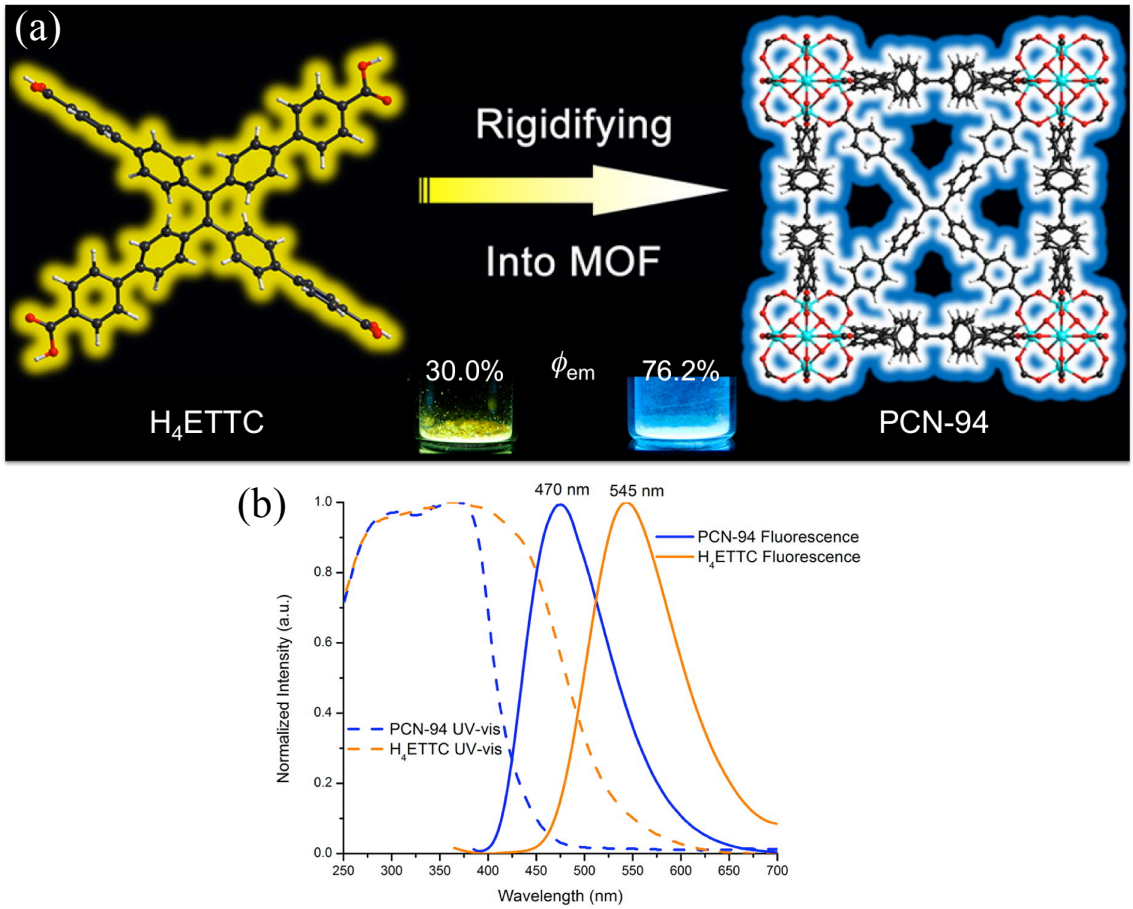

Figure 2. (a) Structures and photoluminescence images with the quantum yields of PCN-94 and H_4ETTC. (b) UV-vis reflectance spectra (dash lines) and emission spectra (solid lines) of PCN-94 (blue) and H_4ETTC (orange) at room temperature.

For LMCT and MLCT luminescent PCPs, d^{10} metal ions including Zn^{2+}, Cd^{2+}, Cu^{+} and Ag^{+}, are often used because other paramagnetic metal ion with unpaired electrons act as efficient quenchers. The d^0 Zr^{4+} can also be used in linker-centered luminescent PCPs. Many reports regarding charge-transfer luminescence of PCPs are available in the literature.[10] In many cases, these PCPs contain the d^{10} ions, Zn^{2+} and Cd^{2+} as well as benzene derivatives (particularly benzene-dicarboxylate and benzene-tricarboxylate derivatives). For example, $\{Zn_4O(1,4\text{-BDC})_3\}_n$ (IRMOF-1, 1,4-BDC = 1,4-benzene-dicarboxylate ion) was first reported in 1999 by Yaghi *et. al.* and its photophysical properties were reported in 2004 by Zecchina (**Figure 3**).[15] IRMOF-1 was the first example of a luminescent framework called a "MOF". The luminescence of IRMOF-1 was red-shifted compared to that of the free ligand, due to LMCT from the π* orbital of BDC^{2-} to the Zn_4O_{13} cluster.

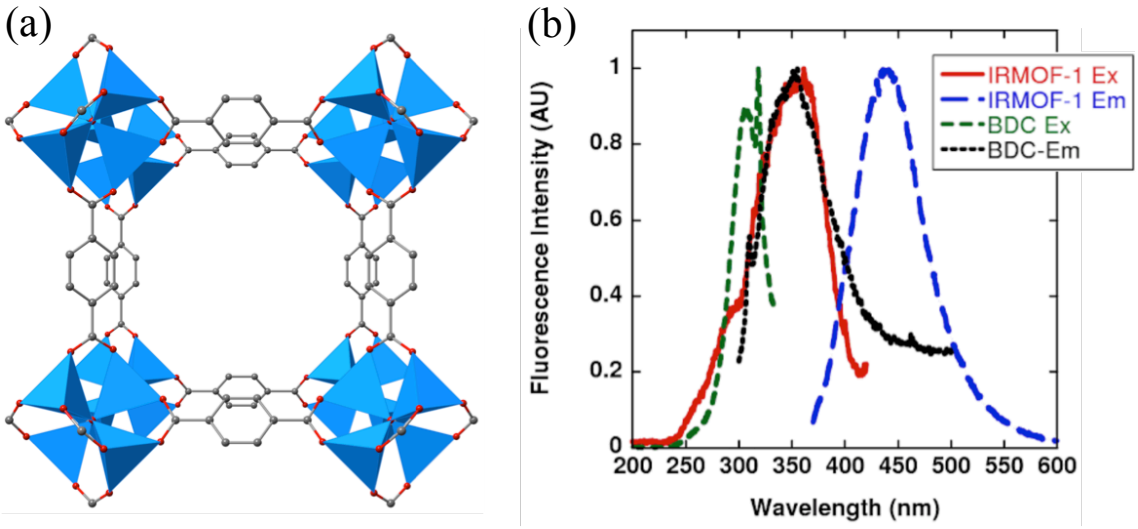

Figure 3. (a) Crystal structure of IRMOF-1. (b) The photoluminescence excitation and emission spectra of IRMOF-1 and BDC.

Lanthanide ions also exhibit strong emission attributed to 4f-4f transitions upon the coordination with appropriate light-harvesting antenna molecules. The general electron configuration of trivalent lanthanide (Ln^{3+}) is expressed as $[Xe](4f)^n(5s)^2(5p)^6$ (n = 0–14). The 4f orbitals are gradually filled from $4f^0$ for La^{3+} to $4f^{14}$ for Lu^{3+} and

their 4f electronic energy levels are characteristic for each ion and defined because of the shielding of the unoccupied 4f orbitals by the occupied $5s^2 5p^6$ subshells.[16] The shielded 4f orbitals are unsusceptible to the conditions of the surrounding environment such as ligands, solvents, and gases. Therefore, each lanthanide ion can exhibit sharp and unique 4f-4f transitions depending on their characteristic electronic energy level. However, the lanthanide luminescence exhibits inherently weak absorbance and low quantum yields because the transitions are Laporte forbidden. A common method to circumvent this problem is coordination of light-harvesting organic linkers to the lanthanide ions.[17] The antenna linker absorbs the excitation light strongly and transfers to the excited energy levels of the lanthanide ion directly and readily, resulting in metal-centered emission. Daiguebonne *et al*. systematically synthesized a series of lanthanide PCPs $[Ln_2(1,4\text{-BDC})_3(H_2O)_4]_n$ (Ln = Y, La–Tm, except for Pm) by reaction in water between each lanthanide ion and $Na_2(1,4\text{-BDC})$.[18] The produced frameworks were confirmed to be isostructural. The lanthanide PCPs containing Eu, Tb, and Dy ions exhibited unique luminescence based on the red, green, and yellow 4f-4f transition emissions, respectively (**Figure 4**). In addition to this series, many reports regarding the luminescent properties of lanthanide-based PCPs have been published, showing that all emission originates from the 4f-4f transition.

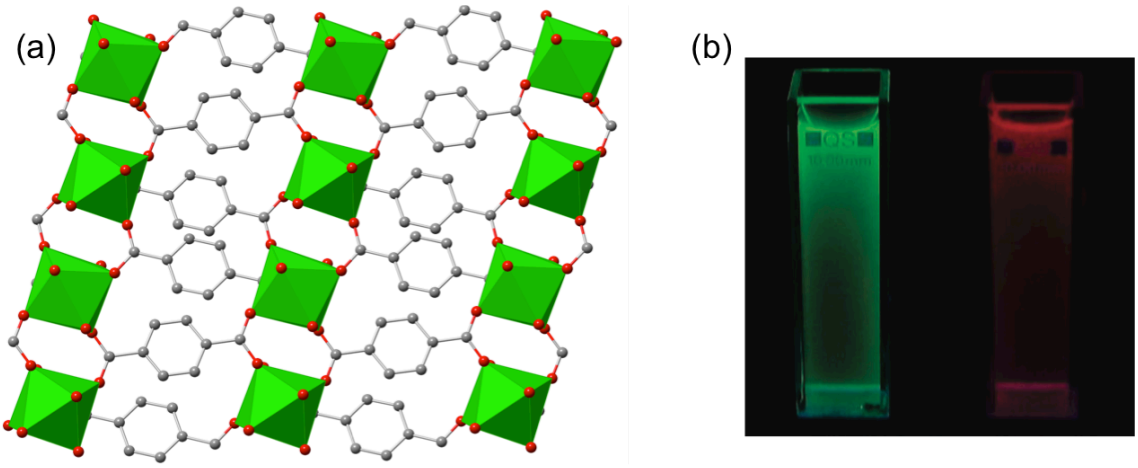

Figure 4. (a) The cystal structure of $[Ln_2(1,4\text{-BDC})_3(H_2O)_4]_n$. (b) Photograph of luminescence under UV light (312 nm) of the nanoparticles dispersed solutions of $[Tb_2(1,4\text{-BDC})_3(H_2O)_4]_n$ (green) and $[Eu_2(1,4\text{-BDC})_3(H_2O)_4]_n$ (red).

2.2. Luminescent changes in PCPs

Luminescent PCPs can potentially be used for chemical sensing by utilizing emission behavior changes upon adsorption of target adsorbates. A strong guest responding process is involved in the host-guest interaction. Hydrogen/metal-metal bonds, π-π, CH-π, electrostatic, and van der Waals interactions stabilize or destabilize the ground and/or excited state of the luminogens.[19] Framework structural changes are often caused by encapsulating guest molecules depending on their size, shape, and affinity. These changes in the frameworks directly affect the physical, magnetic, electro-conductive, and luminescent properties of the clathrate compounds.

For linker-based luminescent PCPs, maximum emission wavelength changes are often induced by host-guest interaction, where the luminogens are stabilized or destabilized, or exciplexes are generated between organic linkers in the frameworks and guest molecules. Kitagawa *et. al*. reported wide range emission color changeable PCPs $[Zn_2(1,4\text{-BDC})_2\text{-}(dpNDI)_3 \cdot 4DMF]_n$ (dpNDI = *N,N'*-di(4-pyridyl)-1,4,5,8-naphthalene-diimide) containing the naphthalene derivative dpNDI as a guest responsive luminophore in the frameworks (**Figure 5**).[20] In the void space of the two-fold interpenetrated framework structures, $[Zn_2(1,4\text{-BDC})_2\text{-}(dpNDI)_3]_n$ can accommodate volatile organic compounds (VOCs) containing aromatic groups ($[Zn_2(1,4\text{-BDC})_2\text{-}(dpNDI)_3]_n \supset$ VOC). Different colored emissions of $[Zn_2(1,4\text{-BDC})_2\text{-}(dpNDI)_3]_n \supset$VOC were observed from 420 to 640 nm depending on the chemical substituents of the encapsulated aromatic species. Differing electron-donating capabilities of the aromatic guest molecules induced maximum emission wavelength shifts as the host-guest interactions between the dpNDI building units and aromatic guest molecules depend on the guest molecule characteristics. However, in this system, the guest molecules were limited to aromatic groups. The same is true of LMCT- and MLCT-based luminescent PCPs because changes in the HOMO-LUMO gaps involved in luminescence are induced by the interaction extent of the organic linker in the frameworks and guest molecules.

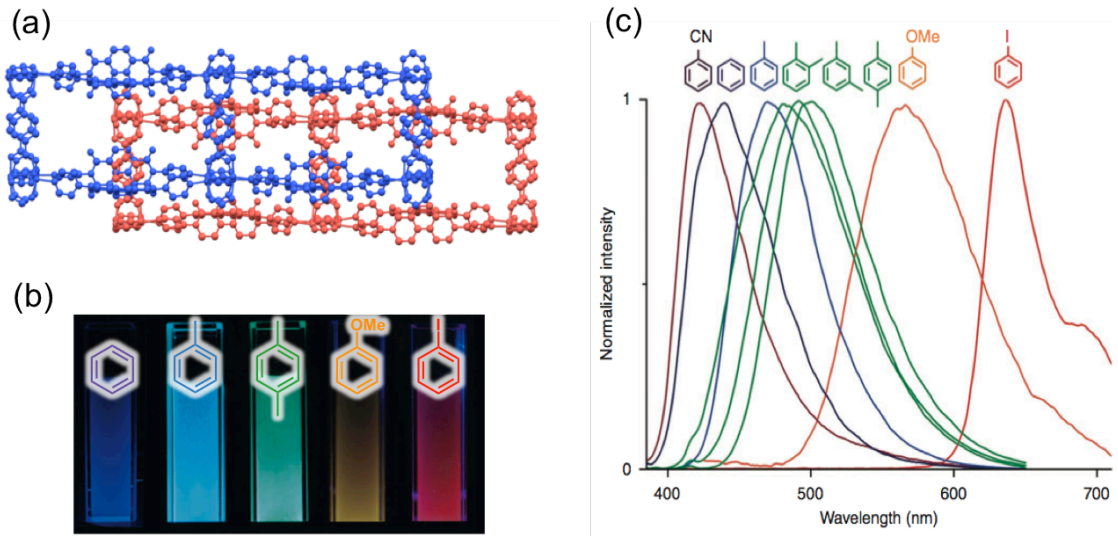

Figure 5. (a) Crystal structure of $[Zn_2(1,4\text{-BDC})_2\text{-}(dpNDI)_3]_n$. (b) Photoluminescent images of the crystal powders of $[Zn_2(1,4\text{-BDC})_2\text{-}(dpNDI)_3]_n$ suspended in each VOC liquid under UV irradiation at 365 nm. (c) Photoluminescent spectra of $[Zn_2(1,4\text{-BDC})_2\text{-}(dpNDI)_3]_n \supset$ VOC under UV irradiation at 370 nm.

Lanthanide-based PCPs with guest responsivity exhibit emission intensity changes because the lanthanide-centered luminescence cannot be shifted due to their shielded f-orbitals.[21] No clearly visible color changes can be observed, which complicates visual observation of changes as changes in emission intensity are difficult to detect with the naked eye.

Herein, we introduced luminescence properties based on d-d transitions to the coordination frameworks. The energy gap of the d-d transitions corresponds sensitively to the change in ligand field rather than f-f transition. For flexible PCPs, the guest molecules can induce framework transformations. Consequently, d-d transition-based luminescence could be shifted by changes in the ligand field splitting of the d orbitals through the structural conversion of the PCP upon interaction with the guest molecule.

2.3. d-d transition-based luminescence in PCPs

However, only a few previous reports have shown that luminescent MOFs exhibit d-d transition emission because the d-d transition is strictly spin-forbidden and Laporte-forbidden in an octahedral coordination environment. However, due to spin-orbit coupling a certain forbidden transition becomes allowed, resulting in the luminescence of some metal complexes from d-d transitions. Luminescent Cr(III) and Co(III) complexes were studied actively in the 1960s and 1970s but their complexes are unsuitable as building units for PCPs because d^3 and d^6 metal ions form largely inert complexes. However, the hexacyanometallate ion $[M^{III}(CN)_6]^{3-}$ (M = Cr and Co) can be used to create cyanide bridges. Thus, only a part of Prussian blue analogues (PBAs), which lack terminal cyano ligands and are expressed as $\{AT[M^{III}(CN)_6]\}_n$ (A; alkaline metal ion, T; divalent transition metal ion e.g. Zn^{2+}), show photo-emission at room temperature. Realization of luminescence at room temperature is important to be applied for guest responsive sensing materials. Unfortunately, PBAs do not show any emission band shifts due to their robust structure.

Recently, luminescent Mn(II) complexes with both octahedral and tetrahedral geometry have attracted significant attention due to their high emissive quantum yields originating from d-d transitions at room temperature.[23] Chen *et. al.* reported a one-dimensional Mn(II) coordination polymer $[MnBr_2(dppeO_2)]_n$ ($dppeO_2$ = 1,2-Bis(diphenylphosphino)ethane dioxide) that showed d-d transition emission. The luminescent color of $[MnBr_2(dppeO_2)]_n$ is switchable between green and red based on the transition between tetrahedral and triangle bipyramidal ligand fields, respectively.[23b] The conversion of coordination geometry can be induced by the coordination/elimination process of DMF (**Figure 6**). However, changes in coordination structure without geometry conversion induced only minor changes in the d-d energy gap of d^5 metal complexes due to the lack of crystal field stabilization energy. Consequently, sensitive guest-responses have not yet been achieved.

In this thesis, we focused on the nitridotetracyanorhenate(V) ion, $[Re^{V}N(CN)_4]^{2-}$, as a luminescent building unit of the PCP framework. The explanation for our choice of $[Re^{V}N(CN)_4]^{2-}$ will be described in detail in the subsequent sections.

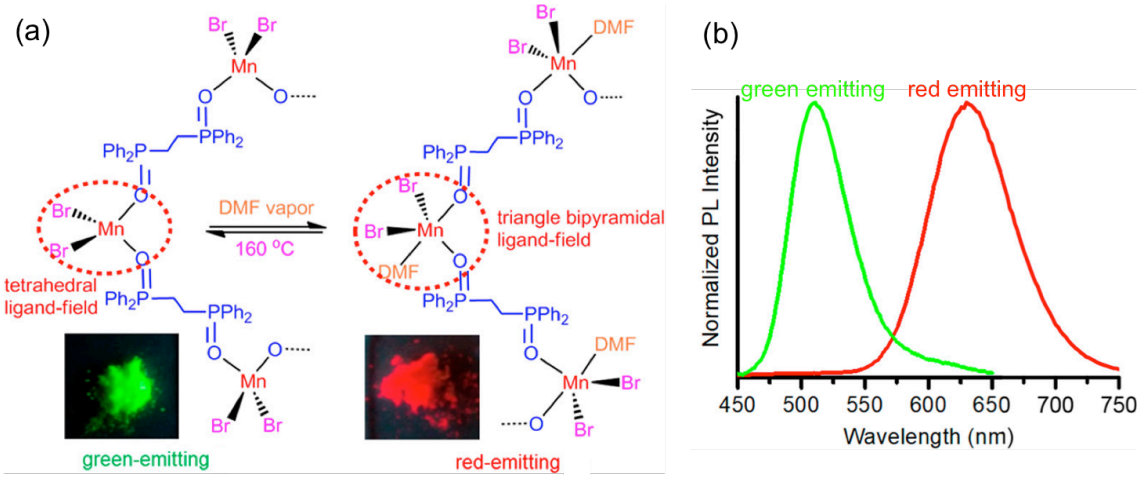

Figure 6. (a) The scheme of reversible transformation of $[MnBr_2(dppeO_2)]_n$ by adsorption/desorption process of DMF and the corresponding photoluminescent images under light at 365 nm. (b) Photoluminescent spectra of $[MnBr_2(dppeO_2)]$ without DMF (green emitting) and with DMF (red-emitting).

3. Nitridotetracyanorhenate(V) unit

3.1. Nitridotetracyanorhenate(V) ion; $[Re^{V}N(CN)_4]^{2-}$

$[M^{V}N(CN)_4]^{2-}$ (M = Mn, Cr, Re) is square pyramidal pentacoordinate complex with the triple bonds of the nitrido ligand at apical position and an open-metal site at the trans position of the nitrido ligand.[24-26] This complex can extend cyanide-bridges in four directions, similar to the $[M^{II}(CN)_4]^{2-}$ ion (M = Pt, Pd, Ni) (**Figure 7a**).[27-31] In addition, $[ReN(CN)_4]^{2-}$ exhibits photoluminescence with a lifetime on the order of microseconds originating from the triplet $^3[(d_{xy})^1(d_{\pi*})^1]$ ($d_{\pi*}$ = d_{xz} and d_{yz}) excited state (**Figure 7b**).[25] The emission wavelength of $[ReN(CN)_4]^{2-}$ shifts because the energy states of its d orbitals change depending on the coordination environment, which is affected by structure distortion and coordination/elimination of ligands. Yoshimura and Shinohara *et. al.* reported the photoluminescent changes of $[ReN(CN)_4]^{2-}$ depending on coordinating guest solvent molecules in the solid state. $[PPh_4]_2[ReN(CN)_4(L)]\cdot n$sol (L = acetone, acetonitrile, ethanol, and methanol) showed interconversion of photoluminescence and multiple emission color changes (λ_{em} = 527–

548 nm) depending on the nature of the axial ligands L upon excitation at 365 nm (**Figure 7c**).[25] However, no correlation was observed between the maximum emission wavelength and chemical properties of the guest molecules, including their permeability as well as electron-donating and -accepting parameters. According to the Walsh diagram of pentacoordinate square pyramidal geometry (**Figure 8**),[32] energy gaps between the ground state d_{xy} and excited states $d_{\pi*}$ ($d_{\pi*}$ = d_{xz} and d_{yz}) increase with increased distortion to the square pyramidal geometry. In other words, acute bending angles of the diagonal L_{basal}–M–L_{basal} bonds result in larger energy gaps of d_{xy}–$d_{\pi*}$, and vice versa. However, the relative emission energies of $[ReN(CN)_4]^{2-}$ were not correlated with the coordination structure. This lack of correlation is considered to originate from the complicated effects on the energy levels of d orbitals by both the chemical properties of the guest molecules and the overall coordination structure.

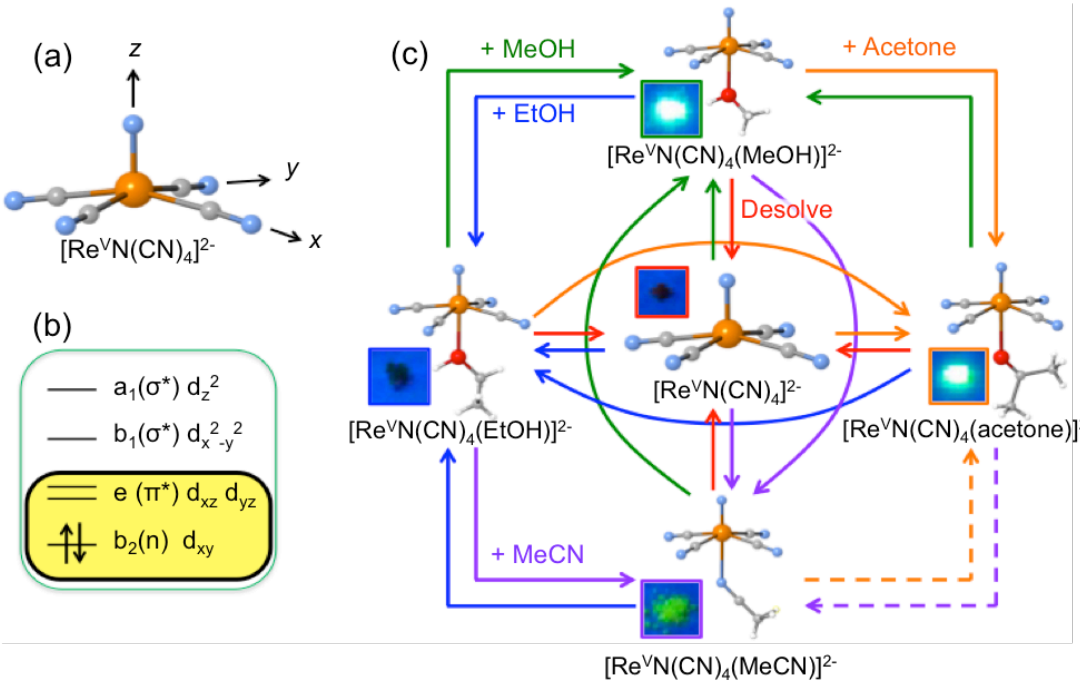

Figure 7. (a) Structure, (b) d electron configuration and (c) interconversion of photoluminescence of the $[Re^{V}N(CN)_4]^{2-}$ unit

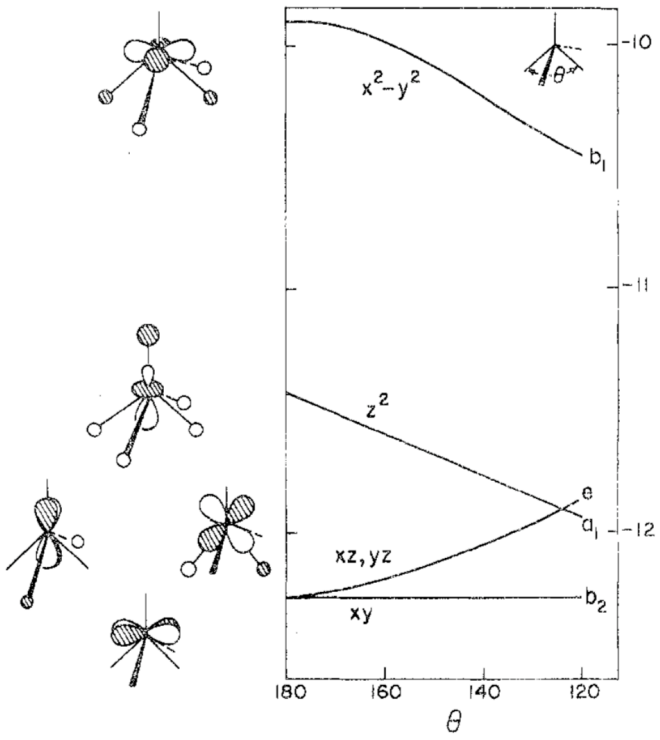

Figure 8. Walsh diagram of pentacoordinated square pyramidal geometry as a function of bending angles of the diagonal L_{basal}–M–L_{basal} bonds (θ).

3.2. Nitridotetracyanorhenate(V) complexes with co-ligands; $[Re^{V}N(CN)_4(co\text{-}L)]^{2-}$

The open-metal site of $[ReN(CN)_4]^{2-}$ can be coordinated with solvent molecules or organic ligands. Yoshimura and Shinohara *et. al.* reported a series of $[Re^{V}N(CN)_4(co\text{-}L)]^{2-}$ complexes coordinated with N-heteroaromatic ligands as co-ligands (co-L), including 4-(dimethylamino)pyridine (dmap), 3,5-lutidine (lut), 4-picoline (pic), 4-phenylpyridine (ppy), pyridine (py), 3-benzoylpyridine (3bzpy), 4,4'-bipyridine (bpy), pyrazine (pz), 4-cyanopyridine (cpy), and 4-benzoylpyridine (4bzpy), and reported their photoluminescent properties in the solid state (**Figure 9a**).[26] This phosphorescence originates from the triplet $^3[(d_{xy})^1(d_{\pi*})^1]$ or ^{3}MLCT excited states depending on the coordinating N-heteroaromatic ligand. The nitridotetracyanorhenate complexes with dmap, lut, pic, ppy, and py showed similar maximum emission wavelengths (λ_{em}) between 539 and 545 nm originating from the $^3[(d_{xy})^1(d_{\pi*})^1]$ excited state with high emission quantum yields (ϕ_{em}) of 0.39–0.93 (**Figure 9b**). In contrast, the nitridotetracyanorhenate complexes with bpy, pz, cpy, and 4bzpy showed red-shifted

λ_{em} at 564–669 nm originating from the ^{3}MLCT excited state, and an obviously lower ϕ_{em} of ≦0.01–0.18 compared to the luminescence of the $^3[(d_{xy})^1(d_{\pi*})^1]$ excited state of $[Re^VN(CN)_4(co\text{-}L)]^{2-}$. These results originate from the LUMO energy level of the N-heteroaromatic ligands, which is lower than the energy level of $d_{\pi*}$. This, the λ_{em} from the ^{3}MLCT excited state and molecular vibrations of co-L enhance non-radiative decay because the ^{3}MLCT excited state is involved in the condinating organic ligands.

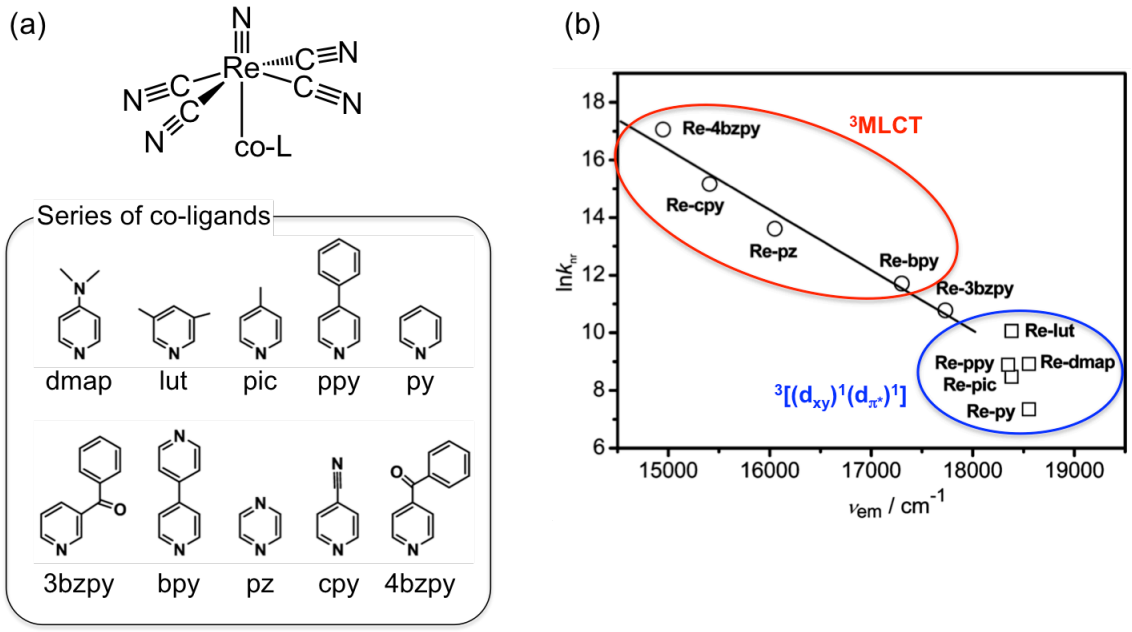

Figure 9. (a) The chemical structure of $[Re^VN(CN)_4(co\text{-}L)]^{2-}$ and series of co-ligands. (b) Plot of lnk_{nr} against the emission maximum energy (ν_{em}) of the complexes in the group emitting based on $^3[(d_{xy})^1(d_{\pi*})^1]$ excited state (open squares), and the group emitting based on ^{3}MLCT excited state and Re-3bzpy (open circles) in the crystalline phase at 296 K.

In our previous studies, we investigated the photoluminescent properties of $[Re^{V}N(CN)_4(co\text{-}L)]^{2-}$ complexes with ppy, bpy, cpy, 1-methylimidazole, 4-pyridylboronic acid or 4-aminopyridine as co-L.[33] It was observed that the emission wavelength of $[Re^{V}N(CN)_4(cpy)]^{2-}$ at 625 nm was blue-shifted by approximately 100 nm with enhanced ϕ_{em} from 0.02 to 0.36 in response to methanol vapor (**Figure 10**). For this response, the emissive excited state was converted from ^{3}MLCT to $^3[(d_{xy})^1(d_{\pi*})^1]$ by swichting the lowest excited state due to the ligand exchange between cpy and methanol. The conversion of emission excited state from MLCT to d-d transition was reversibly switchable.

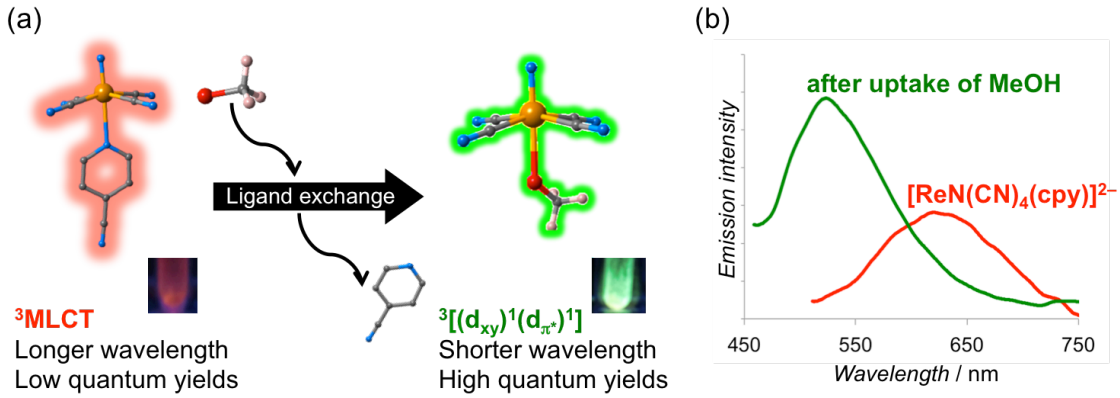

Figure 10. (a) The chart of emission mechanism conversion of $[Re^{V}N(CN)_4(cpy)]^{2-}$ by by the ligand exchange to MeOH and the corresponding photoluminescent images under light at 365 nm. (b) The photoluminescent spectrum of $[Re^{V}N(CN)_4(cpy)]^{2-}$ and the resulting photoluminescent spectrum after uptake of MeOH.

4. Purpose of this research

In this study, we attempted to incorporate $[ReN(CN)_4]^{2-}$ into the frameworks of PCPs and succeeded in the synthesis of novel luminescent PCPs. No previous reports regarding luminescent nitridotetracyanometallate-based PCPs are available in the literature. As described above, mononuclear $[ReN(CN)_4]^{2-}$ exhibits no correlation between luminescent wavelength and coordination structure. However, the coordination structure of $[ReN(CN)_4]^{2-}$ embedded in the PCP frameworks was expected to couple directly and strongly with the structural transformation of the frameworks due to $[ReN(CN)_4]^{2-}$ showing d-d transition emission and the energy level of d-orbitals changing by coordination structure.

In Chapter 1, we investigated a photoluminescent PtS-type PCP $\{Zn[ReN(CN)_4]\}$ using $[ReN(CN)_4]^{2-}$ as a luminescent building unit in the frameworks and discussed the maximum emission wavelength shifts depending on the nature of the guest molecules based on the structure of the prepared PCPs. A simple framework structure using tetracyanometallate ligands as a building unit is typified by PtS-type PCPs $\{M[\mathbf{M'}(CN)_4]\}$ which are fabricated by linking divalent transition-metal ions of tetrahedral geometry with tetracyanometallate ligands $[\mathbf{M'}(CN)_4]^{2-}$ (**M'** = Pt, Pd, Ni, Mn≡N) (**Figure 11**).[29,34] Zn^{2+} was used as a counter cation to prepare $\{Zn[ReN(CN)_4]\}$ because d^{10} metal ions cannot quench the luminescence

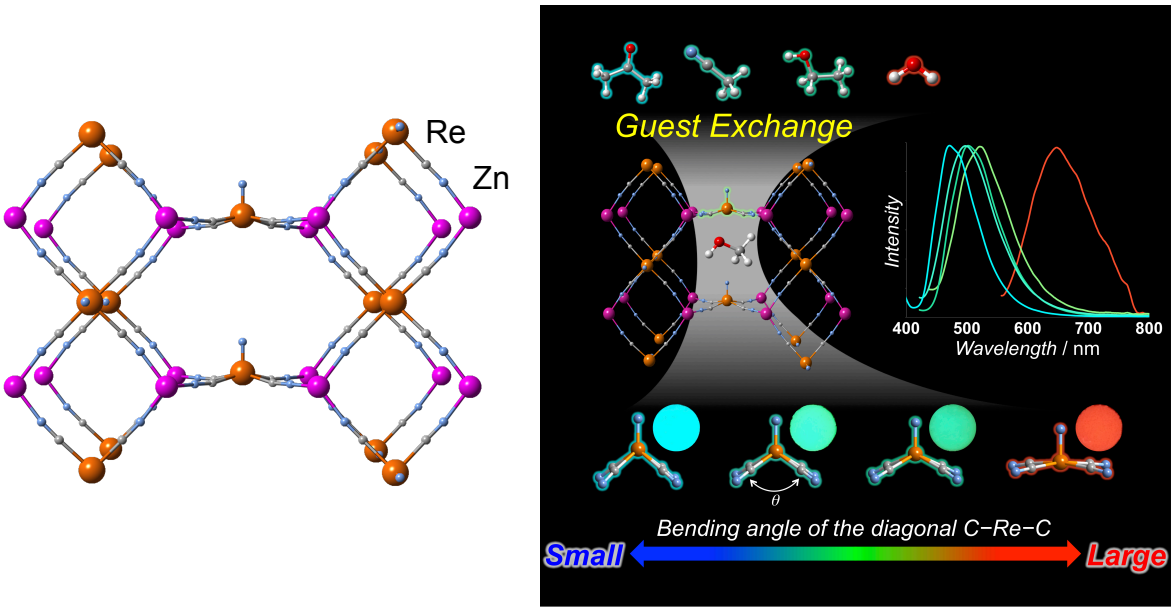

Figure 11. PtS-type framework structure of $\{Zn[ReN(CN)_4]\}$ and a schematic representation of guest-responsive luminescence of $\{Zn[ReN(CN)_4]\}$.

In Chapter 2, we have discussed our interest in effects of co-L on constructed framework structure consisted of $[ReN(CN)_4]^{2-}$ unit and their guest-responsivity. Two-dimensional luminescent coordination polymers $\{[Zn(co\text{-}L)_2][ReN(CN)_4(co\text{-}L)]\}$ (**ZnReco-L**; co-L = pyridine (py) and 3-chloropyridine (Clpy)) with pyridine derivatives at the trans position of their nitrido ligands were reported as part of the synthesis of luminescent nitridotetracyanorhenate(V)-based PCPs with co-L and their photophysical properties were investigated. The strong and rich π-π interactions in the intra- and inter-layers prohibited the guest responsivity. However, we confirmed that the emission property changed depending on the crystallinity (**Figure 12**).

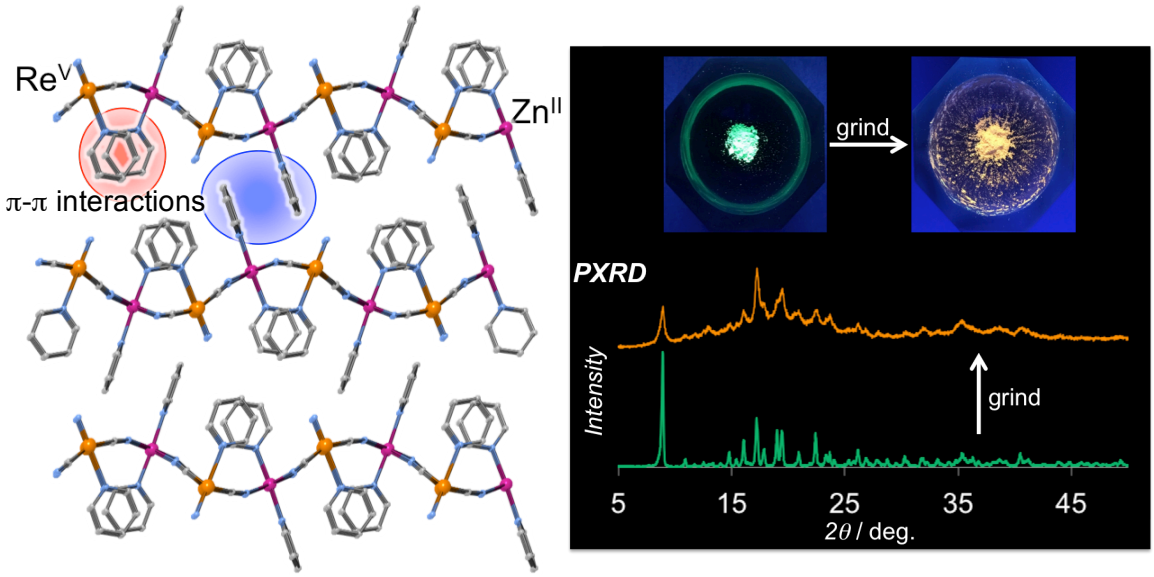

Figure 12. 2D-layer framework structure of $\{[Zn(py)_2][ReN(CN)_4(py)]\}$ and the luminescent images and PXRD patterns of $\{[Zn(py)_2][ReN(CN)_4(py)]\}$.

In Chapter 3, another class of luminescent coordination polymers $\{[M(PPh_3)_2]_2[ReN(CN)_4(MeCN)]\}$ (M = Cu and Ag) which form one-dimensional ladder type structures is reported; Cu^+ and Ag^+ also do not exhibit any quenching. We expected that one-dimensional strucutre provided a flexible framework and an unique guest-responsivity. The crystals of $\{[M(PPh_3)_2]_2[ReN(CN)_4(MeCN)]\}$ exhivited phase transiton with the change of photophysical properties (**Figure 13**). Moreover, selective guest-responsive luminescence in response to acetonitrile was confirmed in the amorphous state samples.

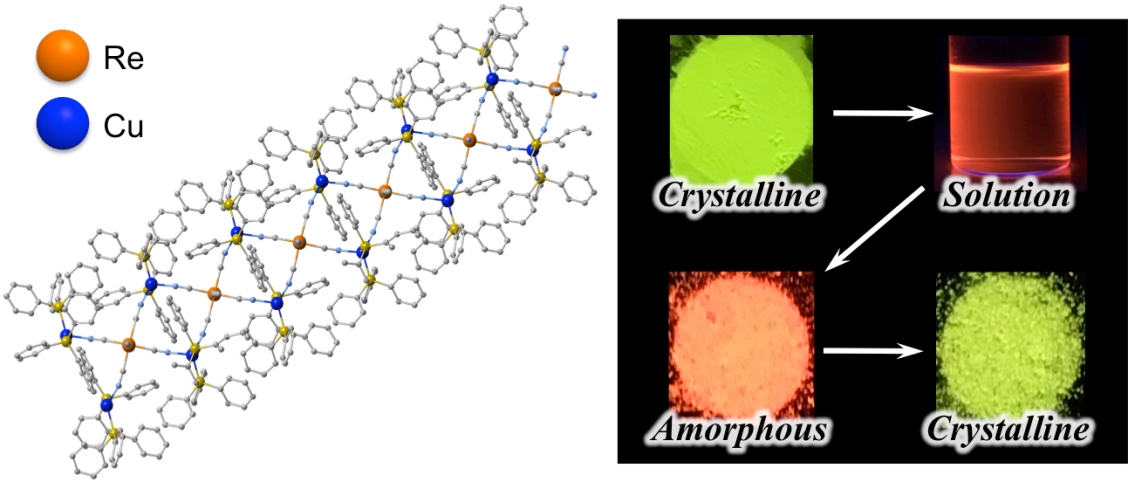

Figure 13. 1D-ladder framework structure of $\{[Cu(PPh_3)_2]_2[ReN(CN)_4(MeCN)]\}$ and the luminescent images with the phase transition of $\{[Cu(PPh_3)_2]_2[ReN(CN)_4(MeCN)]\}$.

References

1. (a) M. O'Keeffe, M. Eddaoudi, H. Li, T. Reineke, O. M. Yaghi, *J. Solid State Chem.* **2000**, *152*, 3–20; (b) O. M. Yaghi, M. O'Keeffe, N. W. Ockwig, H. K. Chae, M. Eddaoudi, J. Kim, *Nature* **2003**, *423*, 705–714; (c) J. L. C. Rowsell, O. M. Yaghi, *Microporous Mesoporous Mater.* **2004**, *73*, 3–14; (d) S. Kitagawa, R. Kitaura, S. I. Noro, *Angew. Chem. Int. Ed.* **2004**, *43*, 2334–2375; (e) S. Kitagawa, K. Uemura, *Chem. Soc. Rev.* **2005**, *34*, 109–119; (f) S. Kitagawa, S. I. Noro, T. Nakamura, *Chem. Commun.* **2006**, 701–707; (g) G. Férey, *Chem. Soc. Rev.* **2008**, *37*, 191–214; (h) G. Férey, C. Serre, *Chem. Soc. Rev.* **2009**, *38*, 1380–1399.
2. (a) M. Fujita, Y. J. Kwon, S. Washizu, K. Ogura, *J. Am. Chem. Soc.* **1994**, *116*, 1151–1152; (b) M. Dincă, J. R. Long, *J. Am. Chem. Soc.* **2005**, *127*, 9376–9377; (c) A. G. Wong-Foy, A. J. Matzger, O. M. Yaghi, *J. Am. Chem. Soc.* **2006**, *128*, 3494–3495.
3. (a) S. T. Wilson, B. M. Lok, C. A. Messina, T. R. Cannan, E. M. Flanigen, *J. Am. Chem. Soc.* **1982**, *104*, 1146–1147; (b) J. V. Smith, *Chem. Rev.* **1988**, *88*, 149–182.
4. (a) A. G. Pandolfo, A. F. Hollenkamp, *J. Power Sources* **2006**, *157*, 11–27; (b) J. Lee, J. Kim, T. Hyeon, *Adv. Mater.* **2006**, *18*, 2073–2094.
5. (a) B. Moulton, M. J. Zaworotko, *Chem. Rev.* **2001**, *101*, 1629–1658; (b) G. S. Papaefstathiou, L. R. MacGillivray, *Coord. Chem. Rev.* **2003**, *246*, 169–184.
6. (a) A. R. Millward, O. M. Yaghi, *J. Am. Chem. Soc* **2005**, *127*, 17998–17999; (b) M. Dincă, A. F. Yu, J. R. Long, *J. Am. Chem. Soc* **2006**, *128*, 8904–8913.
7. (a) R. Matsuda, R. Kitaura, S. Kitagawa, Y. Kubota, R. V. Belosludov, T. C. Kobayashi, H. Sakamoto, T. Chiba, M. Takata, Y. Kawazoe, et al., *Nature* **2005**, *436*, 238–241; (b) R. V. Belosludov, M. Takata, S. Kitagawa, H. Sato, R. Matsuda, S. Sakaki, W. Kosaka, Y. Hijikata, A. Hori, *Science* **2014**, *343*, 167–170.
8. (a) J. Lee, O. K. Farha, J. Roberts, K. A. Scheidt, S. T. Nguyen, J. T. Hupp, *Chem. Soc. Rev.* **2009**, *38*, 1450–1459; (b) J. S. Seo, D. Whang, H. Lee, S. I. Jun, J. Oh, Y. J. Jeon, K. Kim, **2000**, *404*, 982–986.
9. (a) Z. Ma, B. Moulton, *Coord. Chem. Rev.* **2011**, *255*, 1623–1641; (b) A. C. McKinlay, R. E. Morris, P. Horcajada, G. Férey, R. Gref, P. Couvreur, C. Serre, *Angew. Chem. Int. Ed.* **2010**, *49*, 6260–6266.

10. (a) M. D. Allendorf, C. A. Bauer, R. K. Bhakta, R. J. T. Houk, *Chem. Soc. Rev.* **2009**, *38*, 1330–1352; (b) Y. J. Cui, Y. F. Yue, G. D. Qian, B. L. Chen, *Chem. Rev.* **2012**, *112*, 1126–1162.
11. (a) G. J. Halder, C. J. Kepert, B. Moubaraki, J. D. Cahion, *Science (80-.).* **2002**, *298*, 1762–1766; (b) M. Kurmoo, H. Kumagai, S. M. Hughes, C. J. Kepert, *Inorg. Chem.* **2003**, *42*, 6709–6722; (c) M. Kurmoo, *Chem. Soc. Rev.* **2009**, *38*, 1353–1379.
12. (a) S. Dorbes, L. Valade, J. A. Real, C. Faulmann, *Chem. Commun.* **2005**, 69–71; (b)E. Coronado, J. R. Galán-Mascarós, *J. Mater. Chem.* **2005**, *15*, 66–74.
13. (a) G. C. Bazan, W. J. J. Oldham, R. J. Lachicotte, S. Tretiak, V. Chernyak, S. Mukamel, *J. Am. Chem. Soc* **1998**, *120*, 9188–9204; (b) J. Cornil, D. Beljonne, J. P. Calbert, J. L. Brédas, *Adv. Mater.* **2001**, *13*, 1053–1067.
14. (a) Z. F. Chen, R. G. Xiong, J. Zhang, X. T. Chen, Z. L. Xue, X. Z. You, *Inorg. Chem.* **2001**, *40*, 4075–4077; (b) Z. Wei, Z.-Y. Gu, R. K. Arvapally, Y.-P. Chen, R. N. McDougald, J. F. Ivy, A. A. Yakovenko, D. Feng, M. A. Omary, H.-C. Zhou, *J. Am. Chem. Soc.* **2014**, *136*, 8269–8276.
15. (a) H. Li, M. Eddaoudi, M. O'Keeffe, O. M. Yaghi, *Nature* **1999**, *402*, 276–279; (b) M. Eddaoudi, J. Kim, N. Rosi, D. Vodak, J. Wachter, M. O. Keeffe, O. M. Yaghi, *Science* **2002**, *295*, 469–472; (c) S. Bordiga, C. Lamberti, G. Ricchiardi, L. Regli, F. Bonino, A. Damin, K. P. Lillerud, M. Bjorgen, A. Zecchina, *Chem. Commun.* **2004**, 2300–2301.
16. G. H. Dieke, H. M. Crosswhite, *Appl. Opt.* **1963**, *2*, 675–686.
17. N. Sabbatini, M. Guardigli, J.-M. Lhen, **1993**, *123*, 201–228.
18. (a) T. M. Reineke, M. Eddaoudi, M. Fehr, D. Kelley, O. M. Yaghi, *J. Am. Chem. Soc* **1999**, *121*, 1651–1657; (b) C. Daiguebonne, N. Kerbellec, O. Guillou, J.-C. Bünzli, F. Gumy, L. Catala, T. Mallah, N. Audebrand, Y. Gérault, K. Bernot, et al., *Inorg. Chem.* **2008**, *47*, 3700–3708.
19. (a) Z. Hu, B. J. Deibert, J. Li, *Chem. Soc. Rev.* **2014**, *43*, 5815–5840; (b) W. P. Lustig, S. Mukherjee, N. D. Rudd, A. V. Desai, J. Li, S. K. Ghosh, *Chem. Soc. Rev.* **2017**, *46*, 3242–3285; (c) Y. Zhang, S. Yuan, G. Day, X. Wang, X. Yang, H. C. Zhou, *Coord. Chem. Rev.* **2018**, *354*, 28–45.
20. Y. Takashima, V. M. Martínez, S. Furukawa, M. Kondo, S. Shimomura, H. Uehara, M. Nakahama, K. Sugimoto, S. Kitagawa, *Nat. Commun.* **2011**, *2*, 168.

21. Y. Cui, B. Chen, G. Qian, *Coord. Chem. Rev.* **2014**, *273–274*, 76–86.
22. (a) A. Wölpl, D. Oelkrug, *Ber. Bunsenges. Phys. Chem* **1934**, *79*, 394–400; (b) P. D. Fleischauer, P. Fleischauer, *Chem. Rev.* **1970**, *70*, 199–230; (c) Y. Yuske, *J. Spectrosc. Soc. Japan* **1982**, *31*, 2–18.
23. (a) J. Chen, Q. Zhang, F.-K. Zheng, Z.-F. Liu, S.-H. Wang, A.-Q. Wu, G.-C. Guo, *Dalton Trans.* **2015**, *44*, 3289–3294; (b) Y. Wu, X. Zhang, L. J. Xu, M. Yang, Z. N. Chen, *Inorg. Chem.* **2018**, *57*, 9175–9181; (c) A. V. Artem'ev, A. S. Berezin, V. K. Brel, V. P. Morgalyuk, D. G. Samsonenko, *Polyhedron* **2018**, *148*, 184–188; (d) M. Bortoluzzi, J. Castro, E. Trave, D. Dallan, S. Favaretto, *Inorg. Chem. Commun.* **2018**, *90*, 105–107.
24. (a) N. P. Johnson, *J. Chem. Soc. (A).* **1969**, 1843–1845; (b) W. Pureell, I. Z. Potgieter, L. J. Damoense, J. S. Leipolldt, *Transit. Met. Chem.* **1991**, *16*, 473–475; (c) J. Bendix, K. Meyer, T. Weyhermu, E. Bill, N. Metzler-nolte, K. Wieghardt, *Inorg. Chem.* **1998**, *37*, 1767–1775; (d) J. Bendix, R. J. Deeth, T. Weyhermüller, E. Bill, K. Wieghardt, *Inorg. Chem.* **2000**, *39*, 930–938; (e) H. J. Van Der Westhuizen, W. Purcell, S. S. Basson, *Transit. Met. Chem.* **2002**, *27*, 506–511; (f) T. N. Mtshali, W. Pureell, H. G. Visser, *Acta Crystallogr. Sect. E Struct. Reports Online* **2007**, *63*, 80–82; (g) H. J. Van Der Westhuizen, R. Meijboom, M. Schutte, A. Roodt, *Inorg. Chem.* **2010**, *49*, 9599–9608; (h) W. Purcell, H. G. Visser, *J. Chem. Crystallogr.* **2016**, *46*, 15–20.
25. H. Ikeda, T. Yoshimura, A. Ito, E. Sakuda, N. Kitamura, T. Takayama, T. Sekine, A. Shinohara, *Inorg. Chem.* **2012**, *51*, 12065–12074.
26. H. Ikeda, A. Ito, E. Sakuda, N. Kitamura, T. Takayama, T. Sekine, A. Shinohara, T. Yoshimura, *Inorg. Chem.* **2013**, *52*, 6319–6327.
27. J. F. Guo, W. F. Yeung, S. Gao, G. H. Lee, S. M. Peng, M. H. W. Lam, T. C. Lau, *Eur. J. Inorg. Chem.* **2008**, 158–163.
28. T. D. Keene, M. J. Murphy, J. R. Price, D. J. Price, C. J. Kepert, *Dalton Trans.* **2011**, *40*, 11621–11628.
29. M. J. Murphy, D. M. D'Alessandro, C. J. Kepert, *Dalton Trans.* **2013**, *42*, 13308–13310.
30. R. Ohtani, S. Kitagawa, M. Ohba, *Polyhedron* **2013**, *52*, 591–597.
31. R. Ohtani, M. Inukai, Y. Hijikata, T. Ogawa, M. Takenaka, M. Ohba, S. Kitagawa, *Angew. Chem. Int. Ed.* **2015**, *54*, 1139–1143.

32. A. R. Rossi, R. Hoffmann, *Inorg. Chem.* **1975**, *14*, 365–374.
33. H. Yamate, Master's Thesis **2017**.
34. A. H. Yuan, R. Q. Lu, H. Zhou, Y. Y. Chen, Y. Z. Li, *CrystEngComm* **2010**, *12*, 1382–1384; (b) X. Chen, H. Zhou, Y. Y. Chen, A. H. Yuan, *CrystEngComm* **2011**, *13*, 5666–5669.

Chapter 1

Guest-Responsive Luminescence Properties of Three-Dimensional Porous Coordination Polymer

Abstract

Porous coordination polymers (PCPs) are expected to be a platform for multifunction with coupling between porous function and physical properties. Here, we focused on guest responsive luminescence of PCPs, and prepared a new luminescent PCP $\{Zn^{II}[Re^{V}N(CN)_4]\}$ (**ZnRe**), which formed 3D PtS-type structure, by using the luminescent nitridotetracyanorhenate(V) ion as a building unit. $[Re^{V}N(CN)_4]^{2-}$ ion shows photoluminescence originating from the d-d excited state. **ZnRe** adsorbed various guest molecules, such as acetone, acetonitrile, ethanol, methanol, water and so on. The maximum emission wavelength shifted from 471 to 644 nm depending on the guest molecules. The energy level of d orbitals is susceptible to surrounding coordination environment. Since the structure transformation of the frameworks accompanying with uptake of guest molecules was directly affected to each maximum emission wavelength. The guest-responsive emission band shift could be explained by the change in the energy levels of the d-orbitals corresponding to the bending angle of the diagonal C–Re–C bond. The guest responsivity was discussed based on the structural changes and property of guest molecule from results of powder X-ray diffraction, IR spectra and emission spectra.

Introduction

Porous coordination polymers (PCPs) having highly regular, designable, and flexible pores based on coordination bonds have attracted much attention as new class of porous materials.[1] PCPs have potential applications in gas storage[2] and separation[3] sensing[4-6] and so on, with choosing appropriate components such as metal ion, inorganic/organic ligands and so on. Among various applications, luminescence of PCPs is promising property for visible, selective and sensitive molecular sensor with coupling porous functions with luminescence of the framework.

Various luminogens can be embedded in the frameworks, and luminescent organic linkers and lanthanide ions have mainly been used as the luminogens. However, the guest molecules are usually limited to aromatic volatile compounds in the case of luminescent organic linkers because the maximum emission wavelength shifts depending on the host-guest charge transfer interaction between aromatic compounds and luminescent organic linkers.[4,5] On the other hand, the lanthanide-based PCPs can exhibited strong emission originating from the f-f transitions[4,6] but the guest response is shown mainly emission intensity changes because the changes of the surrounding coordination environment almost unaffected the energy levels of the f orbital and affected only the emission efficiency. The energy levels the d orbitals are more sensitive to the change in the coordination environment, such as bond lengths, bond angles, geometry, coordination chemical species and so on, in comparison to the f orbitals.

The frameworks in the most of flexible PCPs show structure transformation accompanying with guest adsorption/desorption and exchange due to host-guest interactions. Such structure transformation is expected to affect the coordination environment in the frameworks and to cause the shift of energy gap between d orbitals. However, there are still a small number of reports of d-d transition-based luminescence in the PCPs.[7,8] In addition, a various and sensitive guest-responsive d-d luminescence has not been reported yet.

In this study, we focused on nitridotetracyanorhenate(V) ion $[Re^{V}N(CN)_4]^{2-}$ as a building unit of PCPs. $[M^{V}N(CN)_4]^{2-}$ (M = Mn, Cr, Re) can extend cyanide-bridges in four directions like $[M^{II}(CN)_4]^{2-}$ ion[9-13] and also provides an open-metal site at the trans position of nitrido ligand.[14-16] In addition, $[ReN(CN)_4]^{2-}$ ion shows photoluminescence originated from the $^3[(d_{xy})^1(d_{\pi*})^1]$ ($d_{\pi*}$ = d_{xz} and d_{yz}) excited state by excitation of 365 nm UV light.[15] The maximum emission wavelength of $[ReN(CN)_4]^{2-}$

ion shifts because the d-d energy gap changes depending on the coordination environment.[16] The mononuclear complex $[PPh_4]_2[ReN(CN)_4(L)]\cdot n$sol (L = methanol, ethanol acetonitrile and acetone) showed an interconversion of photoluminescence in solid state and smultiple emission color change (λ_{max} = 527–548 nm) depending on axial ligands L.[15] PCPs incorporated $[ReN(CN)_4]^{2-}$ unit are expected to exhibit more remarkable guest responsivity, because $[ReN(CN)_4]^{2-}$ units supply open metal sites in the pore surface with Re−CN−Zn linkages and get open space for guest molecules accessing. Althogh the formation of Re−CN−Zn linkages limits molecular motion of $[ReN(CN)_4]^{2-}$, the change of coordination structure of $[ReN(CN)_4]^{2-}$ are expected to be coupled with structure transformation of PCPs by assembled structures.

Here, we prepared a new luminescent PtS-type PCP $\{Zn^{II}[Re^{V}N(CN)_4]_2\}\cdot n$sol (**ZnRe**) by reaction of $[ReN(CN)_4]^{2-}$ with of Zn^{II} ion. For the synthesis, Zn^{II} ion was chosen as a secondary metal ion because Zn^{II} ions can easily form tetrahedral structure which is an elemental structure for PtS-type structure, and avoid absorbing excitation light to $[ReN(CN)_4]^{2-}$ units and emission from $[ReN(CN)_4]^{2-}$ units. In addition, **ZnRe** showed remarkable guest-responsive luminescence through guest exchanges. We investigated the guest responsive luminescence and elucidated correlation between changes of coordination environment of Re^{V} center and luminescent property depending on guest molecules.

Experiments

Physical Measurements

Single-crystal X-ray diffraction data were collected on a Bulker SMART APEX II ULTRA CCD-detector Diffractometer, a rotating-anode (Bruker Tourbo X-ray source) with graphite-monochromated $Mo_{K\alpha}$ radiation (λ = 0.71073 Å) was used. Computations were carried out on APEX2 crystallographic software package and OLEX2 software.[18] A single crystal was mounted on a polymer film with liquid paraffin and the temperature kept –173ºC under flowing N_2. All of the structures were solved by a standard direct method (XSHELL V6.3.1 crystallographic software package of the Bruker AXS) and expanded using Fourier techniques. Fullmatrixleast-squares refinements were carried out with anisotropic thermal parameters for all non-hydrogen atoms. The SQUEEZE program was used to remove the contribution of the highly disordered solvent molecules from the structural calculations.[19] X-ray powder diffraction (XRPD) was carried out on a Rigaku Ultima IV diffractrometer with graphite-monochromated $Cu_{K\alpha}$ radiation. X-ray fluorescence analysis was carried out on a Rigaku ZSX-100S. Infrared spectra were measured with a JASCO FT/IR-4200 using ATR method. Thermogravimetry analysis (TGA) was carried out on a Perkin Elmer STA6000. Elemental analysis of carbon, hydrogen and nitrogen was carried out by the staff of technical support division graduate school of science, Kyushu University. The emission spectra and emission quantum yields were measured by an absolute emission quantum yield measurement system C9920-02 (Hamamatsu Photonics K. K.) composed of an integrating sphere, a multi-channel photodetector PMA-12 (Hamamatsu Photonics K. K.), and a xenon lamp as an excitation light source (excitation wavelength = 365 nm) at room temperature. PL quantum yield was calculated with the following equation:

$$\phi = \frac{\int I_{em} d\lambda}{\int \left(I_{ex}^{before} - I_{ex}^{after} \right) d\lambda}$$

I_{em} is the amount of photon from emission, $I^{before}{}_{em}$ is amount of photon from excitation light that nothing absorbed, and $I^{after}{}_{em}$ is amount of photon from excitation light that something absorbed. The emission decay curves were acquired at room temperature using a Quantaurus-Tau C11367-24 (Hamamatsu Photonics K. K.) with excitation via a xenon flash lamp with a band-path filter (λ_{ex} = 370 nm). Theoretical

value of emission lifetime was calculated with the following equation.

$$\sum_i A_i \exp\left(-\frac{t}{\tau_i}\right)$$

A_i is a coefficient, t is current time, τ_i is emission lifetime. A_i and τ_i are given by fitting of luminescent lifetime measurement.

Theoritical Caluculation

All calculations were performed with the B3LYP functional[20] and the LANL2DZ basis[21] set using the Gaussian 09 program.[22] Graund state geometry was optimized in vacuo condition. The vertical excitation energies were calculated by TD-DFT method with the fixed each diagonal bending angles (θ) from 180 to 120 degrees.

Materials

All chemicals were purchased from commercial sources and used without further purification.

Method

Preparation of compounds

$ReO(OEt)Cl_2(PPh_3)_2$

The $ReO(OEt)Cl_2(PPh_3)_2$ was prepared according to the literature method.[23-24] A solution of triphenilphosphine (19.93 g, 75.98 mmol) and hydrazine dihydrochloride (3.95 g, 37.6 mmol) in ethanol (200 ml) was heated under refluxed over 1 hour with vigorous stirring. This suspension was added a solution of perrhenic acid [prepared from rhenium powder (4.00 g, 21.5 mmol) dissolved in 30% hydrogen peroxide (20 ml) was added in several batches with icing and evaporated to dryness on a hot plate] in ethanol (80 ml). The mixture was heated for 5 min. and filtered. The solid was washed successively with hot ethanol and acetone to give green silver microcrystals. Yield :

11.11 g (61.3 %). IR (cm^{-1}): 1482, 1435 ($\nu_{C\text{-}H}$ of PPh_3), 950 ($\nu_{Re=O}$), 909 (ν_{C-C}).

$ReNCl_2(PPh_3)_2$

The $ReNCl_2(PPh_3)_2$ was prepared according to the literature method.[23-24] A suspension of $ReO(OEt)Cl_2(PPh_3)_2$ (8.98 g, 10.7 mmol) (prepared as described above), triphenylphosphine (4.00 g, 15.3 mmol) and hydrazine sulphate (4.40 g, 33.8mmol) in ethanol (200 ml) and water (10 ml) was heated under reflux overnight under an atmosphere of nitrogen. The product was washed successively with hot ethanol, hot water, hot ethanol and diethyl ether to give brown microcrystals. Yield : 6.80 g (80.2 %) IR (cm^{-1}): 1482, 1437 ($\nu_{C\text{-}H}$ of PPh_3), 1095 ($\nu_{Re\equiv N}$).

$K_2[ReN(CN)_4]\cdot H_2O$

The $K_2[ReN(CN)_4]\cdot H_2O$ was prepared according to the literature method[24]. A suspension of $ReNCl_2(PPh_3)_2$ (4.00 g) and potassium cyanide (2.50 g) in methanol (250 ml) was heated under reflux in a stream of nitrogen for two hours. After the yellow suspension was filtered, the yellow powder was dissolved in a solution of a potassium cyanide (2.0 g) in water (20 ml) and then precipitated methanol (100 ml). The yellow powder dissolved in water (18 ml) and precipitated with methanol (90 ml) as salmon pink powder. Yield : 1.59 g (74.3 %). IR (cm^{-1}) 2118 ($\nu_{C\equiv N}$), 990, 965 ($\nu_{Re\equiv N}$).

$[PPh_4]_2[ReN(CN)_4(MeOH)]\cdot 3MeOH$

The $[PPh_4]_2[ReN(CN)_4(MeOH)]\cdot 3MeOH$ was prepared according to the literature method[15]. $K_2[ReN(CN)_4]\cdot H_2O$ (1.00 g, 2.35 mmol) was dissolved in 12 mL of water, and $(PPh_4)Cl$ (2.65 g, 7.08 mmol) in 2 mL of water was added to the solution. The yellow suspension that formed immediately was heated to give a yellow solution, and then the solution was cooled to room temperature. The yellow solid obtained by filtration was dissolved in 10 mL of MeOH, and 35 mL of Et_2O was layered on the solution. The solution was allowed to stand for several days, and the yellow crystals formed were filtered. Yield: 2.06 g (79.8%). IR (cm^{-1}) 2103 ($\nu_{C\equiv N}$), 1085 (δ_{H-O-C}), 1036 (ν_{C-O}), 1107 ($\nu_{Re\equiv N}$).

Single crystals of {$Zn[ReN(CN)_4]$ }·*n*solv (ZnRe(sc))

Single crystals of **ZnRe(sc)** was prepared by diffusion method used straight tubes.

A mixed solvent of water / ethanol (1.5 ml, water : ethanol = 1 : 1 v/v) was layered on an aqueous solution of $K_2[ReN(CN)_4]\cdot H_2O$ (3.2 mg, 0.0080 mmol) in water (1 ml) at the bottom of the straight tube. Then, an ethanoic solution of $Zn(NO_3)\cdot 6H_2O$ (3.0 mg, 0.010 mmol) in ethanol (1 ml) added slowly. After a few weeks, clear pale yellow single crystals were prepared.

Single crystals of $\{Zn[ReN(CN)_4(MeOH)]\}\cdot H_2O$

Single crystals of $\{Zn[ReN(CN)_4(MeOH)]\}\cdot H_2O$ were prepared by diffusion method used straight tubes. A mixed solvent of water / ethanol (1.5 mL, water:ethanol = 1:1 v/v) was layered on a solution of $Zn(NO_3)\cdot 6H_2O$ (3.0 mg, 1.0×10^{-3} mmol) in 1.0 mL of water at the bottom of the straight tube. Then, a solution of $[PPh_4]_2[ReN(CN)_4(MeOH)]\cdot 3MeOH$ (3.2 mg, 8.0×10^{-4} mmol) and trans,trans,trans-1,4-Bis[2-(4'-pyridyl)ethenyl]benzene (1.0 mg, 3.5×10^{-3} mmol) in 1.0 mL of ethanol added slowly. After two months, clear pale yellow single crystals were prepared.

Powder samples of $\{Zn[ReN(CN)_4]\}\cdot n$solv (ZnRe_MeOH)

ZnRe_MeOH was prepared by slow addition by used dropping funnel. A solution of $[PPh_4]_2[ReN(CN)_4(MeOH)]\cdot 3MeOH$ (327.6 mg, 0.2983 mmol) in MeOH (30 ml) was added to a solution of $Zn(NO_3)\cdot 6H_2O$ (95.0 mg, 0.319 mmol) in MeOH (30 ml) with slowly stirring. After a few days of stirring, yellow solid was separated by centrifugation. Pale yellow powder was obtained by dryness in desiccator without vacuum condition. Yield : 117.0 mg. IR (cm^{-1}) 3400-2850 ($\nu_{O\text{-}H}$), 2168 ($\nu_{C\equiv N}$), 990, 965 ($\nu_{Re\equiv N}$).

Fabrication of ZnRe_MeOH in sample holder for analysis of sensitivity to acetone

To perform analysis of sensitivity to acetone, a side-arm cell A10095-02 (Hamamatsu Photonics K. K.) inserted a glass tube of which inner-wall coated by **ZnRe_MeOH** was fabricated. Powder sample of **ZnRe_MeOH** was dispersed into methanol. The inner-wall of grass tube was covered on the suspension and the outer-wall of the glass tube was rubbed carefully and entirely with a cotton swab dipped in methanol to remove the residue of **ZnRe_MeOH** other than on inner-wall. The glass tube, which was sealed by septa on the opposite side coated with **ZnRe_MeOH**, was

inserted into a side-arm cell through septa having a small hole at the center.

Preparation of acetone-water mixture gas for analysis of detection limit of acetone

A schlenk flask of which whole internal volume is 1336 mL was used in this treatment. The air in the schlenk was removed by vacuum flask and a 23.1 μL of water putted into the schlenk flask. The amount of water was approximately 0.1 mmol/L and was adjusted to coincide with the value of the almost saturated vapor pressure of water at 20ºC under the atmospheric pressure based on the ideal gas law; $PV = nRT$. Then, a 94.0 μL, 18.8 μL, 9.4 μL, 3.8 μL, 1.9 μL, 1.3 μL or 0.9 μL of acetone was also putted into the schlenk flask to prepare the mixture gas at the water/acetone ratio of 1/1, 1/5, 1/10, 1/25, 1/50, 1/75, or 1/100, respectively. After vaporization of water and acetone, the schlenk flask including the water and acetone vapor gas was filled up with nitrogen gas and the internal pressure was regulated at atmospheric pressure. The acetone-nitrogen gases excluding water vapor were also prepared in four different acetone vapor concentration of 1.0, 0.2, 0.1 and 0.04 mmol/L in the same procedure.

Analysis of guest sensitivity to mixture gas

The 30 mL of preparation mixture gases excluding/including water vapor were flowed to **ZnRe_MeOH** fabricated in the sample holder described above after measurement of photoluminescence spectra at initial state. A few minutes after flow of the mixture gas, photoluminescence spectra of the responded sample was measured.

Results and discussion

X-Ray Structural Characterization

Pertinent crystallographic parameters of {Zn[ReN(CN)$_4$] }·*n* solv (**ZnRe(sc)**) are given in **Table 1**. Selected bond distances and angles are given in **Table 2**. The drawing of the asymmetric unit for **ZnRe(sc)** at 100 K is shown in **Figure 1**, together with to atom numbering scheme. The basic unit structure and packing structures are shown in **Figures 2-4**. Because positions of solvents were not refined sufficiently, R value was not so good. The asymmetric unit consists of Zn(II) ion and $[ReN(CN)_4]^{2-}$. The geometry of $[ReN(CN)_4]^{2-}$ unit is distorted square pyramidal, where the angles of trans C-Re-C are 157.2(3) degree. In the lattice, Re≡N bond is disordered at opposite side and exists at each side at the ratio of 50%. The geometry of Zn(II) ion is tetrahedral with four cyanide nitrogen atoms of $[ReN(CN)_4]^{2-}$ unit. **ZnRe** framework formed a PtS-type 3D porous structure extended by Re-CN-Zn linkages. A coordinating solvent with open metal site and lattice solvents, considered H_2O and EtOH, are not determined completely due to positional disorder. In the structures, accessible solvated void was estimated to be 58.9 % (488 Å^3) at 100 K.

Table 1 Crystallographic parameters for {Zn[ReN(CN)$_4$] }·*n* solv (**ZnRe(sc)**)

Complex	**ZnRe(sc)**
Formula	C_4N_5ReZn
Formula weight	370.52
Temperature / K	100
Crystal color	pale yellow
Crystal Habit	dipyramid
Crystal System	tetragonal
Space Group	$P4_2/mmc$
$a = b$ / Å	7.819(3)
c / Å	13.581(5)
$\alpha = \beta = \gamma$ / deg.	90
V / Å^3	830.2(6)
Z	2
R	0.0509
wR	0.1526

Table 2 Selected bond distances and angles for **ZnRe(sc)**

Bond distances (Å)			
Re1-C1	2.11(3)	Re1-N1	1.52(5)
Re1-C1$^{\#1}$	2.11(3)	Re1$^{\#1}$-N1$^{\#1}$	1.52(5)
Re1-C1$^{\#2}$	2.11(3)	C1-N2	1.18(5)
Re1-C1$^{\#3}$	2.11(3)	Zn1-N2	1.93(4)
Re1$^{\#1}$-C1	2.11(3)	Zn1-N2$^{\#1}$	1.93(4)
Re1$^{\#1}$-C1$^{\#1}$	2.11(3)	Zn1-N2$^{\#2}$	1.93(4)
Re1$^{\#1}$-C1$^{\#2}$	2.11(3)	Zn1-N2$^{\#3}$	1.93(4)
Re1$^{\#1}$-C1$^{\#3}$	2.11(3)		
Bond angles (deg)			
C1-Re1-C1$^{\#1}$	87. (2)	Re1-C1-N2	168.2(8)
C1-Re1-C1$^{\#2}$	157.2(3)	C1-N2-Zn1	173.(3)
C1-Re1-C1$^{\#3}$	88. (2)	N2-Zn1-N2$^{\#4}$	109.7(8)
N1-Re1-C1	101.39(16)	N2-Zn1-N2$^{\#5}$	109.7(8)
C1$^{\#1}$-Re1-C1$^{\#2}$	87.(2)	N2-Zn1-N2$^{\#6}$	108.9(16)
C1$^{\#1}$-Re1-C1$^{\#3}$	157.2(3)	N2$^{\#4}$-Zn1-N2$^{\#5}$	108.9(16)
C1$^{\#2}$-Re1-C1$^{\#3}$	88.(2)	N2$^{\#4}$-Zn1-N2$^{\#6}$	109.7(8)
N1$^{\#1}$-Re1-C1$^{\#1}$	101. 39(16)	N2$^{\#5}$-Zn1-N2$^{\#6}$	109.7(8)

Symmetry operations:

#1 (1-x, -y, z) #2 (1-x, y, -z) #3 (x, -y, -z)

#4 (-y, -x, 1/2-z) #5 (y, x, 1/2-z) #6 (-x, -y, z)

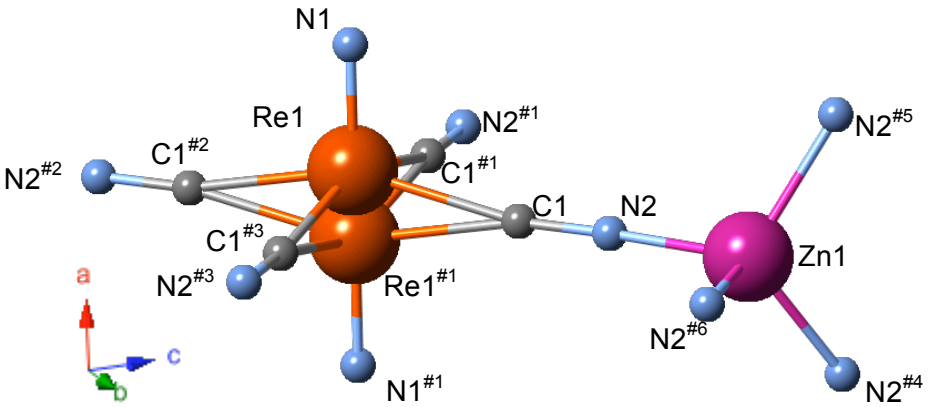

Figure 1. The drawing of the asymmetric unit for **ZnRe(sc)** with the atom numbering scheme

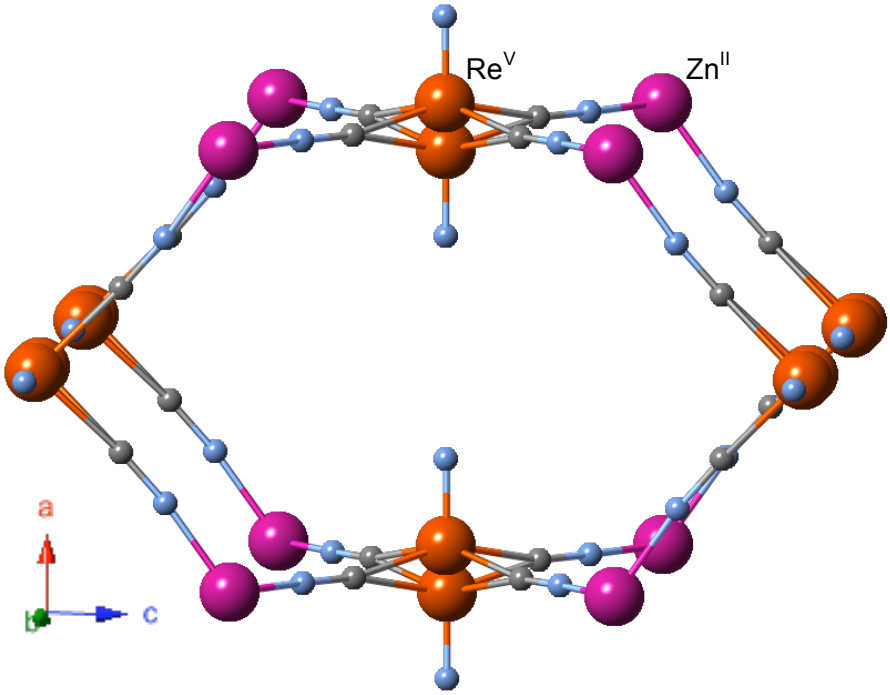

Figure 2. A basic unit consisted porous structure of **ZnRe(sc)**

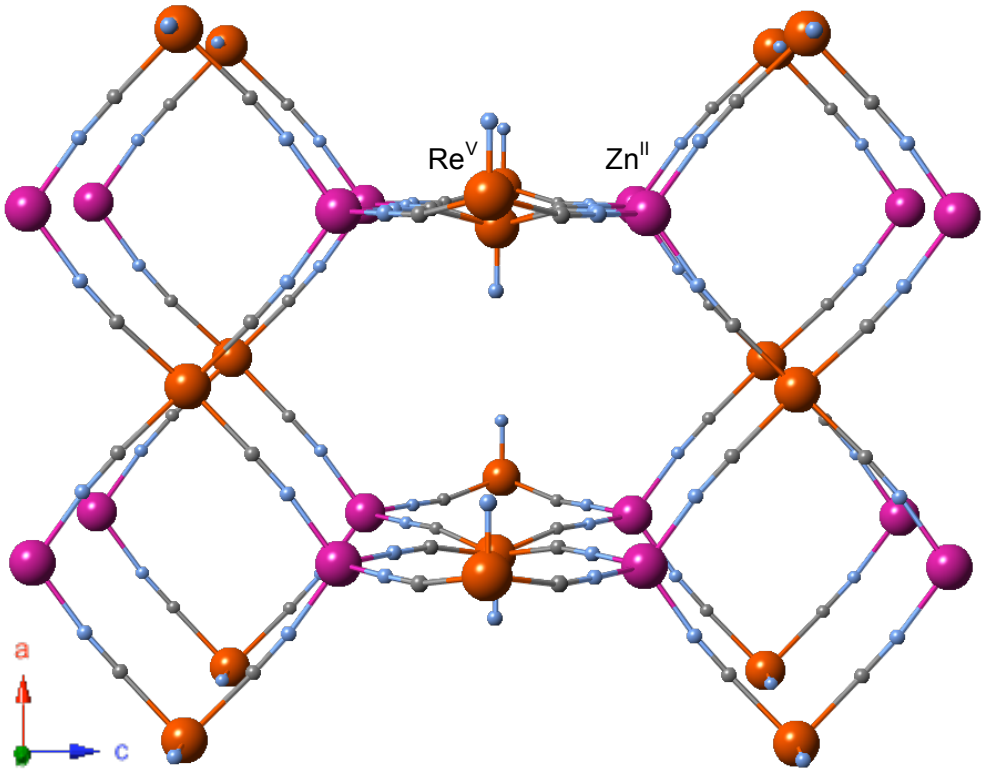

Figure 3. A polymeric structure for **ZnRe(sc)**

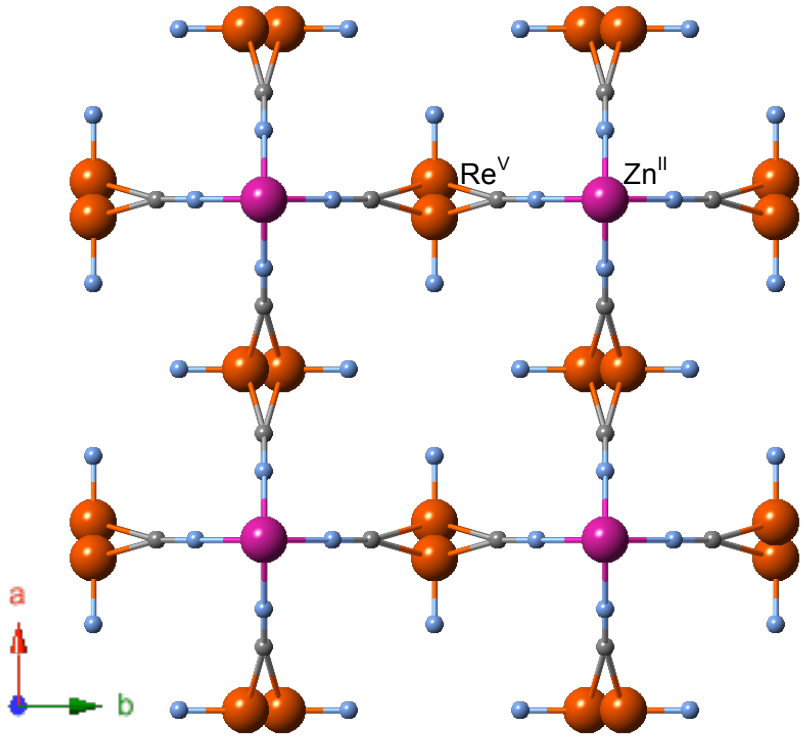

Figure 4. A projection of the polymeric structure for **ZnRe(sc)** onto *ac* plane

As described above, Re≡N bond is disorder at opposite side and exists at each side at the ratio of 50% so **ZnRe** has four kinds of pores depending on orientation of Re≡N bond (**Figure 5(a)-(d)**). If the four kinds pore exists on the average, 50% of the pores have one Re≡N bond and one open-metal-site (**Figure 5(a)-(b)**), 25% of the pores have two Re≡N bond and no open-metal-site (**Figure 5(c)**), and 25% of the pores have no Re≡N bond and two open-metal-site (**Figure 5(d)**).

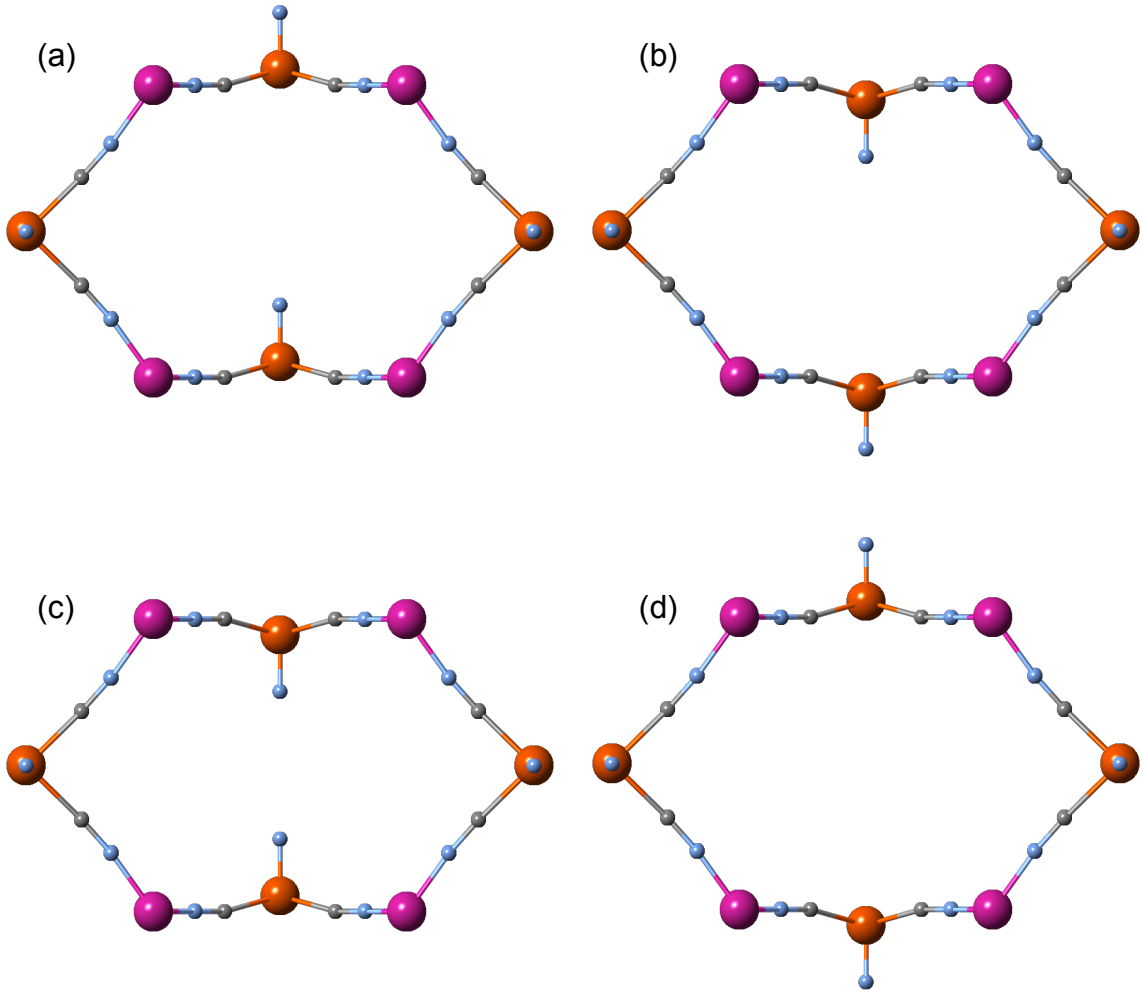

Figure 5. Four kinds of pores in **ZnRe**

Guest Responsivity

Emission Spectroscopic and Photophysical Properties

ZnRe adsorbed various guest molecules in the gas phase. The emission color of **ZnRe** was changed accompanying the guest adsorption. Here, acetone, acetonitrile, ethanol, methanol and water were picked up as representative guest molecules showing unique guest responsevity. Each guest adsorbed **ZnRe** (**ZnRe_Guest**) was prepared by guest exchange through vapor diffusion to as-synthesized **ZnRe_MeOH**, because desolvated framework of **ZnRe** did not recover the initial structure after adsorbing guest molecules (**Figure 6**). In detail procedure, a few ml guest solvent and powder **ZnRe** in a sample tube (1.5 ml) were putted in a sample tube (50 ml) (**Scheme 1**).

All of the **ZnRe_Guest** showed photoluminescence by excitation of 365 nm UV light in the solid state at room temperature. **Figure 7** shows the emission spectra of the **ZnRe_Guest** in the solid state at room temperature. **Table 3** summarizes the luminescence peak wavelength, emission quantum yield and luminescence images observed in the solid state at room temperature, with the literature data of $[PPh_4]_2[ReN(CN)_4(Guest)]$.

The emission maximum wavelength (λ_{em}) was observed at longer wavelength in the order **ZnRe_acetone** (471 nm) < **ZnRe_MeCN** (495 nm) < **ZnRe_EtOH** (502 nm) < **ZnRe_MeOH** (522 nm) < **ZnRe_H_2O** (644 nm). **ZnRe_Guest** showed remarkable guest responsivity with emission band shift rather than $[PPh_4]_2[ReN(CN)_4(Guest)]$. Moreover, the **ZnRe_acetone** showed the largest emission quantum yield (0.61) among **ZnRe_Guest** and the value was about twice as large as ϕ_{em} of $[PPh_4]_2[ReN(CN)_4(acetone)]$ (0.34) which is the largest ϕ_{em} among $[PPh_4]_2[ReN(CN)_4(Guest)]$. The enhancements of quantum yields were thought to be causally related to suppressing vibrational deactivation from excited state by formation of framework.

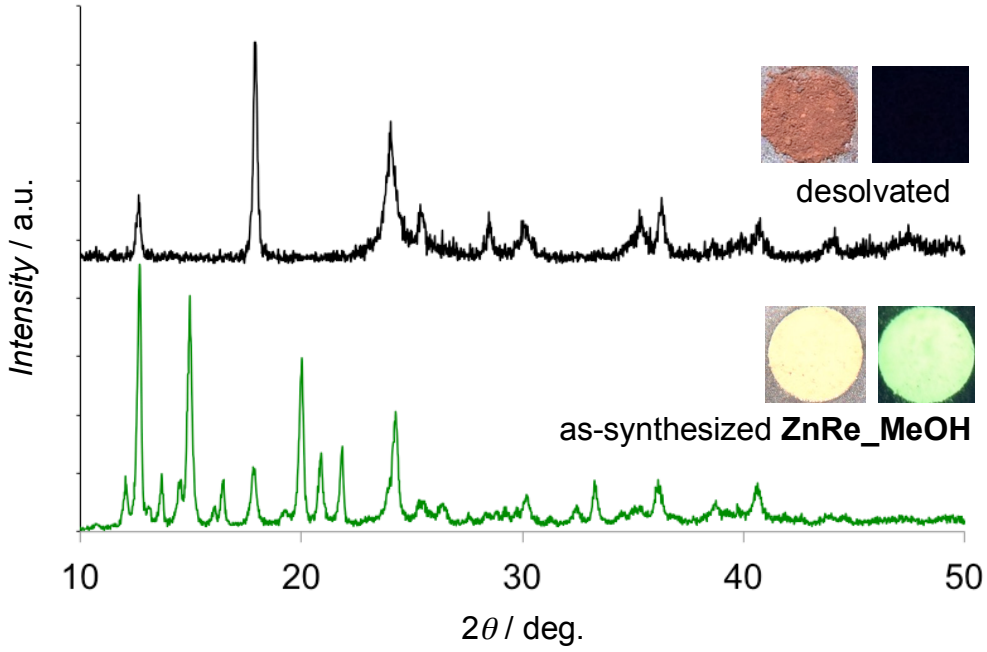

Figure 6. PXRD patterns of as-synthesized **ZnRe_MeOH** and desolvated **ZnRe_MeOH**.

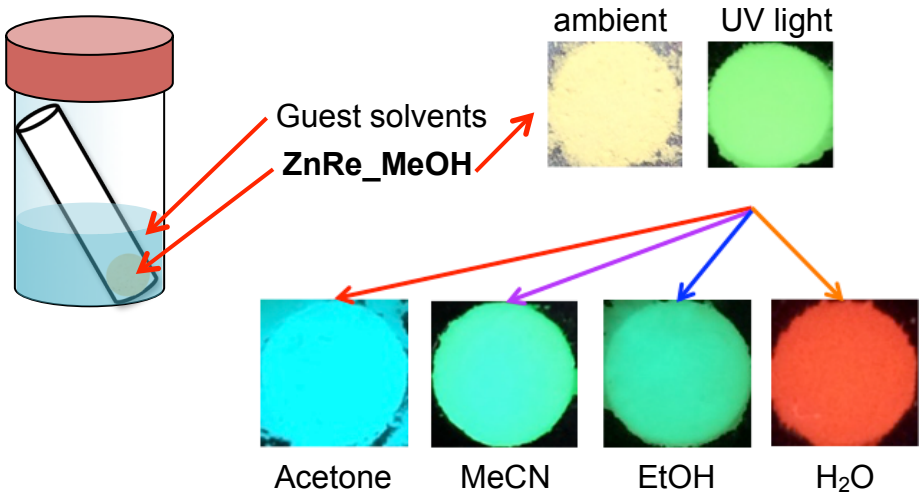

Scheme 1. Guest exchange process and guest responsevity of **ZnRe_Guest**.

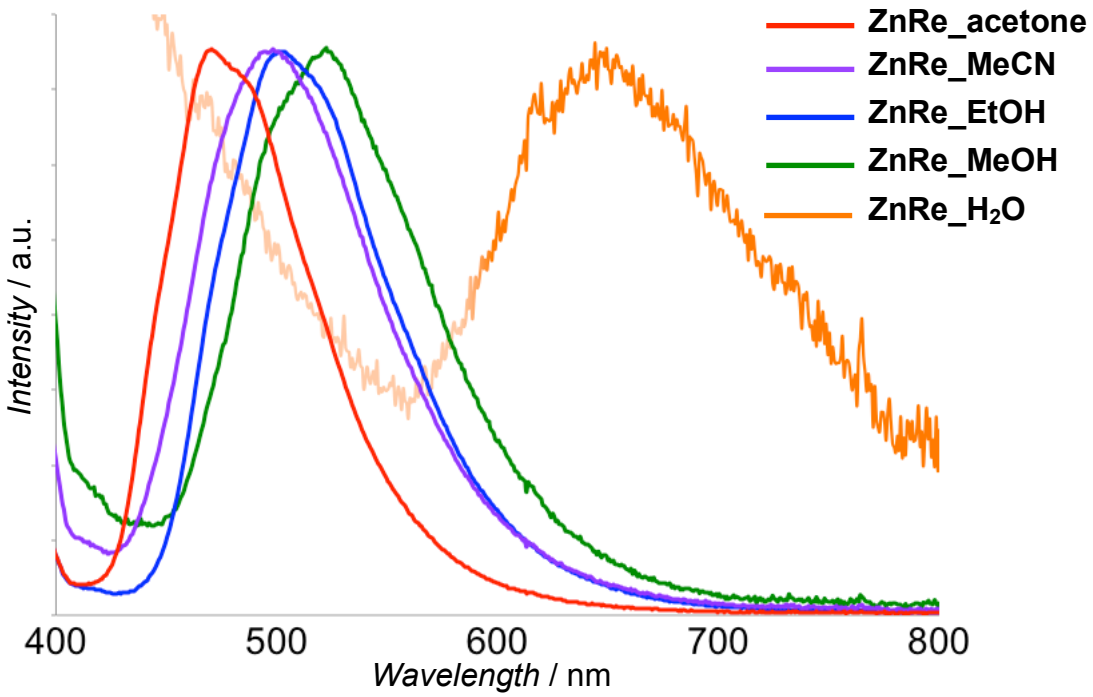

Figure 7 Emission spectra of **ZnRe_Guest** in the solid state at RT by excited at 365 nm.

Table 3. Spectroscopic and photophysical data in the solid state at RT

		Acetone	MeCN	EtOH	MeOH	H_2O
ZnRe	λ_{em} (nm)	471	495	502	522	644
	ϕ_{em}	0.61	0.43	0.46	0.19	0.03
$[PPh_4]_2[ReN(CN)_4]$	λ_{em} (nm)	533	545	548	527	—
	ϕ_{em}	0.34	0.02	<0.01	0.13	

Figure 8 shows the CIE chromaticity diagram of luminescence for the **ZnRe_Guest** by excitation of 365 nm UV light in the solid state at room temperature. **Table 4** summarizes the chromaticity values of **ZnRe_Guest**. All of the plots dispersed so indicated the multiple emission color changes were distinguishable even by visual contact.

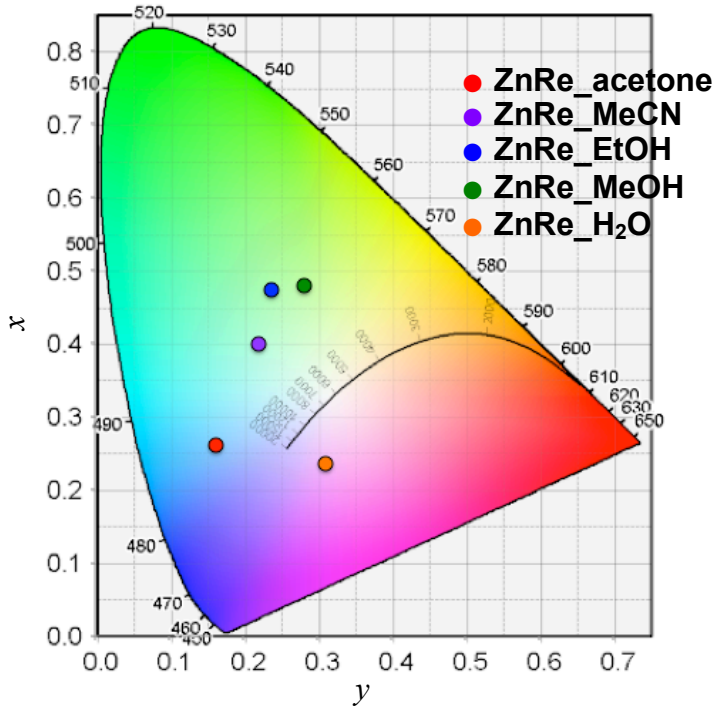

Figure 8. Color diagram showing the location of luminescence for **ZnRe_Guest**

Table 4. Chromaticity values of **ZnRe_Guest**

Guest	***x***	***y***
Acetone	0.16	0.26
MeCN	0.22	0.40
EtOH	0.24	0.47
MeOH	0.28	0.48
H_2O	0.31	0.24

Powder X-ray Diffractions (PXRD)

PXRD patterns of **ZnRe_Guest** (Guest = acetone, acetonitrile, ethanol, methanol and water) are shown in **Figure 9** and compared to the simulation pattern of **ZnRe(sc)** having PtS-type structure. Actually, as-synthesized **ZnRe_MeOH** showed different powder pattern from the simulation pattern. It essentially corresponded to the simulated pattern of the pseudo PtS-type MOF, $\{Zn^{II}[Re^{V}N(CN)_4(MeOH)]\}\cdot H_2O$ (**Figure 10**). This single crystal was obtained accidentally, and the yield was extremely low. On the other hand, the powder patterns of the resulting compounds through the guest exchange processes (**ZnRe_EtOH, ZnRe_MeCN** and **ZnRe_acetone**) were similar to the simulation pattern, which suggested **ZnRe_MeOH** has PtS-type structure with different symmetry. The powder pattern of **ZnRe_H_2O** was obviously changed which low crystallinity because of broaden pattern, but the structure is unclear. In addition, **ZnRe_H_2O** did not recover the initial PXRD pattern by guest exchange treatments. The distorted PtS-type framework of $\{Zn[Ni(CN)_4]\cdot 2MeCN\}$ was reported. In the structure, four coordinated tetrahedral of Zn^{II} ion was quite distorted and a largest N–Zn–N angle was 132.8º although the average N–Zn–N angle in the completely PtS-type framework of $\{Zn[Ni(CN)_4]\}$ was 108.8º. The large distortion of coordination structure of Zn^{II} ion suggested another solvent molecule may coordinate to Zn^{II} ion at an open site by distortion. Then, there is a possibility that the structure of **ZnRe_H_2O** converted accompanying with coordination of a water solvent molecule to Zn^{II} ion, and the structure cannot recover because of coordination water at Zn^{II} ion.

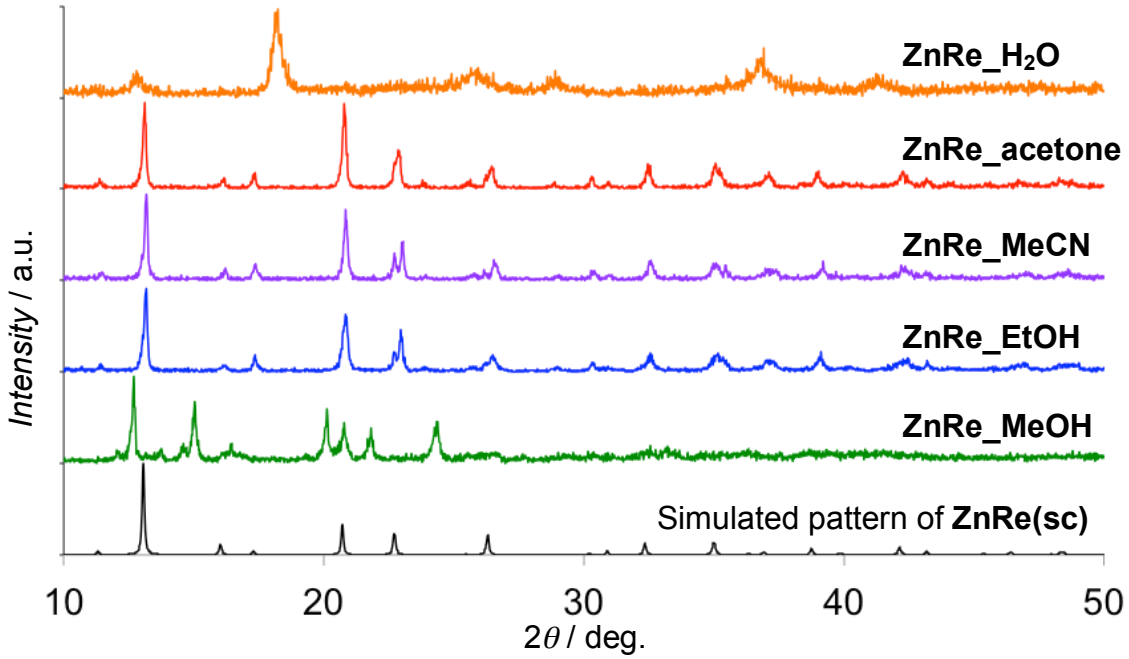

Figure 9. PXRD patterns of **ZnRe_Guest** (at RT) and the simulation pattern of **ZnRe(sc)** (at 100 K).

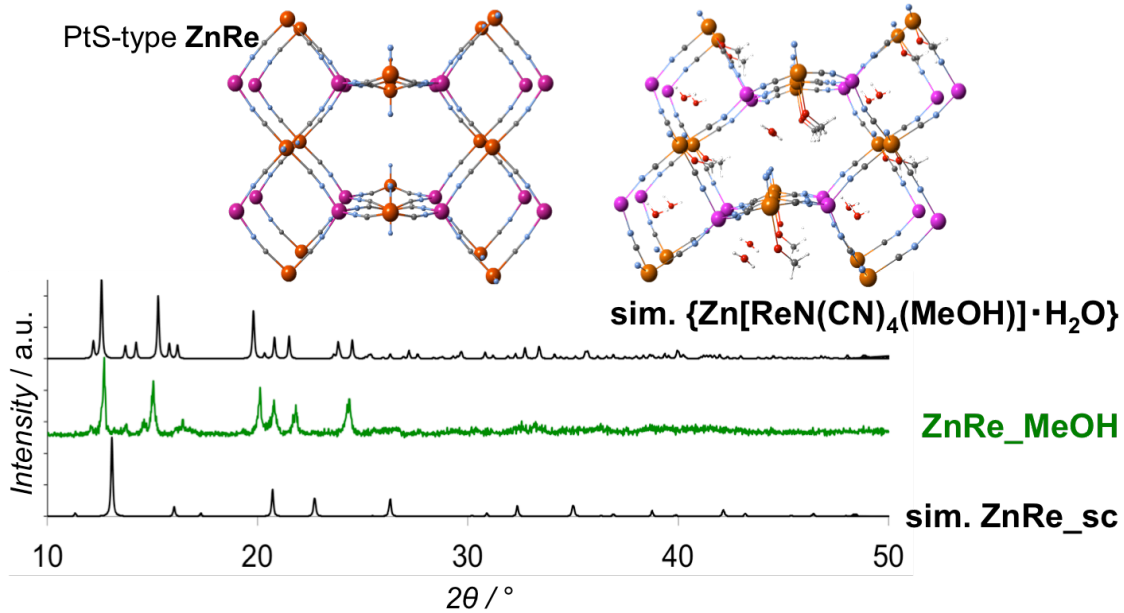

Figure 10. PXRD patterns of **ZnRe_MeOH** (at RT) and the simulation pattern of **ZnRe(sc)** and $\{Zn^{II}[Re^{V}N(CN)_4(MeOH)]\}\cdot H_2O$ (at 100 K) with thier structure.

IR Spectra

Infrared spectra of **ZnRe_Guest** (Guest = acetone, acetonitrile, ethanol, methanol and water) are shown in **Figure 11**. All **ZnRe_guest** were confirmed the peaks nitrido, cyanide and guest molecules.

The strong absorption bands based on stretching vibration of cyano groups ($\nu_{C\equiv N}$) were observed at larger wavenumber in the order (**ZnRe_acetone** (2163 cm^{-1}) < **ZnRe_MeOH** and **ZnRe_MeCN** (2168 cm^{-1}) < **ZnRe_EtOH** (2169 cm^{-1}) < **ZnRe_H_2O** (2178 cm^{-1}). The formation of Re-C≡N-Zn bridges in **ZnRe_Guest** was confirmed by the upshift of the frequency of the $\nu_{C\equiv N}$ band from that of mono-nuclear complexes ($K_2[ReN(CN)_4]\cdot H_2O$; 2107 cm^{-1} and $[PPh_4]_2[ReN(CN)_4(MeOH)]\cdot 3MeOH$; 2105, 2119 and 2135 cm^{-1}).[26] The single or doublet peak of absorption bands based on stretching vibration of nitrido group ($\nu_{Re\equiv N}$) in **ZnRe_Guest** were observed at 1000-1100 cm^{-1}. Because each $[ReN(CN)_4]^{2-}$ unit embedded in pores exists in different environment in the frameworks (**Figure 5**), non-single peaks was observed.

A unique absorption band of guest molecules were also observed at each **ZnRe_Guest**. The broad absorption bands based on stretching vibration of C-H bands ($\nu_{C\text{-}H}$) of methanol, ethanol and acetone were observed at around 3000 cm^{-1} in **ZnRe_MeOH**, **ZnRe_EtOH** and **ZnRe_acetone**, respectively. In **ZnRe_H_2O**, the O-H bands ($\nu_{O\text{-}H}$) of H_2O was observed ranged from 3400 to 3600 cm^{-1}. In **ZnRe_EtOH**, the C-C bands ($\nu_{C\text{-}C}$) of EtOH were observed at 867 cm^{-1}. The $\nu_{C=O}$ of acetone in **ZnRe_acetone** and the $\nu_{C\equiv N}$ of acetonitrile in **ZnRe_MeCN** suggest guest molecules coordinate to open metal site at the trans position of nitrido ligand of $[ReN(CN)_4]^{2-}$ in the **ZnRe** frameworks. The $\nu_{C=O}$ of acetone in **ZnRe_acetone** was observed at 1702 cm^{-1} and smaller than the $\nu_{C=O}$ at free acetone (1715 cm^{-1}), which indicates becoming longer C=O bond of acetone by coordinating to open metal site in **ZnRe**. On the other hand, the $\nu_{C\equiv N}$ of acetonitrile in **ZnRe_MeCN** (2265 cm^{-1}) was larger than the $\nu_{C\equiv N}$ of free acetonitrile (2254 cm^{-1}). The reason was not similar to the situation of the formation of Re-C≡N-Zn bridges. Because of decrease of the contributions of polar resonance structures such as $-C^{+}=N^{-}$ of acetonitrile by coordinating to open metal site in **ZnRe**, the $\nu_{C\equiv N}$ of acetonitrile increases[27].

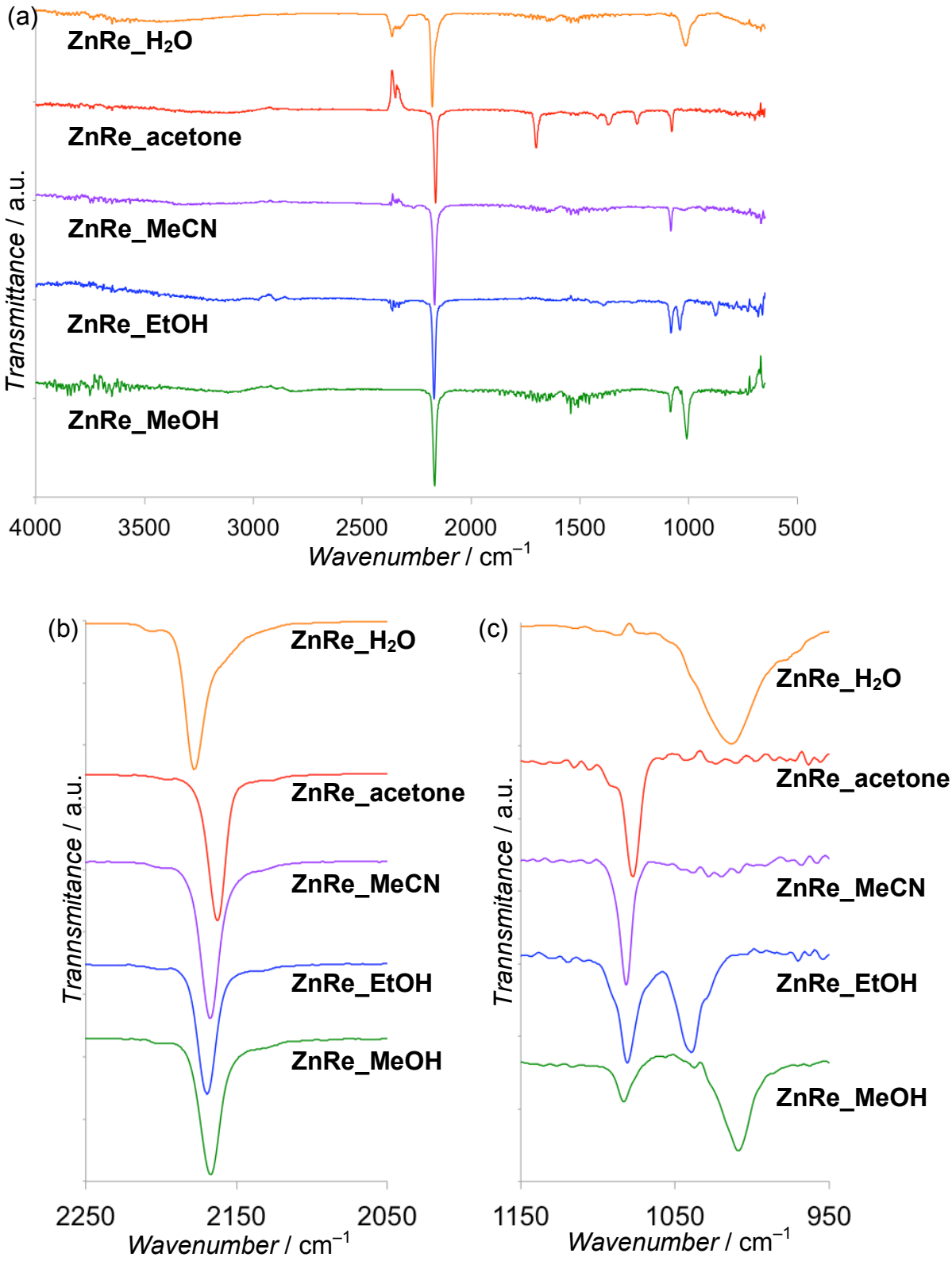

Figure 11. IR spectra of **ZnRe_MeOH** and resulting compounds through the guest exchange processes. All area plots (a), the $\nu_{C\equiv N}$ peaks (b) and the $\nu_{Re\equiv N}$ peaks (c).

Correlation between Luminescent Property and structure

As described above, **ZnRe_Guest** showed more remarkable guest responsivity with emission band shit than $[PPh_4]_2[ReN(CN)_4(Guest)]$. Thanks to $[Re^VN(CN)_4]^{2-}$ unit embedded on the framework of PCP, $[Re^VN(CN)_4]^{2-}$ unit lost the freedom of movement and permitted large structure conversion such as distortion and flat of the plane of tetracyano. The emission wavelength of $[Re^VN(CN)_4]^{2-}$ unit is probably affected the electron-donating and –accepting abilities of guest molecules as the axial ligand. However, no correlation was found between the emission wavelength and the electric permittivity, the electron-donating and -accepting parameters of the solvent ligand (**Figure 12**). This results from d electron energy state involving the coordination structure too.

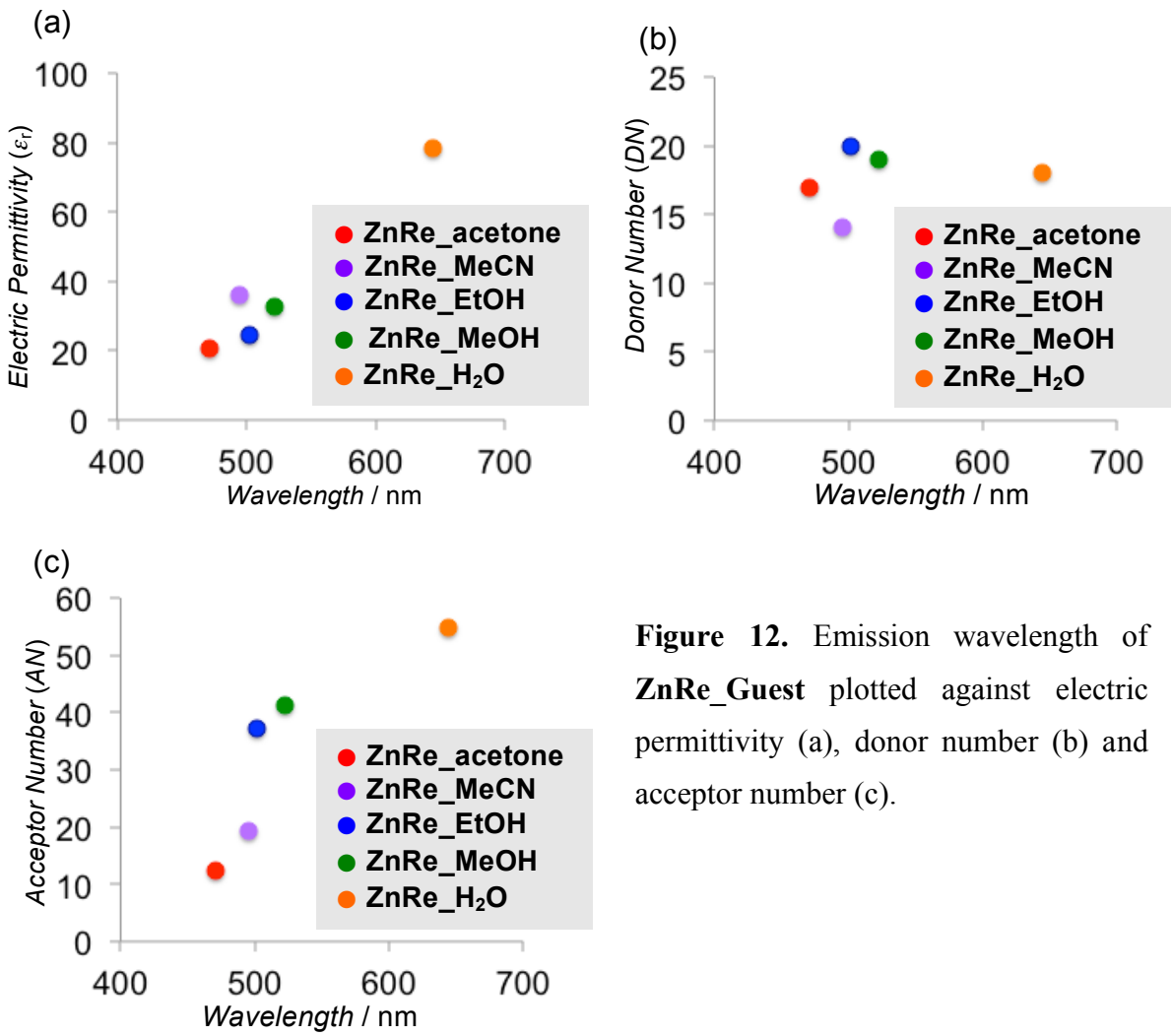

Figure 12. Emission wavelength of **ZnRe_Guest** plotted against electric permittivity (a), donor number (b) and acceptor number (c).

Figure 13 shows the Walsh diagram of square pyramid[17]. This diagram tells that the energy gap of $d_{xy} \rightarrow d_{\pi*}$ ($d_{\pi*}$ = d_{xz} and d_{yz}) increases and decreases with respectively decrease and increase of the angle of square plane. In fact, d_{z^2} and $d_{x^2-y^2}$ of $[Re^{V}N(CN)_4]^{2-}$ unit are inversion in comparison to normal square pyramid structure, and $[Re^{V}N(CN)_4]^{2-}$ unit in **ZnRe_Guest** is six coordinate structure because of having a guest molecule at trans position of nitrido ligand (**Figure 14**). However, the coordination of guest molecules is weak because the Re≡N bond is very strong. The $\nu_{C=O}$ at acetone in **ZnRe_acetone** was observed at 1702 cm^{-1}. The $\nu_{C=O}$ at acetone is larger wavenumber in the order corresponding to $[PPh_4]_2[ReN(CN)_4$(acetone)] (1684 cm^{-1}) < **ZnRe_acetone** (1702 cm^{-1}) < free acetone (1715 cm^{-1}) so acetone weakly coordinates to open metal site at the trans position of nitrido ligand in **ZnRe**. Therefore, Walsh diagram of square pyramid is practically available for $[Re^{V}N(CN)_4]^{2-}$ unit. The qualitative energy gap between dxy and $d_{\pi*}$ orbitals was estimated by changing the diagonal C-Re-C angle (θ) from 180° to 120° (**Figure 15**). The energy gap between d_{xy} and $d_{\pi*}$ orbitals increased with decreasing θ, similar to that observed in a normal square pyramidal geometry, suggesting that the blue shift in λ_{em} of **ZnRe_G** occurred because the environment around the Re^{V} center changed from a square pyramidal geometry (θ = 180º) to an umbrella geometry (θ = 120º) (**Figure 16**).

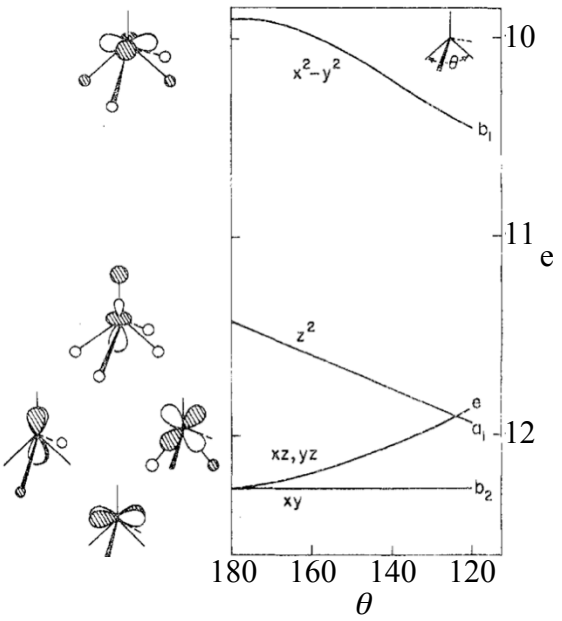

Figure 13. Walsh diagram of square pyramid

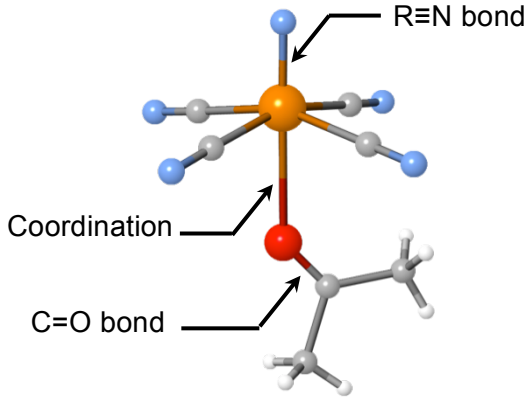

Figure 14. The moiety structure of six-coordinate in **ZnRe_acetone**

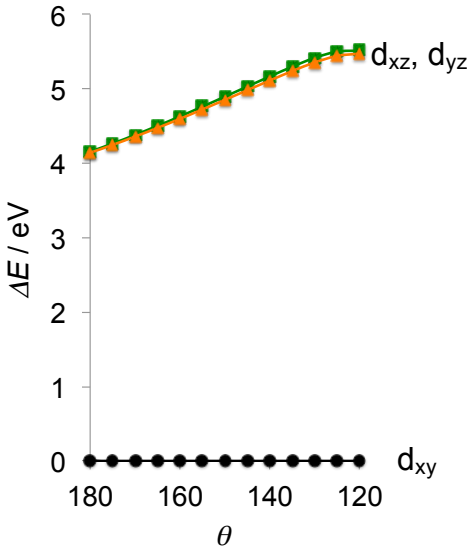

Figure 15. Calculated energy gap (*ΔE*) of 5d orbital of Re^{V} in $[ReN(CN)_4]^{2-}$ in b3lyp/LANL2DZ level.

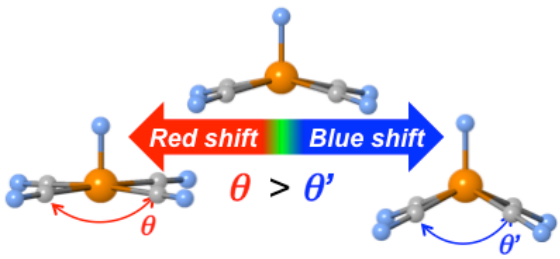

Figure 16. Structure conversion and emission color change

To study correlation between luminescent property and structure, **ZnRe_acetone** and **ZnRe_EtOH** were compared. **Figure 17** shows PXRD patterns of **ZnRe_acetone** and **ZnRe_EtOH** extracted (range from 22 to 24 deg. and from 34 to 36 deg). Here four peaks of (103), (200), (105) and (301) shifted from **ZnRe_EtOH** to **ZnRe_acetone**. According to Bragg's low ($2d\sin\theta = n\lambda$ where d is the interplanar distance, θ is the scattering angle, n is a positive integer and λ is the wavelength of incident wave), d increases or decreases with decrease or increase of θ. Then, θ of (103) and (105) of **ZnRe_acetone** were larger than that of **ZnRe_EtOH**. (200) and (301) were opposite shifts. Here, the four lattice planes show **Figure 18.** (200) and (301) were nearly vertical to the a axis, and (103) and (105) were nearly vertical to the c axis. Therefore, **ZnRe_acetone** suggested an expansion along the *a* axis and a shrinkage along *c* axis. This structure conversion occurred more distorted square planar of $[ReN(CN)_4]^{2-}$. was consistent with the blue shift of luminescence peak wavelength of **ZnRe_acetone**. On the other hand, the structure of **ZnRe_H_2O**, which was observed orange emission at the longest emission wavelength (644 nm) among **ZnRe_Guest,** was not determined. Therefore, we tried to consider correlation between luminescence and structure from IR spectra. Actually, in mono-nuclear complex $[PPh_4]_2[ReN(CN)_4]$, a correlation between the maximum emission wavelength and bond lengths such as Re≡N, Re-C and C≡N bonds was not found. However, the remarkable red-shift of the maximum emission wavelength of **ZnRe_H_2O** suggests that the diagonal angle of C-Re-C in $[ReN(CN)_4]^{2-}$ of **ZnRe_H_2O** became flatter, so it's worth considering from IR spectra due to reveal correlation between luminescence property and structure.

When the diagonal angle of square pyramid in Walsh-diagram becomes larger, the energy level of d_{z^2} and $d_{x^2-y^2}$ orbitals increase. In IR spectra of **ZnRe_Guest,** $\nu_{C\equiv N}$ of **ZnRe_H_2O** was highest wavenumber (2178 cm^{-1}) and $\nu_{Re\equiv N}$ of **ZnRe_H_2O** was only single peak at comparatively low wavenumber (1013 cm^{-1}). (The $\nu_{Re\equiv N}$ of **ZnRe_H_2O** was not lowest, but **ZnRe_MeOH** have two peaks of $\nu_{Re\equiv N}$ (1009 and 1088 cm^{-1}) although one $\nu_{Re\equiv N}$ of **ZnRe_MeOH** was lowest wavenumber.) Also, the Re-C bond becomes weaker with the C≡N bond strengthened. Then Re≡N bond and Re-C bond of **ZnRe_H_2O** are probably longer than that of other **ZnRe_Guest**. This is consistent with the emission band red shift of **ZnRe_H_2O**, which is supported by rise of energy gap of $d_{xy}\rightarrow d_{\pi*}$ associated with the increase of diagonal angle in $[ReN(CN)_4]^{2-}$.

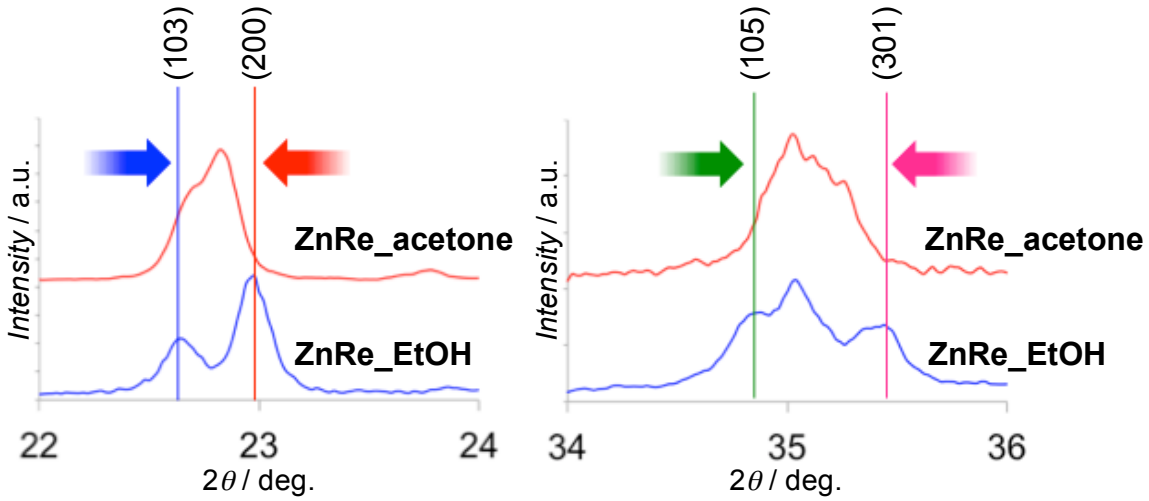

Figure 17. PXRD patterns of **ZnRe_acetone** and **ZnRe_EtOH**

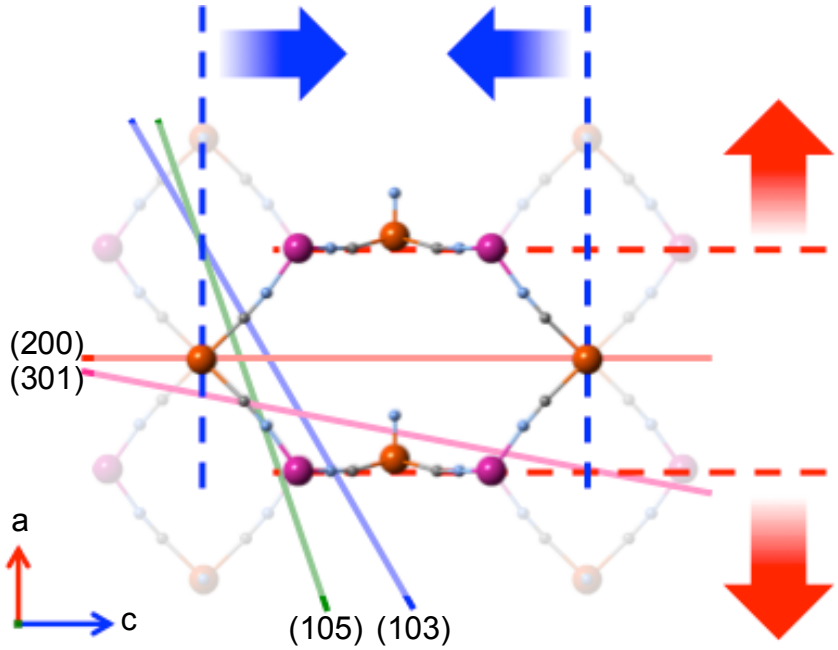

Figure 18. Stracture conversion from **ZnRe_EtOH** to **ZnRe_acetone**

Guest Exchange Reversibility

As described above, the luminescence property and structure of the desolvated **ZnRe** was irreversible, and also H_2O adsorbed **ZnRe** was in a similar state although showed orange emission. However, the reversible guest responsivity of **ZnRe** was observed on guest exchange among volatile organic vapor. **Figure 19** and **Figure 20** show the reversible process of respectively IR spectra and PXRD between methanol and acetone.

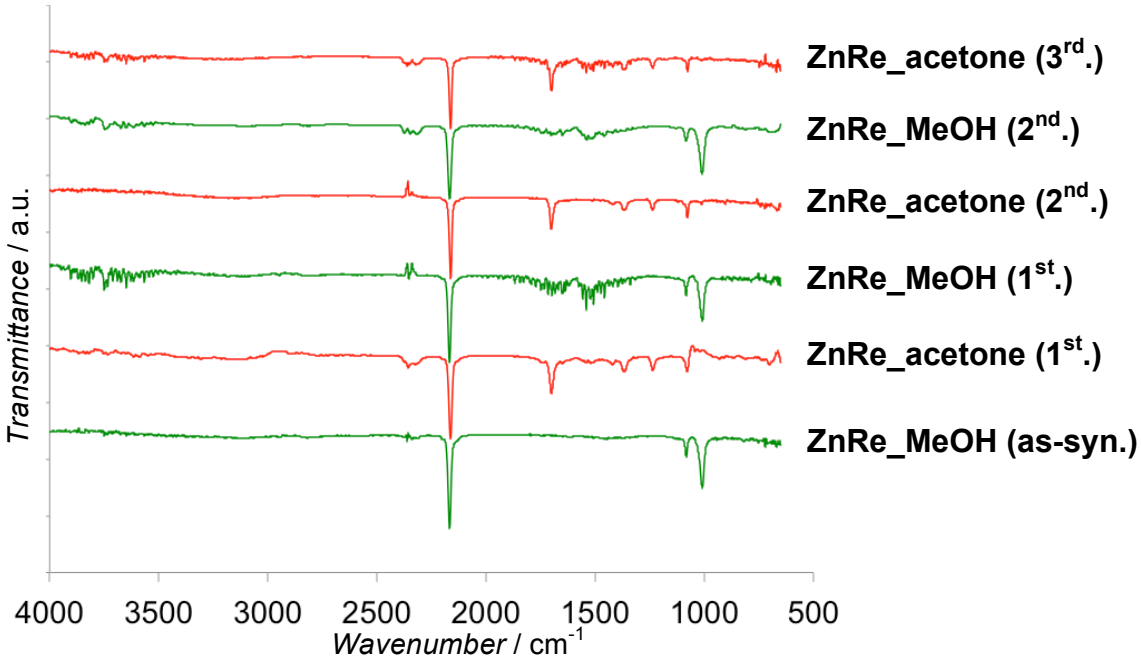

Figure 19. IR spectra of reversible guest exchange of **ZnRe** between methanol and acetone

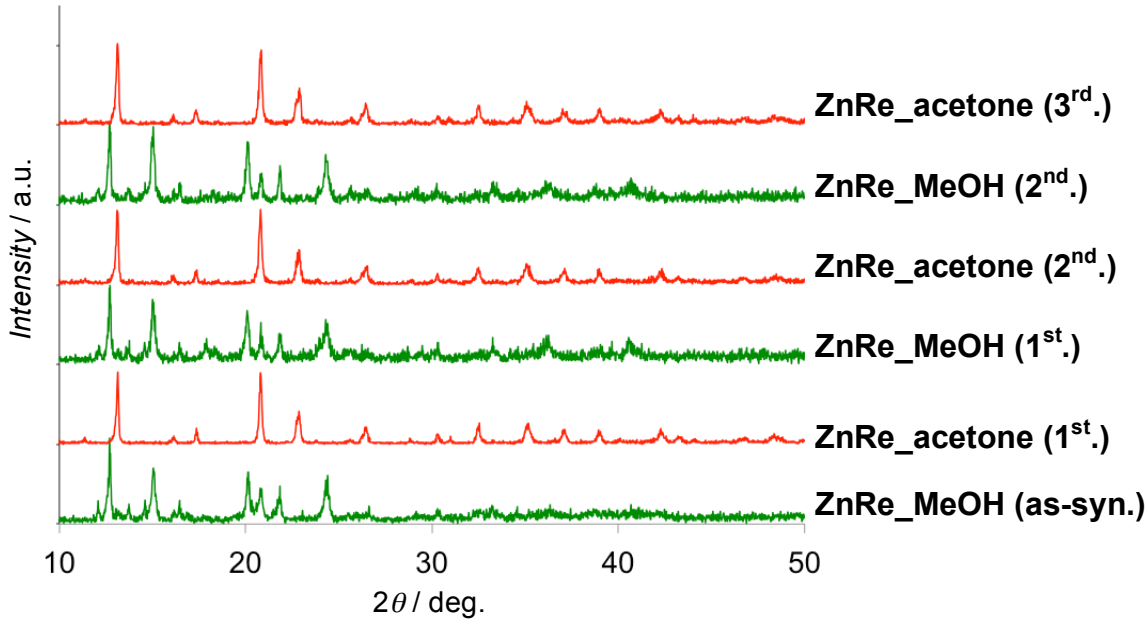

Figure 20. PXRD of reversible guest exchange of **ZnRe** between methanol and acetone

Guest Sensitivity to Acetone

The acetone-water mixture vapor in nitrogen gas for guest sensitivity was prepared according to the method described above. The ratio and concentration of acetone and water in mixture gas were summarized in **Table 5**. When the acetone gases with the concentration of approximately 9.6×10^{-4}, 1.9×10^{-4}, 9.6×10^{-5} and 3.8×10^{-5} mol/L excluding water vapor were flowed to **ZnRe_MeOH**, the emission color changed from lime green to sky blue obviously and quickly and the emission spectra demonstrated emission band blue shift from ca. 530 nm to 495 nm and the increase of emission intensity (**Figure 21**). In the case of coexistence of water vapor in the saturated vapor pressure, adequate responses were observed (**Figure 22**). To consider the difference of the guest sensitivity to acetone ex- and including water vapor, the emission intensity increment at 500 nm after the mixture gas flow were plotted against each acetone concentration (**Figure 22**). Both plots indicated the smaller emission intensity increment with smaller acetone concentration and the slope is steeper when the mixture gases have include water vapor. The result suggested water behaved as competitor guest molecules against acetone. Nevertheless, **ZnRe** showed high sensitivity to acetone vapor regardless of the presence or absence of water. Continuously, the investigation of detection limit of acetone was performed. **Figure 24** showed the emission spectra of **ZnRe_MeOH** before and after flow of acetone-water mixture gas with the acetone concentration of approximately 1.9×10^{-5}, 1.3×10^{-5} and 9.6×10^{-6} mol/L at room temperature by excited at 365 nm. After flow of 1×10^{-5} mol/L acetone vapor, the changes of emission intensity and wavelength did not observed. In our laboratory level, therefore, the detection limit of acetone vapor by **ZnRe_MeOH** was around 300 ppm despite the existence of 75 times the amount of water vapor. In order to detect acetone in a breathing air, the detection of acetone at level of at least a few hundred bpm should be performed. Our detection limit at 300 ppm was far inferior to the practical level in presence. However, it was unconfirmed whether our procedure for the fabrication of **ZnRe_MeOH** in sample holder and the analysis of guest sensitivity to acetone vapor were most appropriate. In addition, the detection limit using changes of photoluminescent behavior is also affected and depends on the performance of a measuring device. Therefore, the detection limit to acetone using **ZnRe_MeOH** maybe still decrease by using an appropriate method and measuring device.

Table 5. The conditions of acetone gas for analysis of detection limit of acetone

293 K	vapor pressure (Pa)	ratio against water content	introduced amount (μL)	ppm	concentration (mol/L)
water	2332	—	23.1	23015	9.6×10^{-4}
	2332	1 / 1	94.0	23015	9.6×10^{-4}
	46.4	1 / 5	18.8	4603	1.9×10^{-4}
	233.2	1 / 10	9.4	2302	9.6×10^{-5}
acetone	93.28	1 / 25	3.8	921	3.8×10^{-5}
	46.64	1 / 50	1.9	460	1.9×10^{-5}
	31.09	1 / 75	1.3	307	1.3×10^{-5}
	23.32	1 / 100	0.9	230	9.6×10^{-6}

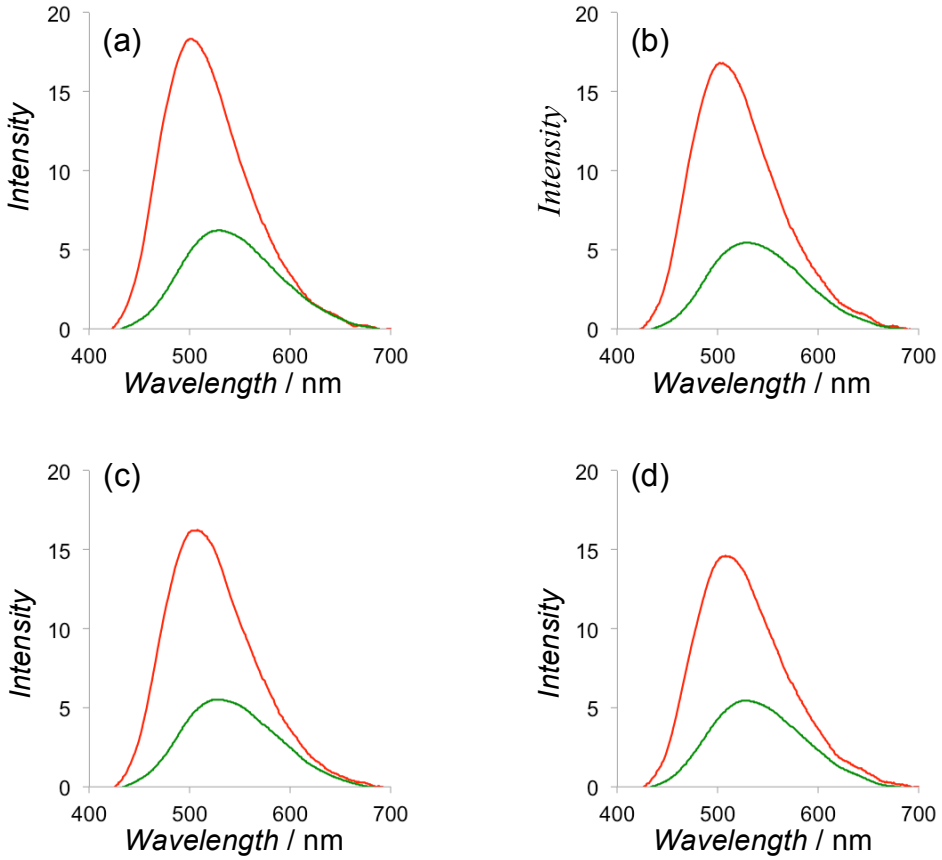

Figure 21. Emission spectra of the initial **ZnRe_MeOH** sample in green line and the responded sample by acetone gas with the concentration of approximately 9.6×10^{-4} mol/L in (a), 1.9×10^{-4} mol/L in (b), 9.6×10^{-5} mol/L in (c) and 3.8×10^{-5} mol/L in (d) in red line at RT by excited at 365 nm.

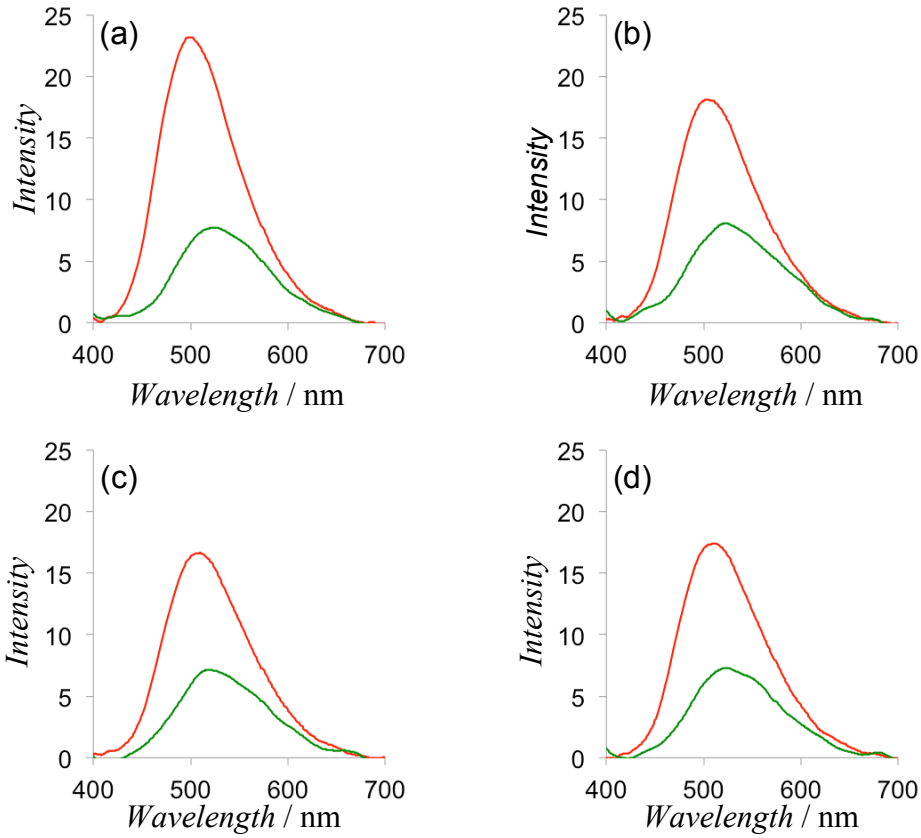

Figure 22. Emission spectra of the initial **ZnRe_MeOH** sample in green line and the responded sample by acetone gas with the concentration of approximately 9.6×10^{-4} mol/L in (a), 1.9×10^{-4} mol/L in (b), 9.6×10^{-5} mol/L in (c) and 3.8×10^{-5} mol/L in (d) including the water vapor of 9.6×10^{-4} mol/L in red line at RT by excited at 365 nm.

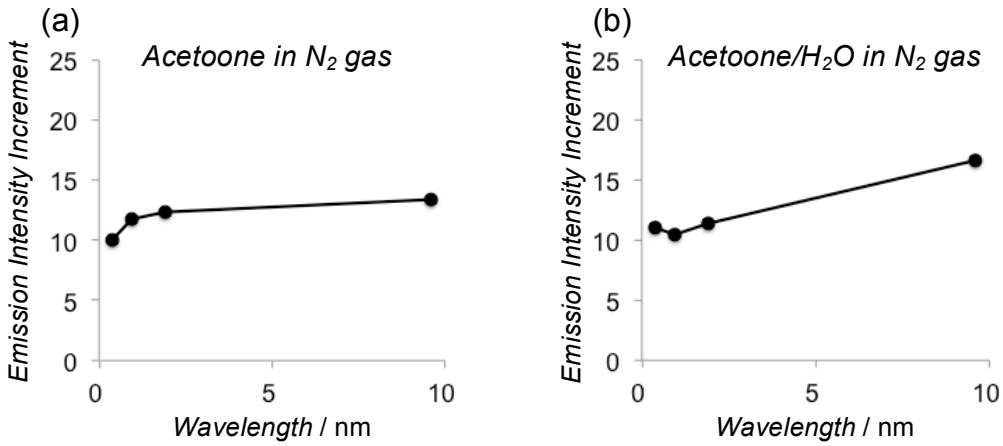

Figure 23. Emission intensity increment at 500 nm of **ZnRe_MeOH** after acetone-nitrogen mixture gas flow without and with water vapor in (a) and (b), respectively.

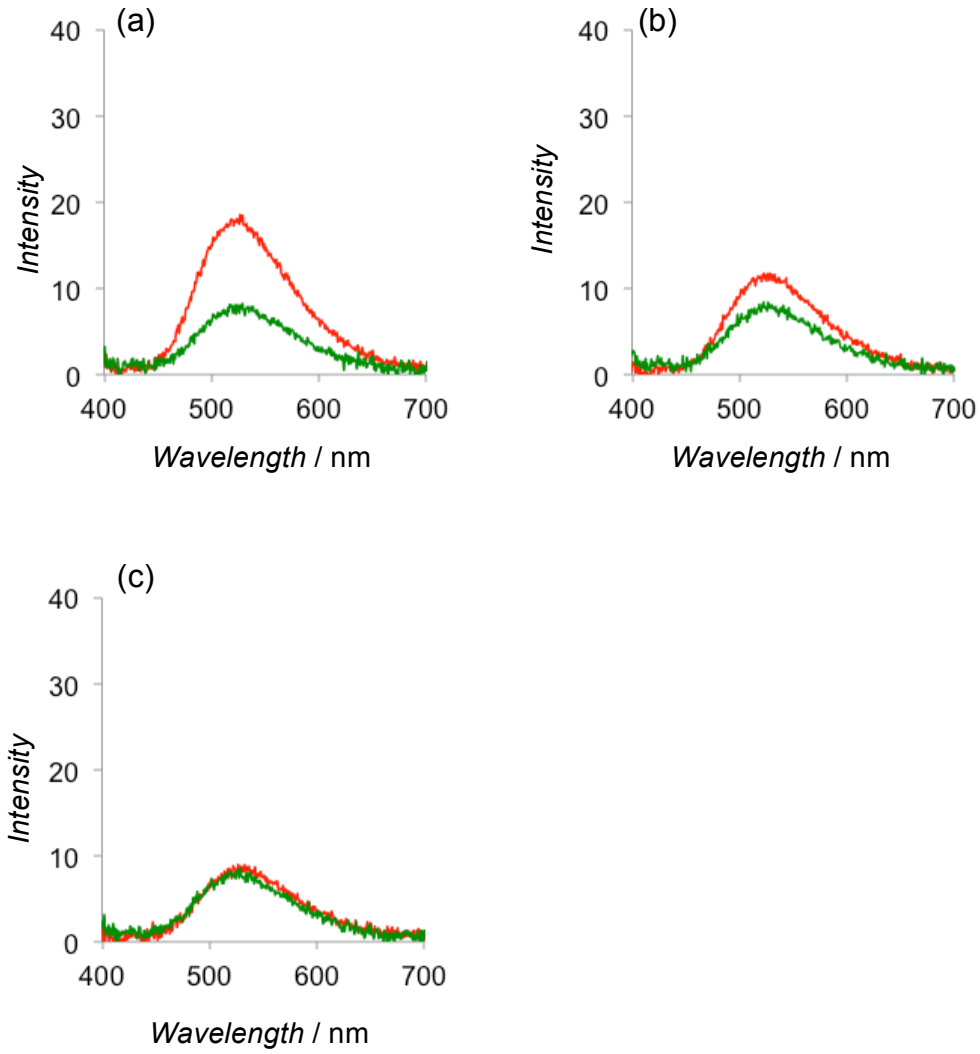

Figure 24. Emission spectra of the initial **ZnRe_MeOH** sample in green line and the responded sample by acetone gas with the concentration of approximately 1.9×10^{-5} mol/L in (a), 1.3×10^{-5} mol/L in (b) and 9.6×10^{-6} mol/L in (c) including the water vapor of 9.6×10^{-4} mol/L in red line at RT by excited at 365 nm.

Conclusion

Guest responsive luminescent 3-D coordination polymer $\{Zn^{II}[Re^{V}N(CN)_4]\cdot n\text{sol}\}$ (**ZnRe**) was prepared by using a nitridotetracyanometalate $[Re^{V}N(CN)_4]^{2-}$ as a building unit. Single crystal and powder X-ray structural analyses revealed that **ZnRe** formed a PtS-type porous structure extended by Re-CN-Zn linkages. As synthesized **ZnRe_MeOH** showed lime green emission (λ_{max} = 522 nm) by excitation of 365 nm UV light. **ZnRe** adsorbed various guest molecules, such as acetone, acetonitrile, ethanol, methanol and water. **ZnRe_Guest** showed remarkable guest responsivity with emission band shift (λ_{max} = 471 - 644 nm) depending on the guest molecules, which was not observed in only $[Re^{V}N(CN)_4]^{2-}$ unit. Guest responsivity of **ZnRe_Guest** was carefully discussed based on the structure and property of guest molecule by powder X-ray diffraction, IR spectra and emission spectra.

We found out correlation between the maximum emission wavelength and structure. The large emission band shifts were associated with change of C–Re–C bond angles in the $[Re^{V}N(CN)_4]^{2-}$ unit. According to Walsh diagram of suquare pyramid, the energy gap of $d_{xy} \rightarrow d_{\pi*}$ ($d_{\pi*} = d_{xz}$ and d_{yz}) increases and decreases with respectively decrease and increase of the angle of square plane. This relation was consistent with emission spectra and structure conversion considered by powder X-ray diffraction and IR spectra. In detail, **ZnRe_acetone** indicates emission blue-shift and becoming narrower C–Re–C bond, and **ZnRe_H_2O** indicates emission red-shift and becoming wider C–Re–C bond.

ZnRe_Guest and **ZnRe** analogue are expected using as gas sensor by additional elucidation of correlation between the maximum emission wavelength and structure, detection limit and response speed.

References

1. (a) M. O'Keeffe, M. Eddaoudi, H. Li, T. Reineke, O. M. Yaghi, *J. Solid State Chem.* **2000**, *152*, 3–20; (b) O. M. Yaghi, M. O'Keeffe, N. W. Ockwig, H. K. Chae, M. Eddaoudi, J. Kim, *Nature* **2003**, *423*, 705–714; (c) J. L. C. Rowsell, O. M. Yaghi, *Microporous Mesoporous Mater.* **2004**, *73*, 3–14; (d) S. Kitagawa, R. Kitaura, S. I. Noro, *Angew. Chem. Int. Ed.* **2004**, *43*, 2334–2375; (e) S. Kitagawa, K. Uemura, *Chem. Soc. Rev.* **2005**, *34*, 109–119; (f) S. Kitagawa, S. I. Noro, T. Nakamura, *Chem. Commun.* **2006**, 701–707; (g) G. Férey, *Chem. Soc. Rev.* **2008**, *37*, 191–214; (h) G. Férey, C. Serre, *Chem. Soc. Rev.* **2009**, *38*, 1380–1399.
2. (a) A. R. Millward, O. M. Yaghi, *J. Am. Chem. Soc* **2005**, *127*, 17998–17999; (b) M. Dincă, A. F. Yu, J. R. Long, *J. Am. Chem. Soc* **2006**, *128*, 8904–8913.
3. (a) R. Matsuda, R. Kitaura, S. Kitagawa, Y. Kubota, R. V. Belosludov, T. C. Kobayashi, H. Sakamoto, T. Chiba, M. Takata, Y. Kawazoe, et al., *Nature* **2005**, *436*, 238–241; (b) R. V. Belosludov, M. Takata, S. Kitagawa, H. Sato, R. Matsuda, S. Sakaki, W. Kosaka, Y. Hijikata, A. Hori, *Science* **2014**, *343*, 167–170.
4. (a) L. E. Kreno, K. Leong, O. K. Farha, M. Allendorf, R. P. Van Duyne, J. T. Hupp, *Chem. Rev.* **2011**, *112*, 1105–1125; (b) Y. J. Cui, Y. F. Yue, G. D. Qian, B. L. Chen, *Chem. Rev.* **2012**, *112*, 1126–1162; (c) Z. Hu, B. J. Deibert, J. Li, *Chem. Soc. Rev.* **2014**, *43*, 5815–5840; (d) W. P. Lustig, S. Mukherjee, N. D. Rudd, A. V. Desai, J. Li, S. K. Ghosh, *Chem. Soc. Rev.* **2017**, *46*, 3242–3285.
5. (a) Y. Takashima, V. M. Martínez, S. Furukawa, M. Kondo, S. Shimomura, H. Uehara, M. Nakahama, K. Sugimoto, S. Kitagawa, *Nat. Commun.* **2011**, *2*, 168; (b) M. Zhang, G. Feng, Z. Song, Y. P. Zhou, H. Y. Chao, D. Yuan, T. T. Y. Tan, Z. Guo, Z. Hu, B. Z. Tang, et al., *J. Am. Chem. Soc.* **2014**, *136*, 7241–7244; (c) I. H. Park, R. Medishetty, J. Y. Kim, S. S. Lee, J. J. Vittal, *Angew. Chem. Int. Ed.* **2014**, *53*, 5591–5595; (d) A. Watanabe, A. Kobayashi, E. Saitoh, Y. Nagao, S. Omagari, T. Nakanishi, Y. Hasegawa, W. M. C. Sameera, M. Yoshida, M. Kato, *Inorg. Chem.* **2017**, *56*, 3005–3013; (e) D. S. Zhang, Q. Gao, Z. Chang, X. T. Liu, B. Zhao, Z. H. Xuan, T. L. Hu, Y. H. Zhang, J. Zhu, X. H. Bu, *Adv. Mater.* **2018**, *30*, 180471; (f) A. Kobayashi, K. Shimizu, A. Watanabe, Y. Nagao, N. Yoshimura, M. Yoshida, M. Kato, *Inorg. Chem.* **2019**, *58*, 2413–2421.
6. (a) K. Miyata, Y. Konno, T. Nakanishi, A. Kobayashi, M. Kato, K. Fushimi, Y. Hasegawa, *Angew. Chem. Int. Ed.* **2013**, *52*, 6413–6416; (b)J. N. Hao, B. Yan,

Chem. Commun. **2015**, *51*, 7737–7740; (c) S. Sato, A. Ishii, C. Yamada, J. Kim, C. Ho Song, A. Fujiwara, M. Takata, M. Hasegawa, *Polym. J.* **2015**, *47*, 195–200; (d) G. Ji, J. Liu, X. Gao, W. Sun, J. Wang, S. Zhao, Z. Liu, *J. Mater. Chem. A* **2017**, *5*, 10200–10205; (e) H. S. Quah, L. T. Ng, J. J. Vittal, *Dalton Trans.* **2018**, *47*, 264–268.

7. (a) P. D. Fleischauer, P. Fleischauer, *Chem. Rev.* **1970**, *70*, 199–230; (b) A. Wölpl, D. Oelkrug, *Ber. Bunsenges. Phys. Chem* **1974**, *79*, 394–400; (c) Y. Yuske, *J. Spectrosc. Soc. Japan* **1982**, *31*, 2–18.
8. Y. Wu, X. Zhang, L. J. Xu, M. Yang, Z. N. Chen, *Inorg. Chem.* **2018**, *57*, 9175–9181. **2018**, *90*, 105–107.
9. J. F. Guo, W. F. Yeung, S. Gao, G. H. Lee, S. M. Peng, M. H. W. Lam, T. C. Lau, *Eur. J. Inorg. Chem.* **2008**, 158–163.
10. T. D. Keene, M. J. Murphy, J. R. Price, D. J. Price, C. J. Kepert, *Dalton Trans.* **2011**, *40*, 11621–11628.
11. M. J. Murphy, D. M. D'Alessandro, C. J. Kepert, *Dalton Trans.* **2013**, *42*, 13308–13310.
12. R. Ohtani, S. Kitagawa, M. Ohba, *Polyhedron* **2013**, *52*, 591–597.
13. R. Ohtani, M. Inukai, Y. Hijikata, T. Ogawa, M. Takenaka, M. Ohba, S. Kitagawa, *Angew. Chem. Int. Ed.* **2015**, *54*, 1139–1143.
14. (a) N. P. Johnson, *J. Chem. Soc. (A).* **1969**, 1843–1845; (b) W. Pureell, I. Z. Potgieter, L. J. Damoense, J. S. Leipolldt, *Transit. Met. Chem.* **1991**, *16*, 473–475; (c) J. Bendix, K. Meyer, T. Weyhermu, E. Bill, N. Metzler-nolte, K. Wieghardt, *Inorg. Chem.* **1998**, *37*, 1767–1775; (d) J. Bendix, R. J. Deeth, T. Weyhermüller, E. Bill, K. Wieghardt, *Inorg. Chem.* **2000**, *39*, 930–938; (e) H. J. Van Der Westhuizen, W. Purcell, S. S. Basson, *Transit. Met. Chem.* **2002**, *27*, 506–511; (f) T. N. Mtshali, W. Pureell, H. G. Visser, *Acta Crystallogr. Sect. E Struct. Reports Online* **2007**, *63*, 80–82; (g) H. J. Van Der Westhuizen, R. Meijboom, M. Schutte, A. Roodt, *Inorg. Chem.* **2010**, *49*, 9599–9608; (h) W. Purcell, H. G. Visser, *J. Chem. Crystallogr.* **2016**, *46*, 15–20.
15. H. Ikeda, T. Yoshimura, A. Ito, E. Sakuda, N. Kitamura, T. Takayama, T. Sekine, A. Shinohara, *Inorg. Chem.* **2012**, *51*, 12065–12074.
16. H. Ikeda, A. Ito, E. Sakuda, N. Kitamura, T. Takayama, T. Sekine, A. Shinohara, T. Yoshimura, *Inorg. Chem.* **2013**, *52*, 6319–6327.

17. A. R. Rossi, R. Hoffmann, *Inorg. Chem.* **1975**, *14*, 365–374.
18. O. V. Dolomanov, L. J. Bourhis, R. J. Gildea, J. A. K. Howard, H. Puschmann, *J. Appl. Crystallogr.* **2009**, *42*, 339–341.
19. A. L. Spek, *Acta Crystallogr. Sect. C, Struct. Chem.* **2015**, *71*, 9–18.
20. (a) C. Lee, W. Yang, R. G. Parr, *Phys. Rev. B - Cover. Condens. matter Mater. Phys.* **1988**, *37*, 785–789; (b) A. D. Becke, *J. Chem. Phys.* **1993**, *98*, 5648–5652.
21. (a) P. J. Hay, W. R. Wadt, *J. Chem. Phys.* **1985**, *82*, 299–310; (b) P. J. Hay, W. R. Wadt, *J. Chem. Phys.* **1985**, *82*, 270–283.
22. Gaussian R 09W, M. J. Frisch, G. W. Trucks, H. B. Schlegel, G. E. Scuseria, M. A. Robb, J. R. Cheeseman, G. Scalmani, V. Barone, B. Mennucci, G. A. Petersson, H. Nakatsuji, M. Caricato, X. Li, H. P. Hratchian, A. F. Izmaylov, J. Bloino, G. Zheng, J. L. Sonnenberg, M. Hada, M. Ehara, K. Toyota, R. Fukuda, J. Hasegawa, M. Ishida, T. Nakajima, Y. Honda, O. Kitao, H. Nakai, T. Vreven, J. A. Montgomery, Jr., J. E. Peralta, F. Ogliaro, M. Bearpark, J. J. Heyd, E. Brothers, K. N. Kudin, V. N. Staroverov, T. Keith, R. Kobayashi, J. Normand, K. Raghavachari, A. Rendell, J. C. Burant, S. S. Iyengar, J. Tomasi, M. Cossi, N. Rega, J. M. Millam, M. Klene, J. E. Knox, J. B. Cross, V. Bakken, C. Adamo, J. Jaramillo, R. Gomperts, R. E. Stratmann, O. Yazyev, A. J. Austin, R. Cammi, C. Pomelli, J. W. Ochterski, R. L. Martin, K. Morokuma, V. G. Zakrzewski, G. A. Voth, P. Salvador, J. J. Dannenberg, S. Dapprich, A. D. Daniels, O. Farkas, J. B. Foresman, J. V. Ortiz, J. Cioslowski, and D. J. Fox, Gaussian, Inc., Wallingford CT, 2009.
23. (a) N. P. Johnson, C. J. L. Lock, G. Wilkinson, *Inorg. Synth.* **1967**, *IX*, 145–148; (b) B. P. Sullivan, J. C. Brewer, H. B. Gray, *Inorg. Synth.* **1992**, *29*, 146–150.
24. N. P. Johnson, *J. Chem. Soc. A Inorganic, Phys. Theor.* **1969**, *0*, 1843–1845.
25. (a) Z. F. Chen, R. G. Xiong, J. Zhang, X. T. Chen, Z. L. Xue, X. Z. You, *Inorg. Chem.* **2001**, *40*, 4075–4077; (b) Z. Wei, Z.-Y. Gu, R. K. Arvapally, Y.-P. Chen, R. N. McDougald, J. F. Ivy, A. A. Yakovenko, D. Feng, M. A. Omary, H.-C. Zhou, *J. Am. Chem. Soc.* **2014**, *136*, 8269–8276.
26. (a) K. Nakamoto, in *Infrared Raman Spectra Inorg. Coord. Compd. Part B Appl. Coord. Organometallic, Bioinorg. Chem.*, John Wiley & Sons, **2009**, pp. 110–117; (b) Y. Yamada, *Bull. Chem. Soc. Jpn.* **2016**, *68*, 16–28.
27. I. Matsubara, *Bull. Chem. Soc. Jpn.* **1961**, *34*, 1710–1719.

Chapter 2

Luminescence Properties of Two-Dimensional Coordination Polymers Incorporated Axial Co-Ligands

Abstract

Hofmann-type coordination polymers (CPs) $\{M(L)_n[M'(CN)_4]\}$ consisted of two-dimensional cyanide bridged sheets have been well researched by using the variety of transition metal ions and complementary ligands. We have been interested in the effects of complementary ligands on luminescent property of nitridotetracyanometallate(V) ion $[Re^{V}N(CN)_4]^{2-}$ and framework structure contained of $[Re^{V}N(CN)_4]^{2-}$. Then, novel 2D nitridotetracyanorhenate-based Hofmann-type PCPs $\{[Zn(co\text{-}L)_2][ReN(CN)_4(co\text{-}L)]\}$ (**ZnRepy** and **ZnReClpy**; co-L = pyridine (py) and 3-chloropyridine (Clpy)) were prepared. Their framework structure had wavy cyanide-bridged layers and co-L coordinated to unoccupied coordination sites at one of the $[ReN(CN)4]^{2-}$ unit and two of the Zn^{II} ion **ZnRepy** and **ZnReClpy** showed lime green emission originating from d-d transition but exhibit no guest responsivity because of strong intra- and inter-layer π-π interactions. **ZnRepy** showed the emission red-shift and the decrease of crystallinity by grinding. After exposure the ground sample of **ZnRepy** to organic vapors, the emission color and PXRD peaks related to the arrangement of pyridine were recovered partially. This result suggested that the order or disorder of the arrangement of co-L in the frameworks affected to the intra- and inter-layer π-π interactions and the coordination environment of Re(V) metal center.

Introduction

Hofmann-type compounds have been known as one of the series of porous coordination polymers (PCPs), also called metal-organic frameworks, since 1897.[1] Hofmann and Küspert reported first example as Hofmann clathrates which were $\{Ni(NH_3)_2[Ni(CN)_4]\cdot(\mathbf{G})\}$ (**G** = benzene, pyrrole, thiophene, furane). The frameworks of Hofmann-type CPs consisted of two-dimensional square mesh sheets, which were constructed by Ni–CN–Ni linkages between square planar $[Ni(CN)_4]^{2-}$ metalloligand linkers and hexacoordinated octahedral Ni^{2+} ions with two coordinated NH_3 at the axial positions, and organic guest molecules accommodated between the layers. Subsequently, using different building components of not only metal ions but also axial ligands coordinating octahedral metal ions expanded the series of Hofmann-type CPs with general formula $\{M(L)_n[M'(CN)_4]\cdot xG\}$, where M and M' are transition metal ions, L is monodentate or bridging ligand and G are guest molecules.[2] By choosing appropriate ligand, the structure of PCPs can be designed. When monodentate ligands represented by pyridine (py) are introduced instead of protruded NH_3 ligands in the sheet of $\{M(NH_3)_2[M'(CN)_4]\}$, the 2D Hofmann-type CPs $\{M(py)_2[M'(CN)_4]\}$ was prepared.[3] In the case of using bridging ligands such as pyrazine (pz), the framework structure forms 3D pillared-layer structure with formula $\{M(pz)[M'(CN)_4]\}$ as resulting from connecting the 2D cyanide bridged sheets with vertical columns of the pyrazine bridges.[4] In addition, the physical properties of PCPs are also varified depending on introduced organic ligands, and in particular the magnetic property in Hofmann-type PCPs have been investigated.[2,4] Nitridotetracyanometallates group could also construct Hofmann-type PCPs as with tetracyanometallate group. 3D Hofmann-type PCPs $\{M^{II}(H_2O)(bpy)_{1/2}[Mn^{V}N(CN)_4(bpy)_{1/2}]\cdot 2H_2O\}$ (bpy = 4,4'-bipyridine; M^{II} = Mn, Fe, Co) having wavy cyanide-bridged layers and $\{M^{II}(bpy)[Mn^{V}N(CN)_4(bpy)_{1/2}]\}$ (M^{II} = Zn, Cd) having planar cyanide-bridged layers were reported by Kepart's group and Ohba's group, respectively.[5]

In this study, we focused on luminescent nitridotetracyanometallate-based PCPs with complementary ligands (co-L), about which have been no reports. T. Yoshimura and A. Shinohara *et. al.* synthesized luminescent mononuclear nitridotetracyanorhenate(V) complexes with N-heteroaromatic ligands as co-L at open-metal site with formula $[Re^{V}N(CN)_4(co\text{-}L)]^{2-}$, and investigated about the photoluminescent property. Their emission mechanisms were categorized to d-d

transition or MLCT transition depending on co-L. Our group also investigated luminescent photoluminescent properties of $[Re^{V}N(CN)_4(co\text{-}L)]^{2-}$ complexes, and found out that $[Re^{V}N(CN)_4(cpy)]^{2-}$ (cpy = 4-cyanopyridine) showed emission mechanism switching between d-d transition and MLCT by responding to methanol vapor. Then, co-L in the PCPs is expected to provide the interaction site for guest molecules. In this chapter, as first trial of synthesis of luminescent nitridotetracyanorhenate(V)-based PCPs having co-L, we report the preparation, identification and luminescence properties of 2D Hofmann-type luminescent coordination polymers having pyridine derivatives $\{[Zn(co\text{-}L)_2][ReN(CN)_4(co\text{-}L)]\}$ (co-L = pyridine or 3-chloropyridine).

Experiments

Physical Measurements

Single-crystal X-ray diffraction data were collected on a Bulker SMART APEX II ULTRA CCD-detector Diffractometer, a rotating-anode (Bruker Tourbo X-ray source) with graphite-monochromated $Mo_{K\alpha}$ radiation (λ = 0.71073 Å) was used. Computations were carried out on a APEX2 crystallographic software package and OLEX2 software.[7] A single crystal was mounted on a polymer film with liquid paraffin and the temperature kept constant under flowing N_2. All of the structures were solved by a standard direct method (XSHELL V6.3.1 crystallographic software package of the Bruker AXS) and expanded using Fourier techniques. Fullmatrixleast-squares refinements were carried out with anisotropic thermal parameters for all non-hydrogen atoms. All of the hydrogen atoms were placed in the measured positions and refined using a riding model. X-ray powder diffraction (XRPD) was carried out on a Rigaku Ultima IV diffractrometer with graphite-monochromated $Cu_{K\alpha}$ radiation. X-ray fluorescence analysis was carried out on a Rigaku ZSX-100S. Infrared spectra were measured with a JASCO FT/IR-4200 using ATR method. Thermogravimetry analysis (TGA) was carried out on a Perkin Elmer STA6000. Elemental analysis of carbon, hydrogen and nitrogen was carried out by the staff of technical support division graduate school of science, Kyushu University. The emission spectra and emission quantum yields were measured by an absolute emission quantum yield measurement system C9920-02 (Hamamatsu Photonics K. K.) composed of an integrating sphere, a multi-channel photodetector PMA-12 (Hamamatsu Photonics K. K.), and a xenon lamp as an excitation light source (excitation wavelength = 365 nm) at room temperature. PL quantum yield was calculated with the following equation:

$$\phi = \frac{\int I_{em} d\lambda}{\int \left(I_{ex}^{before} - I_{ex}^{after} \right) d\lambda}$$

I_{em} is the amount of photon from emission, $I^{before}{}_{em}$ is amount of photon from excitation light that nothing absorbed, and $I^{after}{}_{em}$ is amount of photon from excitation light that something absorbed. The emission decay curves were acquired at room temperature using a Quantaurus-Tau C11367-24 (Hamamatsu Photonics K. K.) with excitation via a xenon flash lamp with a band-path filter (λ_{ex} = 370 nm). Theoretical value of emission lifetime was calculated with the following equation.

$$\sum_i A_i \exp\left(-\frac{t}{\tau_i}\right)$$

A_i is a coefficient, t is current time, τ_i is emission lifetime. A_i and τ_i are given by fitting of luminescent lifetime measurement.

Preparation

All chemicals were purchased from commercial sources and used without further purification. Synthesis of $K_2[ReN(CN)_4]\cdot H_2O$ is described in Chapter 1.

Single crystals of {[Zn(py)$_2$][ReN(CN)$_4$(py)] } (ZnRepy_sc)

Single crystals of ZnRepy_sc was prepared by diffusion method used H-shaped tubes. A 1 mL aqueous solution of $K_2[ReN(CN)_4]\cdot H_2O$ (8.4 mg, 0.0197 mmol) and pyridine (0.05 mL) was placed at the bottom in one side of an H-shaped tube, and a 1 mL aqueous solution of $Zn(NO_3)_2\cdot 6H_2O$ (5.9 mg, 0.0198 mmol) and pyridine (0.05 mL) was introduced into the other side. Then, approximately 25 mL of water was layered over the solutions on both sides to provide a diffusion pathway. After a few weeks, clear pale yellow single crystals were prepared.

Powder samples of {[Zn(py)$_2$][ReN(CN)$_4$(py)] } (ZnRepy_as-syn)

ZnRe_as-syn was prepared by slow addition using dropping funnel. A 40 mL aqueous solution of $K_2[ReN(CN)_4]\cdot H_2O$ (101.0 mg, 0.237 mmol) and pyridine (0.04 mL) was added to a 40 mL aqueous solution of $Zn(NO_3)_2\cdot 6H_2O$ (75.1 mg, 0.252 mmol) and pyridine (0.04 mL) with slowly stirring. After stirring overnight, yellow solid was separated by centrifugation. Pale yellow powder was obtained by dryness in desiccator without vacuum condition. Yield: 133.2 mg (92.7 %).

Single crystals of {[Zn(Clpy)$_2$][ReN(CN)$_4$(py)] } (ZnReClpy_sc)

Single crystals of ZnReClpy_sc was prepared by diffusion method used H-shaped tubes. A 1 mL aqueous solution of $K_2[ReN(CN)_4]\cdot H_2O$ (8.5 mg, 0.0199 mmol) and 3-chloropyridine (0.1 mL) was placed at the bottom in one side of an H-shaped tube,

and a 1 mL aqueous solution of $Zn(NO_3)_2 \cdot 6H_2O$ (5.9 mg, 0.0198 mmol) and 3-chloropyridine (0.1 mL) was introduced into the other side. Then, approximately 25 mL of water was layered over the solutions on both sides to provide a diffusion pathway. After a few weeks, clear pale yellow single crystals were prepared.

Powder samples of {[Zn(Clpy)$_2$][ReN(CN)$_4$(Clpy)] } (ZnReClpy)

ZnReClpy_as-syn was prepared by slow addition using dropping funnel. A 40 mL aqueous solution of $K_2[ReN(CN)_4] \cdot H_2O$ (100.1 mg, 0.235 mmol) and 3-chloropyridine (0.06 mL) was added to a 40 mL aqueous solution of $Zn(NO_3)_2 \cdot 6H_2O$ (72.4 mg, 0.243 mmol) and 3-chloropyridine (0.24 mL) with slowly stirring. After stirring overnight, yellow solid was separated by centrifugation. Pale yellow powder was obtained by dryness in desiccator without vacuum condition. Yield : 156.8 mg.

Preparation of activation samples of ZnRepy and ZnReClpy (ZnRepy_a and ZnReClpy_a)

The activation samples **ZnRepy_a** and **ZnReClpy_a** were prepared by activation of **ZnRepy** and **ZngReClpy** heated at 120ºC and 90ºC for 5 hours with vacuum, respectively.

Preparation of ground sampls of ZnRepy (ZnRepy_gr)

The activation samples **ZnRepy_a** and **ZngReClpy_a** were prepared by grinding homogeneously in an agate motor for 30 min at room temperature under ambient atmosphere.

Results and discussion

X-Ray Structural Characterization

X-ray crystallographic analysis reveals that **ZnRepy_sc** and **ZnReClpy_sc** are isomorphic, respectively. Crystal parameters for complexes are summarized in **Table 1**. The selected bond lengths and angles for complexes are described in **Table 2-5**. **ZnRepy_sc** and **ZnReClpy_sc** crystallize in monoclinic system with space group $P2_1/c$. The asymmetric unit consists of one $[ReN(CN)_4]^{2-}$ unit, one Zn^{2+} ion and three pyridine derivatives (co-L). (**Figures 1** and **3**). The geometry of $[ReN(CN)_4(co\text{-}L)]^{2-}$ unit is distorted octahedral, where the average bending angles of the diagonal C-Re-C in **ZnRepy_sc** and **ZnReClpy_sc** are 160.8 and 160.4 degree, respectivery. Each co-L to the open-metal site at trans position of nitride ligand of $[ReN(CN)_4]^{2-}$ units. The geometry of Zn^{2+} ion is octahedral with each a cyanide nitrogen atom of four $[ReN(CN)_4]^{2-}$ units at the equatorial sites and two pyridine derivatives at axial sites. **ZnRepy_sc** and **ZnReClpy_sc** formed 2D-layer structure extended by Re-CN-Zn linkages in the ratio of one $[ReN(CN)_4(co\text{-}L)]^{2-}$ unit to one $[Zn(co\text{-}L)_2]^{2+}$ unit. Their 2D frameworks have intra- and inter-layer π-π interactions. The co-L of $[ReN(CN)_4(co\text{-}L)]^{2-}$ unit interacts with the one of the co-L of neighboring $[Zn(co\text{-}L)_2]^{2+}$ unit in intra-layer, and the other co-L of $[Zn(co\text{-}L)_2]^{2+}$ unit interacts with another co-L of $[Zn(co\text{-}L)_2]^{2+}$ unit in the neighboring layer (**Figures 2** and **4**).

Table 1 Crystallographic parameters of **ZnRepy_sc** and **ZnReClpy_sc**

Name	**ZnRe_sc**	**ZnReClpy_sc**
Formula	$C_{19}H_{15}N_8ZnRe$	$C_{19}ClH_{14}Cu_2N_{17}ZnRe$
Crystal System	monoclinic	monoclinic
Space Group	$P2_1/c$	$P2_1/c$
a / Å	7.4854(16)	7.439(2)
b / Å	19.581(4)	14.225(4)
c / Å	14.075(3)	21.919(6)
α / deg.	90	90
β / deg.	90.415(2)	96.014(4)
γ / deg.	90	90
Temperature / K	100	100(2)
V / $Å^3$	2062.9(8)	2306.7(11)
Z value	4	4
GOF	1.033	2.870
R1	0.0171	0.1309
wR	0.0398	0.3605

Table 2 Bond length (Å) of **ZnRepy_sc**

Re1-N1	1.669(2)	Zn1-N4$^{\#}$	2.134(3)
Re1-C1	2.102(3)	Zn1-N5$^{\#}$	2.163(3)
Re1-C2	2.115(3)	Zn1-N7	2.163(2)
Re1-C3	2.093(3)	Zn1-N8	2.144(2)
Re1-C4	2.097(3)	C1-N2	1.154(4)
Re1-N6	2.484(2)	C2-N3	1.147(4)
Zn1-N2	2.148(3)	C3-N4	1.149(4)
Zn1-N3	2.159(2)	C4-N5	1.154(4)

Symmetry operation: (#)X, 1/2-Y, 1/2+Z

Table 3 Bond angles (º) of **ZnRepy_sc**

N1-Re1-C1	100.2(1)	N5$^{\#}$-Zn1-N2	89.3(1)
N1-Re1-C2	99.6(1)	N2-Zn1-N7	88.6(1)
N1-Re1-C3	100.1(1)	N3-Zn1-N7	88.9(1)
N1-Re1-C4	98.6(1)	N4$^{\#}$-Zn1-N7	89.3(1)
C1-Re1-C2	87.5(1)	N5$^{\#}$-Zn1-N7	86.1(1)
C2-Re1-C3	89.5(1)	N2-Zn1-N8	92.1(1)
C3-Re1-C4	87.0(1)	N3-Zn1-N8	94.59(9)
C4-Re1-C1	89.7(1)	N4$^{\#}$-Zn1-N8	89.9(1)
C1-Re1-C3	159.7(1)	N5$^{\#}$-Zn1-N8	90.4(1)
C2-Re1-C4	161.8(1)	Re1-C1-N2	177.9(2)
C1-Re1-N6	80.2(1)	Re1-C2-N3	177.4(2)
C2-Re1-N6	79.9(1)	Re1-C3-N4	174.4(3)
C3-Re1-N6	79.5(1)	Re1-C4-N5	176.9(3)
C4-Re1-N6	81.9(1)	Zn1-N2-C1	166.1(2)
N2-Zn1-N3	88.99(9)	Zn1-N3-C2	171.4(2)
N3-Zn1-N4$^{\#}$	90.46(9)	Zn1-N4$^{\#}$-C3$^{\#}$	163.2(2)
N4$^{\#}$-Zn1-N5$^{\#}$	91.0(1)	Zn1-N5$^{\#}$-C4$^{\#}$	160.9(2)

Symmetry operation: (#)x, 1/2-y, 1/2+z

Table 4 Bond length (Å) of **ZnReClpy_sc**

Re1-N1	1.66(2)	Zn1-N4	2.18(2)
Re1-C1	2.10(2)	Zn1-N5	2.11(2)
Re1-C2	2.11(2)	Zn1-N7	2.23(2)
Re1-C3	2.09(2)	Zn1-N8	2.16(2)
Re1-C4$^{\#}$	2.09(2)	C1-N2	1.14(3)
Re1-N6	2.48(2)	C2-N3	1.13(3)
Zn1-N2$^{\#}$	2.13(2)	C3-N4	1.13(3)
Zn1-N3	2.17(2)	C4$^{\#}$-N5$^{\#}$	1.18(3)

Symmetry operation: (#)1-x, 1/2+y, 1/2-z

Table 5 Bond angles (º) of **ZnReClpy_sc**

N1-Re1-C1	99.8(8)	N3-Zn1-N4'	87.4(7)
N1-Re1-C2	99.7(8)	N4'-Zn1-N2$^{\#}$	91.1(7)
N1-Re1-C3	100.0(8)	N2$^{\#}$-Zn1-N5'	89.5(6)
N1-Re1-C4	99.8(8)	N5'-Zn1-N3	91.3(7)
C1-Re1-C2	89.3(8)	N2$^{\#}$-Zn1-N7	87.7(6)
C2-Re1-C3	87.0(8)	N3-Zn1-N7	85.3(7)
C3-Re1-C4$^{\#}$	90.1(8)	N4'-Zn1-N7	85.6(7)
C4$^{\#}$-Re1-C1	86.9(8)	N5'-Zn1-N7	88.5(6)
C1-Re1-C3	160.2(8)	N2$^{\#}$-Zn1-N8	89.1(7)
C2-Re1-C4$^{\#}$	160.5(8)	N3-Zn1-N8	97.9(8)
C1-Re1-N6	79.0(7)	N4'-Zn1-N8	95.4(7)
C2-Re1-N6	81.1(7)	N5'-Zn1-N8	90.6(7)
C3-Re1-N6	81.1(7)	N2$^{\#}$-Zn1-N3	172.9(7)
C4-Re1-N6	79.4(7)	N4'-Zn1-N5'	174.0(7)
Re1-C1-N2	175(2)	Zn1$^{\#}$-N2-C1	171(2)
Re1-C2-N3	179(2)	Zn1-N3-C2	162(2)
Re1-C3-N4	180(2)	Zn1'-N4-C3	164(2)
Re1-C4$^{\#}$-N5$^{\#}$	177(2)	Zn1$^{\#}$'-N5$^{\#}$-C4$^{\#}$	167(2)

Symmetry operation: (#)1-x, 1/2+y, 1/2-z

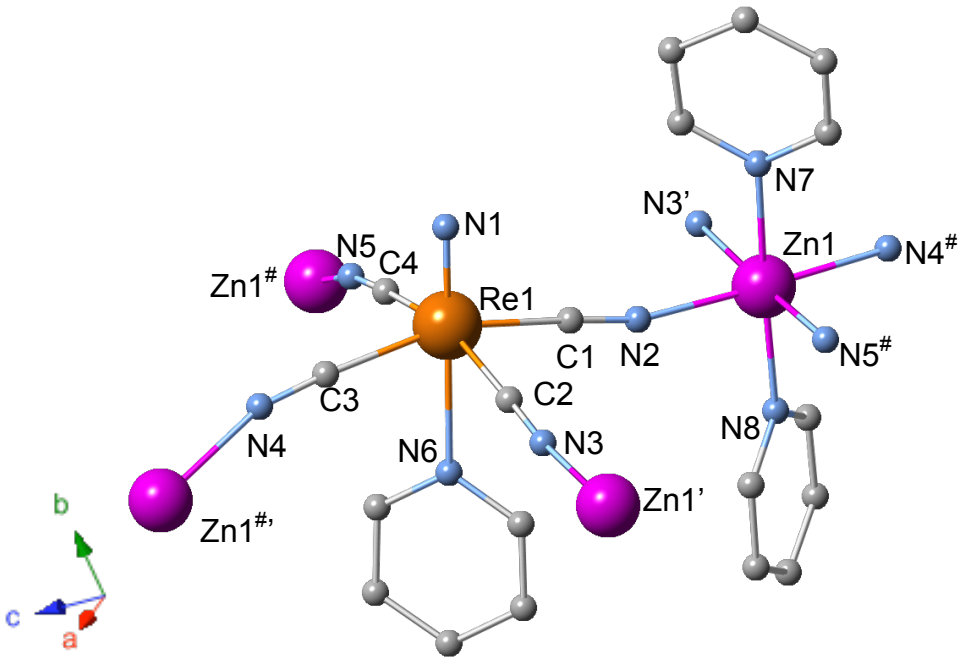

Figure 1. The drawing of the asymmetric unit for **ZnRepy_sc** with the atom numbering scheme. H atoms are omitted.

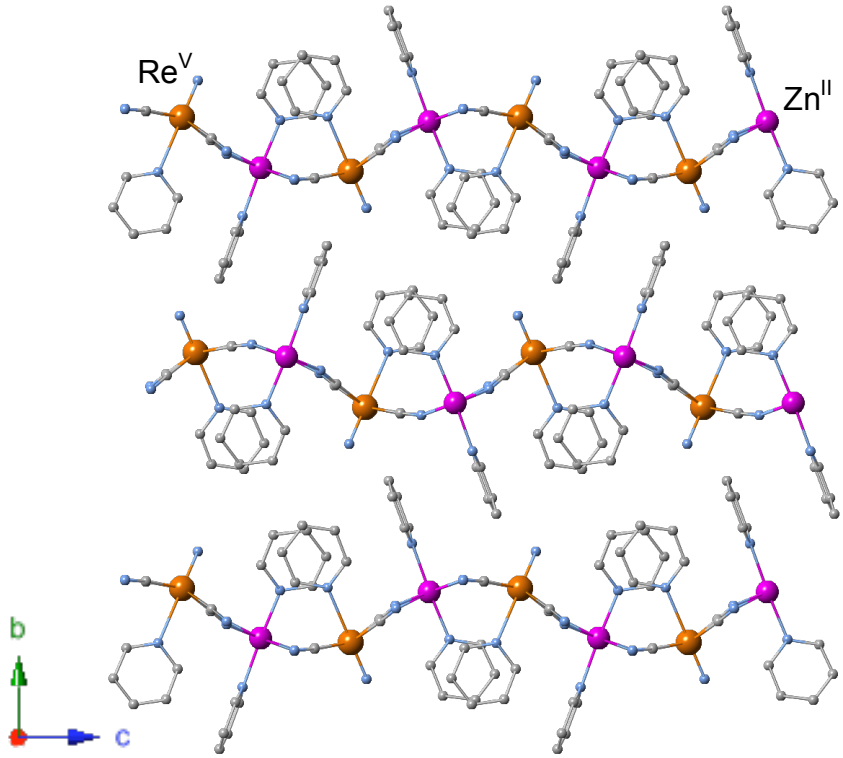

Figure 2. The projection of polymeric structure for **ZnRepy_sc** onto *ac* plane. H atoms are omitted.

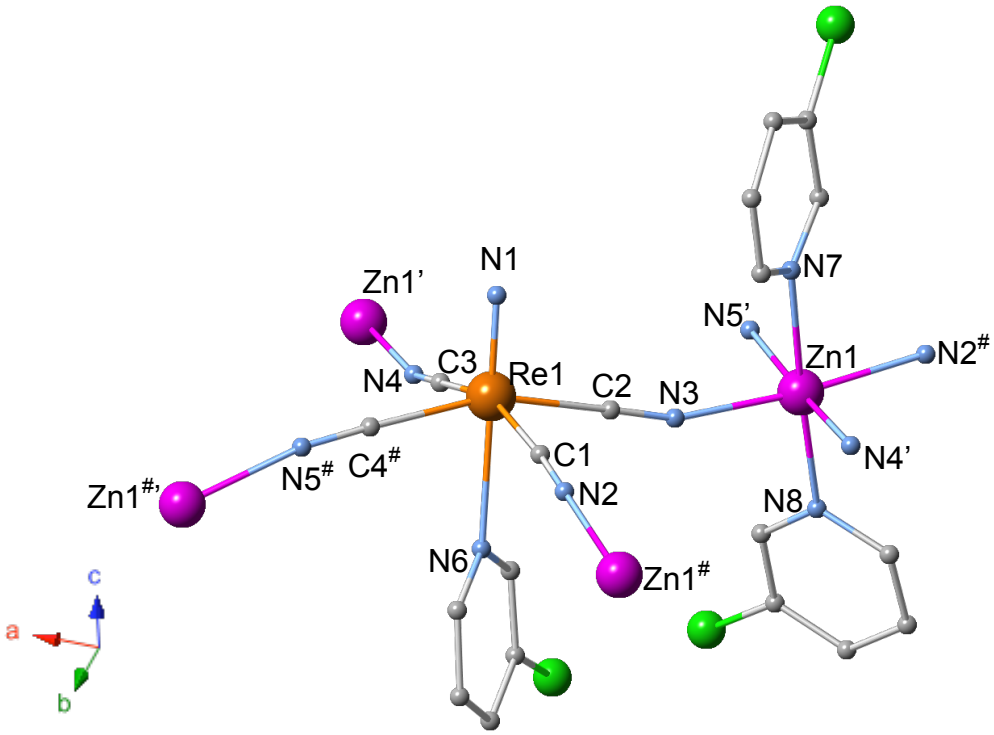

Figure 3. The drawing of the asymmetric unit for **ZnReClpy_sc** with the atom numbering scheme. H atoms are omitted.

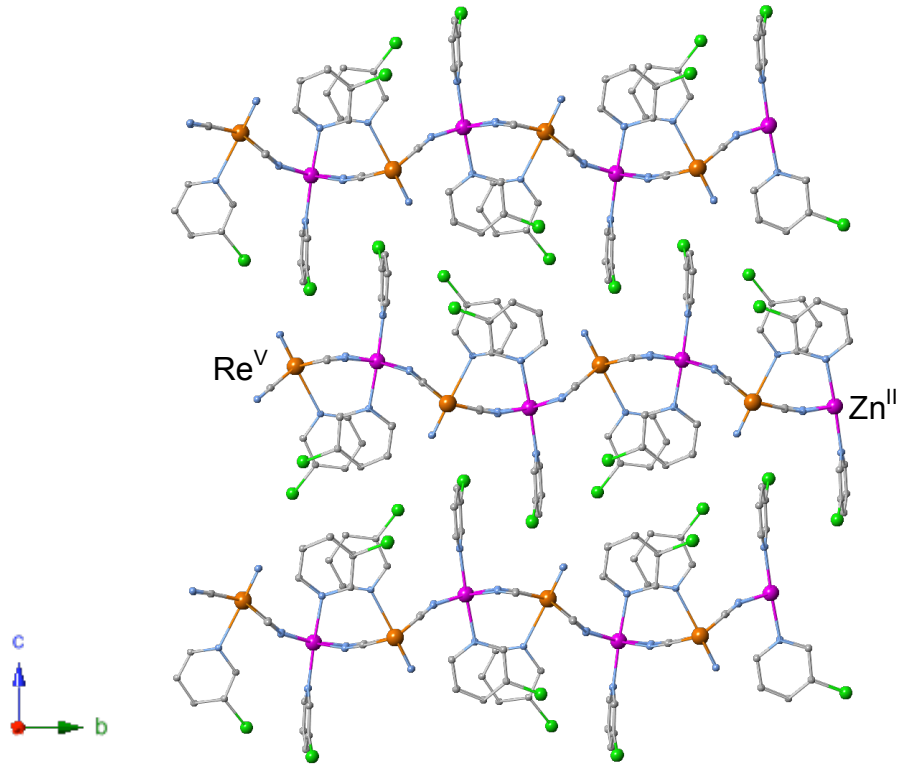

Figure 4. The projection of polymeric structure for **ZnReClpy_sc** onto *ac* plane. H atoms are omitted.

Powder X-Ray Diffraction Patterns

The PXRD patterns of **ZnRepy** and **ZnReClpy** were measured at room temperature under ambient atmosphere and the results show in **Figure 5**. The measured PXRD patterns of bulk samples of **ZnRepy** obviously corresponded with simulated pattern of **ZnRepy_sc** and, the structure of **ZnReClpy** is broadened and has the strong peak in which the simulated pattern does not exhibit. Three peaks in the range of low angles area are assigned (010) at 6.54 degree, (002) at 7.96 degree, and (020) at 12.42 degree. The (002) plane was the direction of layering the frameworks (**Figure 6**). On the other hand, the (010) and (020) planes was the direction of extending the cyano-linkages. Therefore, **ZnReClpy** formed seemingly 2D-layer structure with low crystallinity and high anisotropic structure.

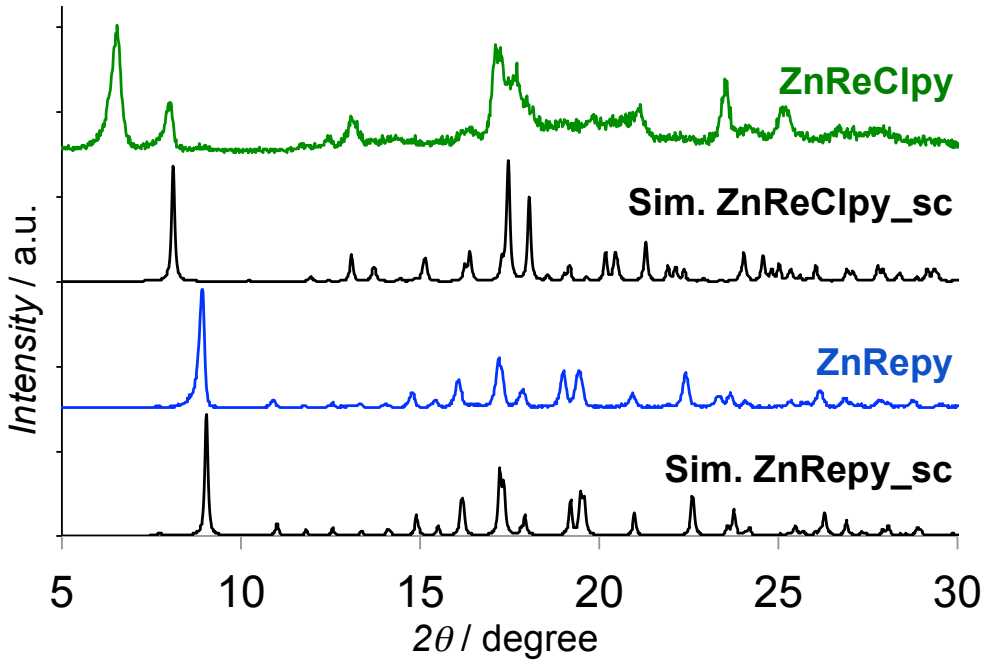

Figure 5. PXRD measured patterns of **ZnRepy** and **ZnReClpy**, and simulated patterns of **ZnRepy_sc** and **ZnReClpy_sc**.

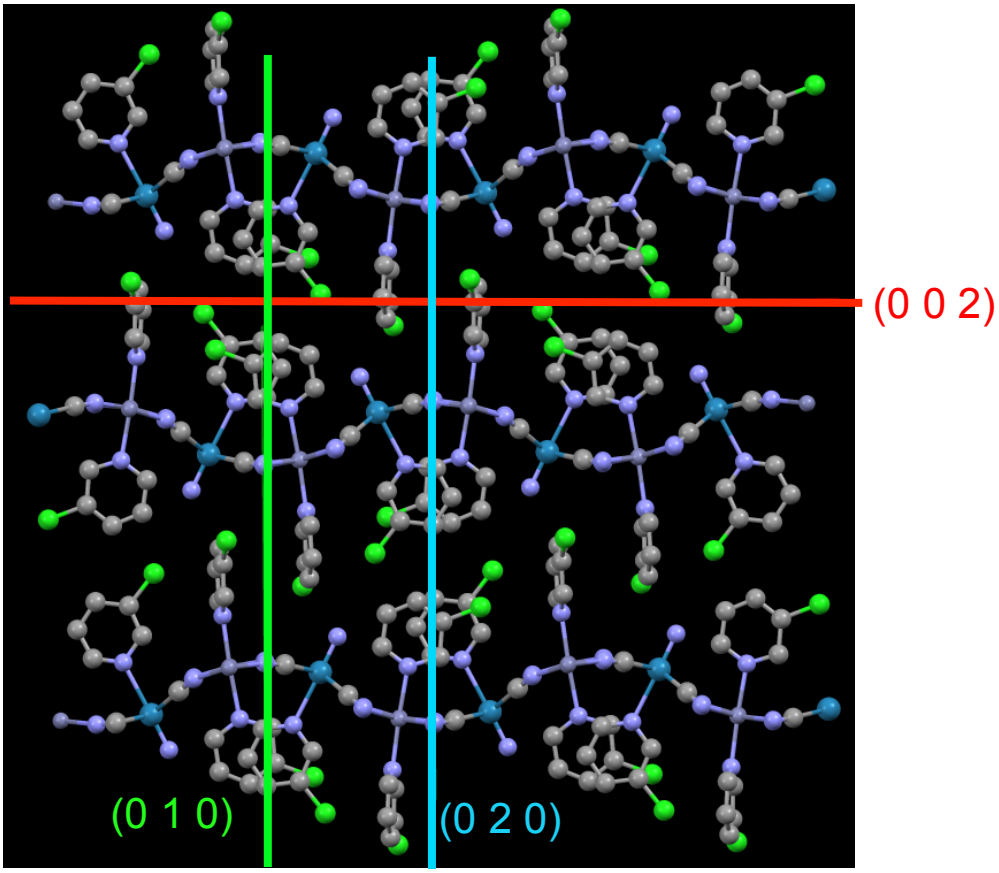

Figure 6. The projection of polymeric structure for **ZnRepy_sc** onto *bc* plane, and the lattice planes of (010), (020) and (002).

IR spectra

FT-IR spectra of $K_2[ReN(CN)_4]\cdot H_2O$, **ZnRepy** and **ZngReClpy** were shown in **Figure 7**. The strong absorption bands based on stretching vibration of cyano groups ($\nu_{C\equiv N}$) were observed at 2139 cm^{-1} in **ZnRepy** and 2140 cm^{-1} in **ZngReClpy**. The formation of Re-C≡N-M bridges were confirmed by the upshift of the frequency of the $\nu_{C\equiv N}$ band from that of mono-nuclear complexes ($K_2[ReN(CN)_4]\cdot H_2O$; 2107 cm^{-1} and $[PPh_4]_2[ReN(CN)_4(MeOH)]\cdot 3MeOH$; 2105 cm^{-1}).[8] In addition, the peaks derived from PPh_4^+ ion were disappeared.

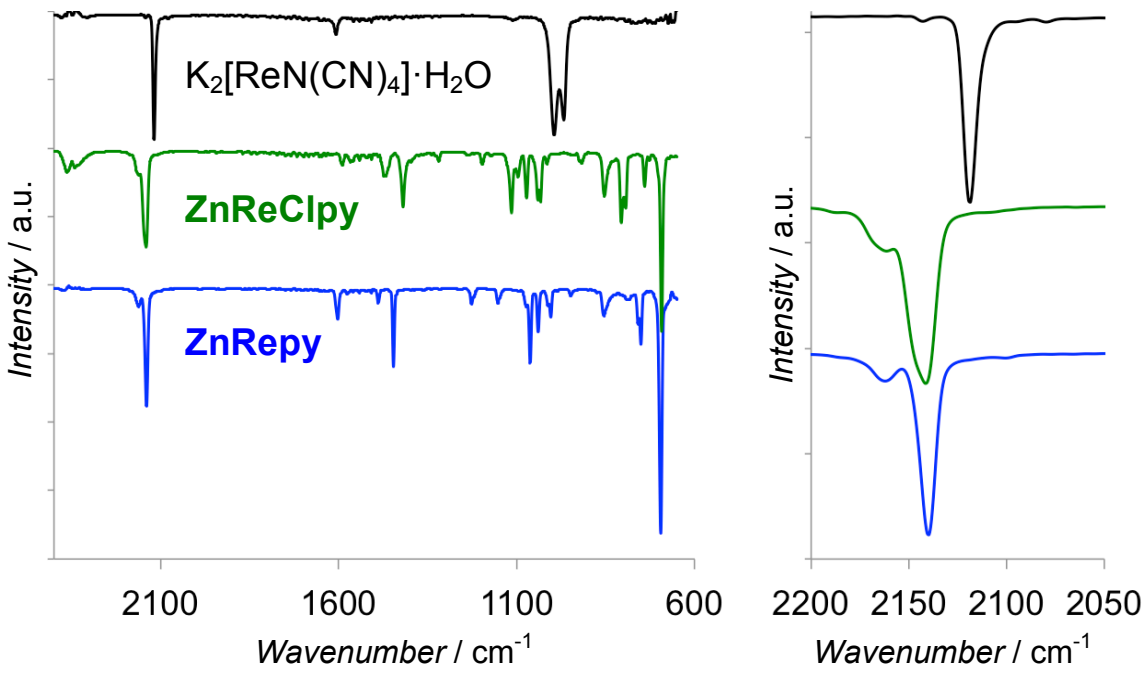

Figure 7. IR spectra of **ZnRepy** (blue), **ZnReClpy** (green) and $[PPh_4]_2[ReN(CN)_4(MeOH)]\cdot 3MeOH$ (black).

Emission Spectroscopic and Photophysical Properties

Photoluminescence spectra of **ZnRepy** and **ZngReClpy** show in **Figure 8** and the emission maximum wavelength (λ_{em}) and the quantum yields summarize in **Table 6**. The emission maximum wavelength (λ_{em}) was observed at 517 nm and 513 nm in **ZnRepy** and **ZngReClpy**, respectively. Their broaden emission spectra and emission color were typical luminescent features based on $[ReN(CN)_4]^{2-}$ unit. However, the quantum yields of **ZnRepy** and **ZngReClpy** were low efficiency with 13.17% and 6.50% although the quantum yield of luminescent components typically increased by rigidifying with attributed to construction of coordination frameworks.[9] The reason of the low quantum yield is unclear at this stage. We could explain the reason if the photoluminescence of **ZnRepy** and **ZngReClpy** originating from ^{3}MLCT excited state involved in co-L. In the case of photoluminescence derived from ^{3}MLCT excited state of $[ReN(CN)_4]^{2-}$ series, the quantum yields are comparatively low by molecular vibration of co-L contributing to noradiative decay, and the emission maximum wavelengths are lower than the emission from d-d excited state. The emission of **ZnRepy** was quite unlikely to originate from ^{3}MLCT excited state because the mononuclear complex $[PPh_4]_2[ReN(CN)_4(py)]\cdot py\cdot H_2O$ showed higher emission maximum wavelength at 539 nm derived from $^3[(d_{xy})^1(d_{\pi*})^1]$ excited state.[6] In addition, the unique adsorption band based on MLCT did not observed in the UV-vis reflectance spectra (**Figure 9**)

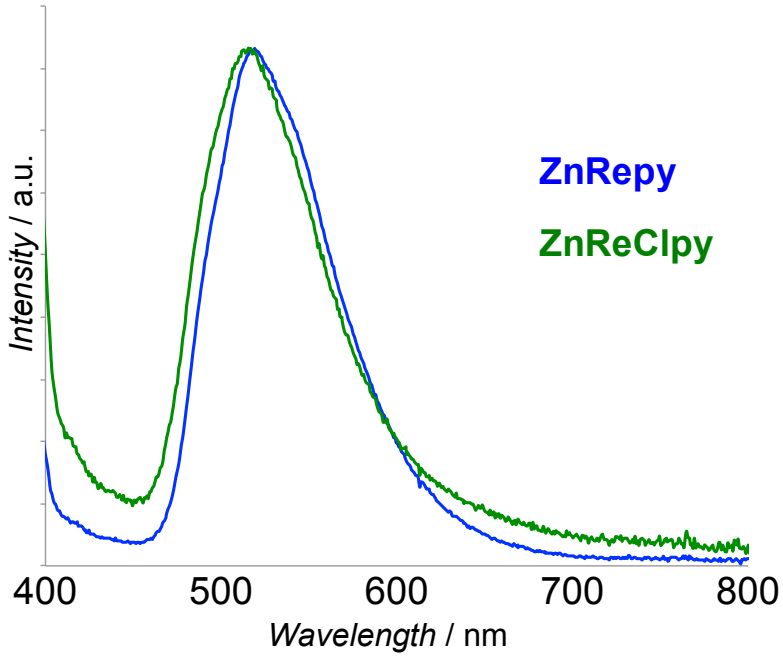

Figure 8. Emission spectra of **ZnRepy** and **ZnReClpy** in solid state at room temperature upon excitation at 365 nm.

Table 6. Emission maximum wavelength, PL quantum yields and life times of **ZnRepy** and **ZnReClpy**.

Compound	λ_{em} [nm]	ϕ [%]
ZnRepy	517	13.17
ZnReClpy	513	6.50

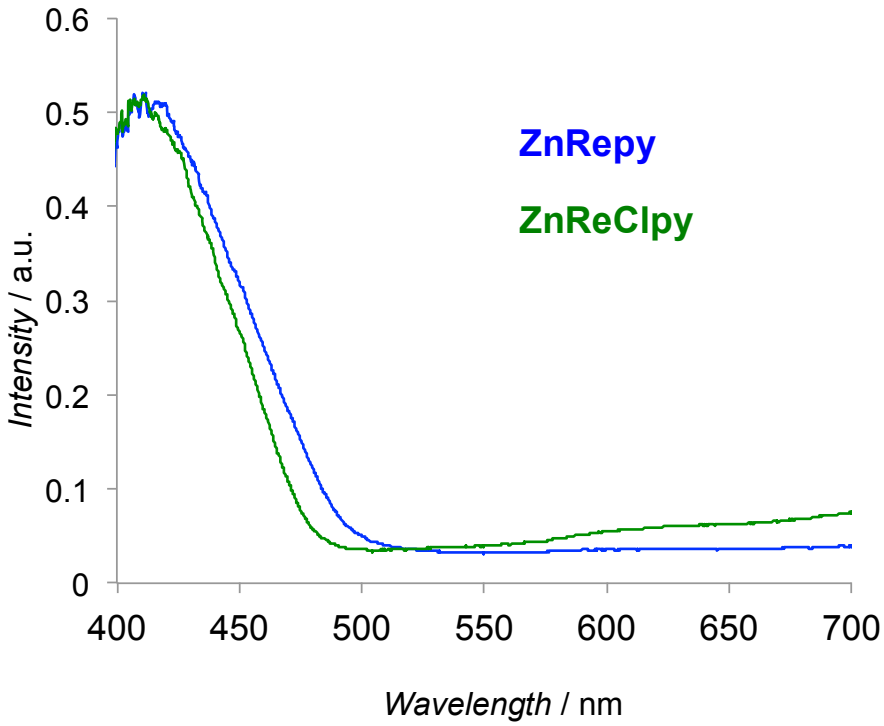

Figure 9. UV-Vis reflectance spectra of **ZnRepy** and **ZnReClpy** in solid state at room temperature.

Physical properties of activated sample

The thermogravimetric analysis of **ZnRepy_a** and **ZngReClpy_a** were performed, and PXRD pattern and emission spectra were measured at room temperature under ambient atmosphere. The TGA of as-synthesized samples **ZnRepy** and **ZngReClpy** showed gradual weight loss of around 12.8 wt% and 15.4 % until 150ºC and 128ºC (**Figures 10-11**). The weight loss corresponds closely to one co-L (calculated. 13.03% and 15.98%). The weight loss of **ZnRepy_a** and **ZngReClpy_a** started from around 150ºC and 128ºC in TGA. These results suggested **ZnRepy_a** and **ZnReClpy_a** lost one co-L from their as-synthesized samples. From PXRD pattern, **ZnRepy_a** and **ZnReClpy_a** became low crystallinity and decreased between each layer structures, which was explained that the peaks of planes in the direction of layering the frameworks shifted to higher angles from 8.9º in **ZnRepy** to 10.1º **ZnRepy_a** and from 8.0º in **ZnReClpy** to 9.2º in **ZnReClpy_a** (**Figure 12**). Photoluminescence spectra of **ZnRepy_a** and **ZngReClpy_a** show in **Figure 13** and the emission maximum wavelength and the quantum yields summarize in **Table 7**. The both emission maximum wavelengths were little changed and the quantum yields of **ZnRepy** and **ZngReClpy** decreased from 13.17% to 3.22% and from 6.50% to 3.40% after activation process, respectively. These decreases were probably induced by degradation of crystallinity because of the increase of terminal cyano-ligands, which occurred the vibrational deactivation.

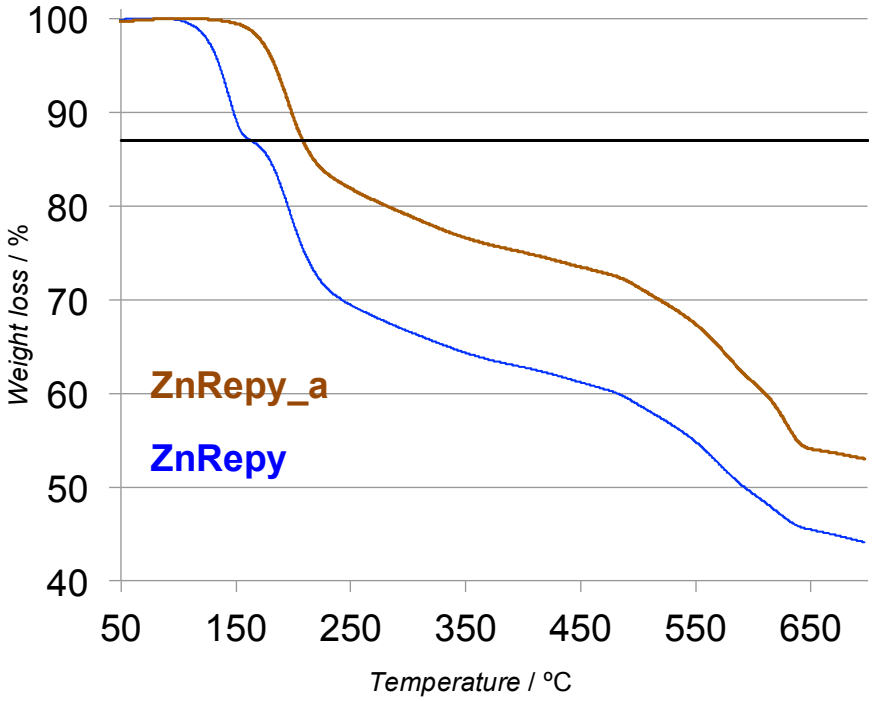

Figure 10. TGA curves of **ZnRepy** (blue) and **ZnRepy_a** (brown).

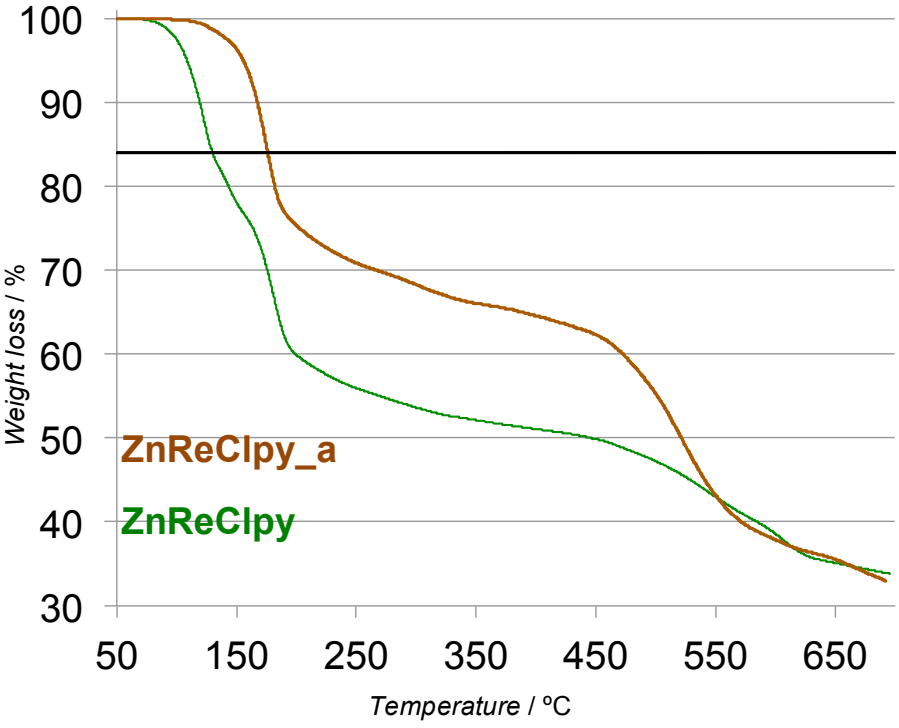

Figure 11. TGA curves of **ZnReClpy** (green) and **ZnReClpy_a** (brown).

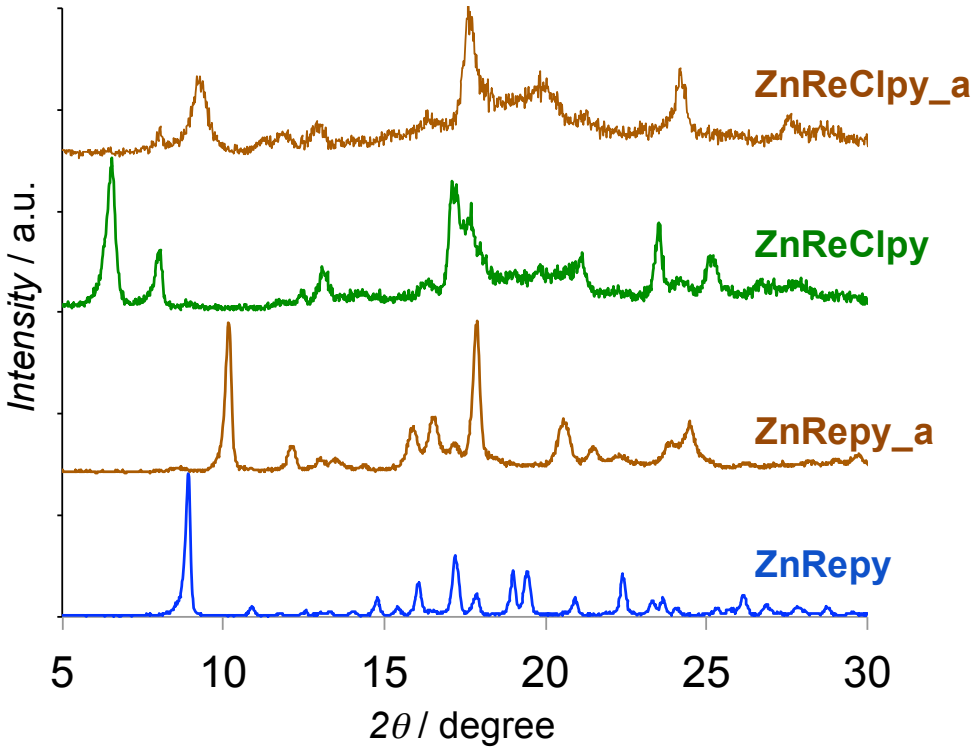

Figure 12. PXRD measured patterns of **ZnRepy**, **ZnRepy_a, ZnReClpy** and **ZnReClpy_a**.

Table 7. Emission maximum wavelength, PL quantum yields and life times of **ZnRepy**, **ZnRepy_a**, **ZnReClpy** and **ZnReClpy_a**.

Compound	λ_{em} [nm]	ϕ [%]
ZnRepy	517	13.17
ZnRepy_a	520	3.22
ZnReClpy	513	6.50
ZnReClpy_a	514	3.40

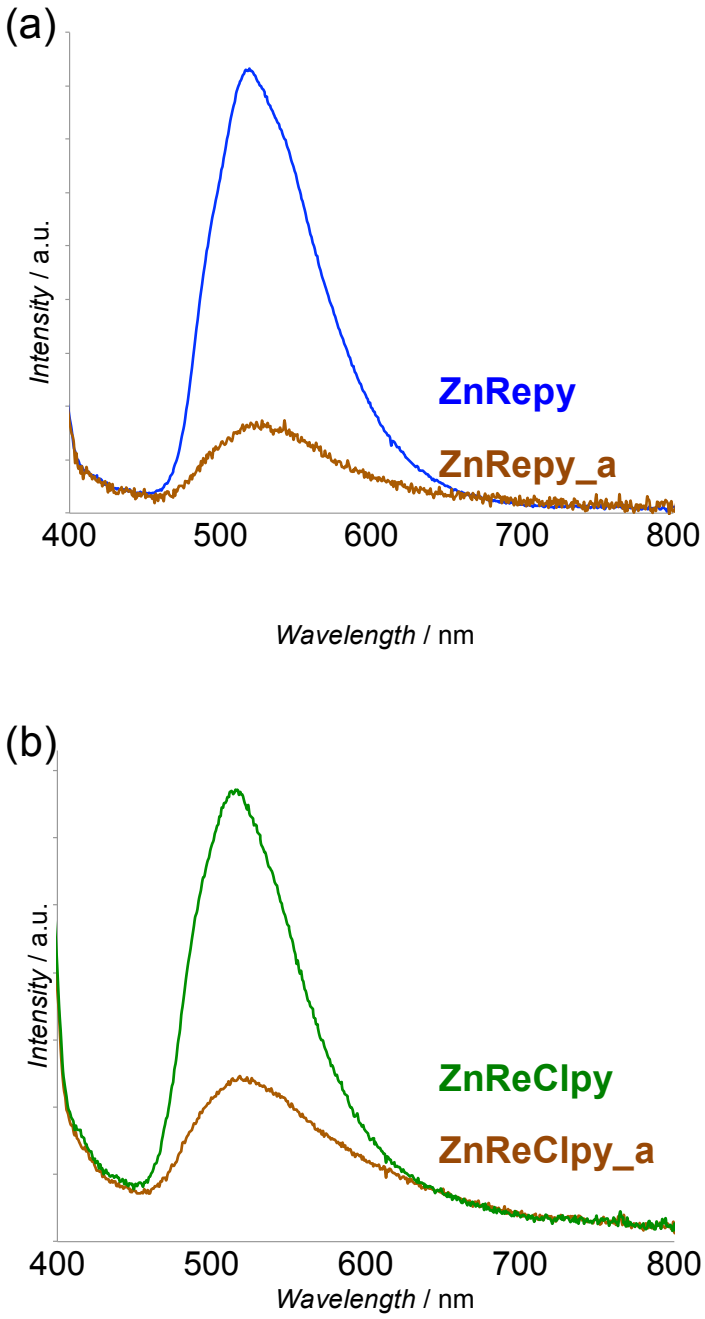

Figure 13. Emission spectra of **ZnRepy** and **ZnRepy_a** in (a), and **ZnReClpy** and **ZnReClpy_a** in (b) in solid state at room temperature upon excitation at 365 nm.

Guest vapor exposure to ZnRepy_a

We tried to expose directly **ZnRepy_a** to several guest vapors such as acetonitrile, ethanol, methanol, and water. Each guest vapor exposure samples (**ZnRe_a_Guest**) were prepared by guest solvent vapor diffusion to activation sample **ZnRepy_a**. Then, PXRD pattern and emission spectra of **ZnRe_a_Guest** were measured at room temperature under ambient atmosphere (**Figure 14** and **Table 8**). However, the PXRD patterns did not show any changes, and their emission maximum wavelength also little changed unfortunately. The reason of no guest responsitivity was expected that the framework of **ZnRepy_a** had insufficient space for access guest molecules

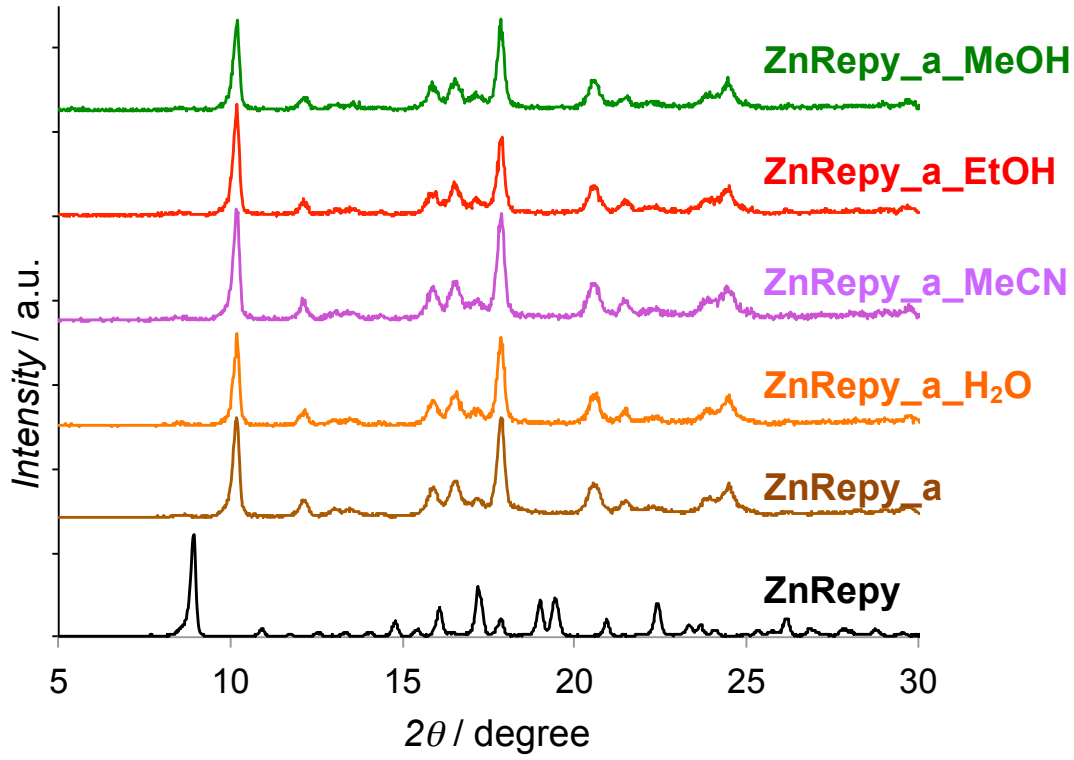

Figure 14. PXRD measured patterns of **ZnRepy**, **ZnRepy_a** and **ZnRepy_a_Guest**.

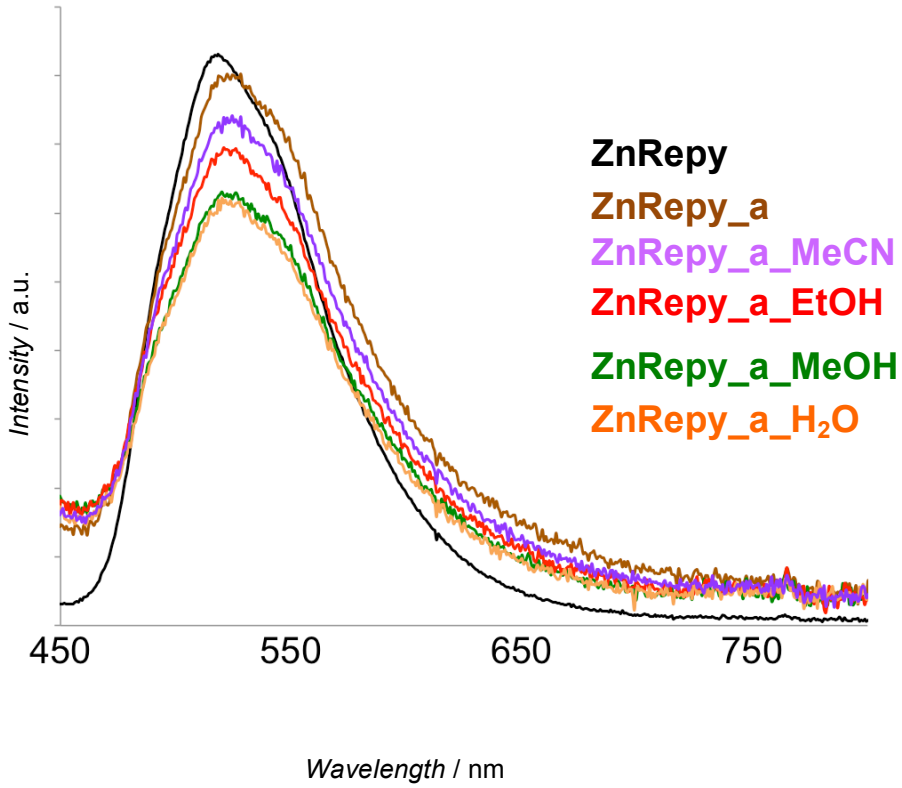

Figure 15. Emission spectra of **ZnRepy**, **ZnRepy_a** and **ZnRepy_a_Guest** in solid state at room temperature upon excitation at 365 nm.

Table 8. Emission maximum wavelength, PL quantum yields and life times of **ZnRepy**, **ZnRepy_a**, and **ZnRepy_a_Guest**.

Guest	λ_{em} [nm]	ϕ [%]	Guest	λ_{em} [nm]	ϕ [%]
ZnRepy	517	13.17	MeOH	519	4.33
ZnRepy_a	520	3.22	EtOH	518	4.55
H_2O	518	3.35	MeCN	518	4.26

Guest responsivity of ground sample ZnRepy_gr

The emission color of **ZnRepy** under UV light irradiation at 365 nm changed from lime-green to orange by grinding homogeneously (**Figure 16**). To investigate the guest responsivity of the ground sample **ZnRepy_gr** was exposed to guest solvent vapor such as acetone, methanol, ethanol, water and pyridine. **Figures 17-18** shows the IR spectra and PXRD pattern of **ZnRepy**, **ZnRepy_gr** and **ZnRepy_gr_Guest** measured at room temperature. **Figure 19** shows the emission spectra in the solid state at room temperature. **Table 9** summarizes the photoluminescent maximum peak wavelength and emission quantum yield. No peak shift was observed in the IR spectra and PXRD pattern but the crystallinity degradation was confirmed in **ZnRepy_gr** and **ZnRepy_gr_Guest** because the peaks of PXRD pattern were broadened. Then, **ZnRepy_gr** and all of **ZnRepy_gr_Guest** showed photoluminescence and guest responsivity although the quantum yields were low efficiency at 4-2%. **ZnRepy_gr** exhibited orange emission at 628 nm, and **ZnRepy_gr_MeOH** showed lime-green again and the emission peak at 530 nm. **ZnRepy_gr_Guest** except **ZnRepy_gr_MeOH** showed a peak and a shoulder peak in the emission spectra (**Figure 19**). The shorter wavelength peak or shoulder peak around 520-550 nm was similar to **ZnRepy**, while the longer wavelength peak or shoulder peak around 620 nm was similar to **ZnRepy_gr**. It means that emision propety recover To elucidate about guest responsivity, the peak counts at 8.9º in PXRD pattern of **ZnRepy_gr** and **ZnRepy_gr_Guest** was plotted against the emission intensity ratio I_{520}/I_{630}, whrere I_{520} and I_{630} are the emission intensity at 520 nm and 620 nm, respectively (**Figure 20**). The peak at 8.9º in PXRD pattern corresponds to (020) plane of **ZnRepy** in the direction of layering the frameworks. According to the plots of peak counts *vs.* I_{520}/I_{630}, suggested that I_{520}/I_{630} tended to increase with higher peak counts. Therefore, although it is necessary to consider in more detail about a coordination environment around Re^{5+} ion and molecular composition after grind and guest exposure process, it is indicated that recovery of crystallinity by guest vapor exposure induced recovery of emission color from orange color emission of **ZnRepy_gr** to initial lime green color emission.

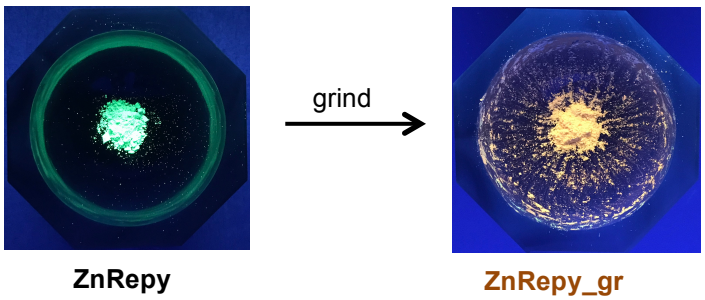

Figure 16. Photoluminescence images of **ZnRepy** before and after grind.

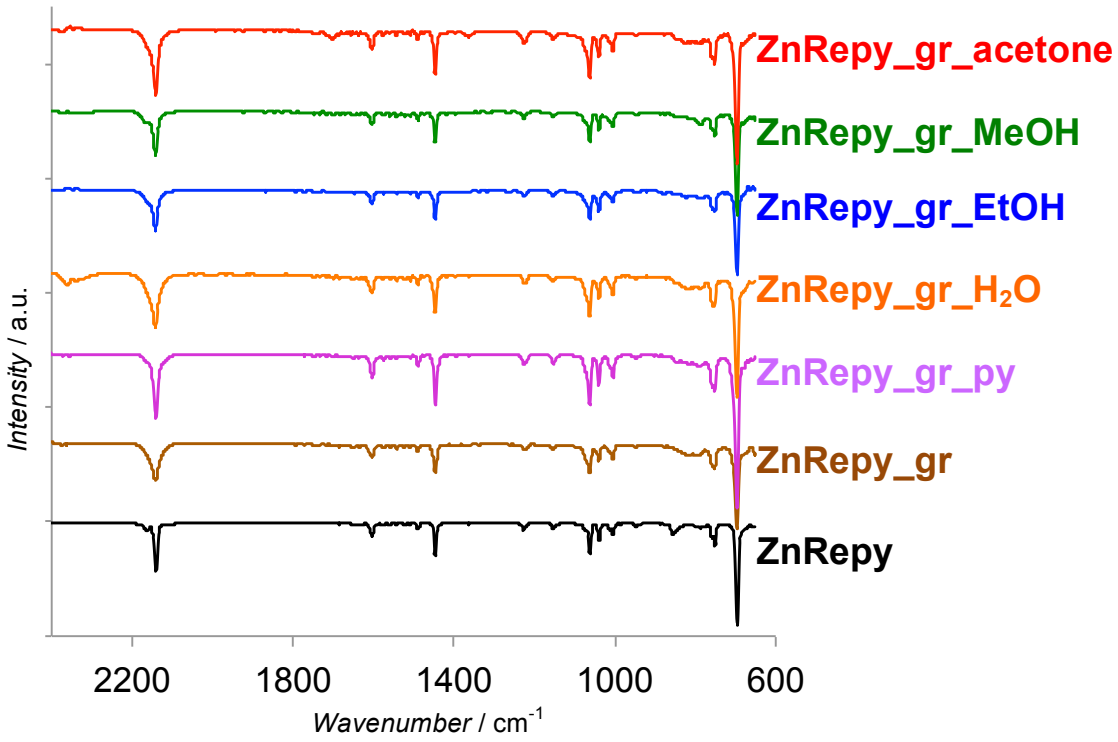

Figure 17. IR spectra of **ZnRepy**, **ZnRepy_gr** and **ZnRepy_gr_Guest**.

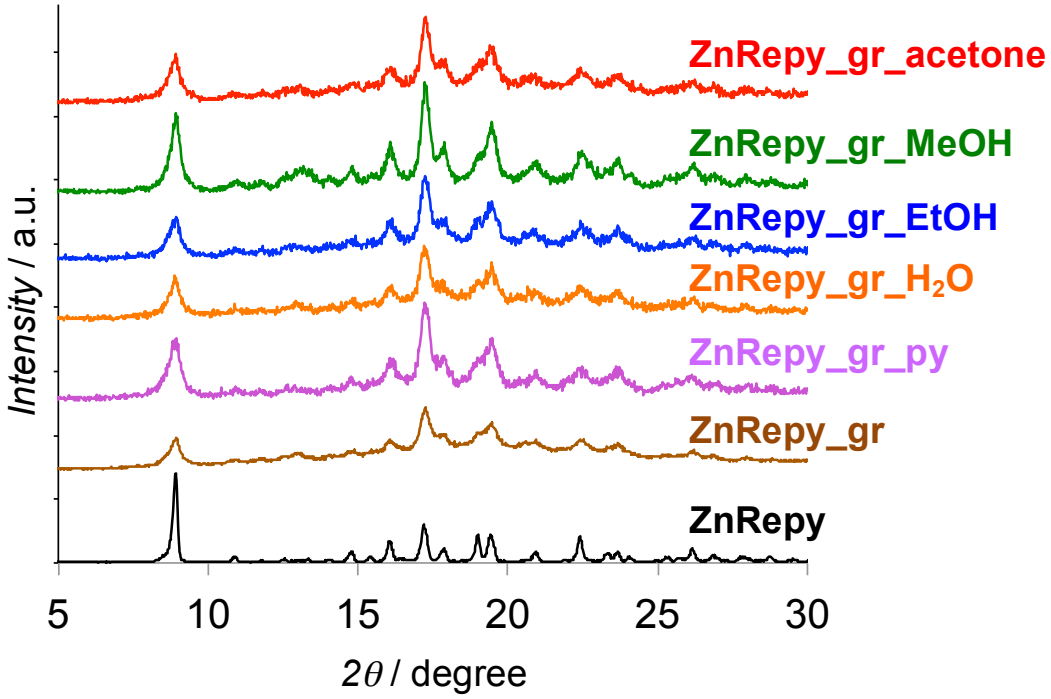

Figure 18. PXRD measured patterns of **ZnRepy**, **ZnRepy_gr** and **ZnRepy_gr_Guest**.

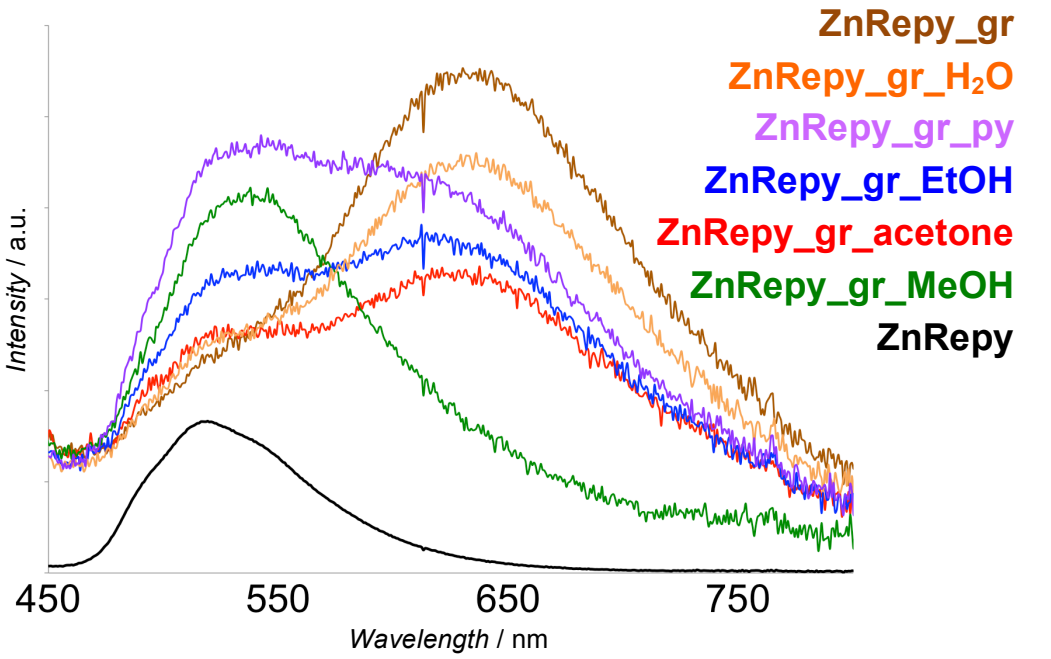

Figure 19. Emission spectra of **ZnRepy**, **ZnRepy_gr** and **ZnRepy_gr_Guest** in solid state at room temperature upon excitation at 365 nm.

Table 9. Emission maximum wavelength, PL quantum yields and life times of **ZnRepy**, **ZnRepy_gr**, and **ZnRepy_gr_Guest**.

Guest	λ_{em} [nm]	ϕ [%]	Guest	λ_{em} [nm]	ϕ [%]
ZnRepy_gr	628	5.6	Acetone	620	3.4
H_2O	628	3.82	Pyridine	537	4.2
EtOH	616	3.51	MeOH	530	2.4

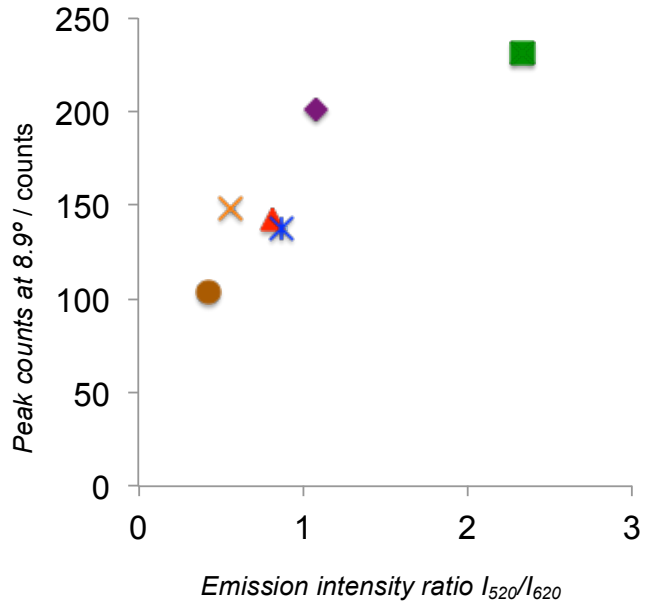

Figure 20. The plot of peak counts at 8.9º in PXRD pattern of **ZnRepy_gr** and **ZnRepy_gr_Guest** against the emission intensity ratio I_{520}/I_{630}.

Conclusion

We prepared two-dimensional nitridotetracyanorhenate(V)-based Hofmann-type PCPs {[Zn(co-L)$_2$][ReN(CN)$_4$(co-L)]} (**ZnReco-L**; co-L = pyridine (py) and 3-chloropyridine (Clpy)) by incorporation of pyridine derivatives as complementary ligands. Their basic framework consisted of cyanide-bridged layers. In addition, co-L coordinated to unoccupied coordination sites at axial position of the $[ReN(CN)_4]^{2-}$ unit and Zn^{II} ion, and formed intra- and inter-layer π-π interactions. **ZnRepy** and **ZnReClpy** showed lime green emission originating from d-d transition but exhibit no guest responsivity because of strong π-π interactions. By grinding procedure, **ZnRepy** showed an emission red-shift and a decrease of crystallinity. The emission color and Xray-diffracyion peaks related to the pyridine arrangement were recovered partially by exposing the ground sample to volatile organic compounds. This result suggested that the order-disorder arrangement of pyridine in the frameworks affected the emission property but no selectivity and sensitivity. The strong and rich π-π interaction provides rigid frameworks and insufficient void space. Therefore, a construction of flexible framework and sufficient void space by using bulky ligands is needed to achieve guest-responsive emission change in luminescent coordination polymers.

References

1. (a) K. A. Hofmann, F. Küspert, *Zeitschrift für Anorg. Chem.* **1897**, *15*, 204–207; (b) K. A. Hofmann, F. Höchtlen, *Berichte der Dtsch. Chem. Gesellschaft* **1903**, *36*, 1149–1151; (c) K. A. Hofmann, H. Arnoldi, *Berichte der Dtsch. Chem. Gesellschaft* **1906**, *39*, 339–344; (d) H. M. Powell, *J. Chem. Soc.* **1948**, 61–73; (e) J. H. Rayner, H. M. Powell, *J. Chem. Soc.* **1952**, 319–328.
2. Z. P. Ni, J. L. Liu, M. N. Hoque, W. Liu, J. Y. Li, Y. C. Chen, M. L. Tong, *Coord. Chem. Rev.* **2017**, *335*, 28–43.
3. (a) M. Kondo, M. Kubo, *J. Phys. Chem.* **1957**, *61*, 1648–1651; (b) D. Ülkü, *Zeitschrift für Krist.* **1975**, *142*, 271–280; (c) R. L. Morehouse, K. Aytaç, D. Ülkü, *Zeitschrift für Krist.* **1977**, *145*, 157–160; (d) T. Kitazawa, Y. Gomi, M. Takahashi, M. Takeda, M. Enomoto, A. Miyazaki, T. Enoki, *J. Mater. Chem.* **1996**, *6*, 119–121.
4. (a) V. Niel, J. M. Martinez-Agudo, M. C. Muñoz, A. B. Gaspar, J. A. Real, *Inorg. Chem.* **2001**, *40*, 3838–3839; (b) J. A. Rodríguez-Velamazán, M. A. González, J. A. Real, M. Castro, M. C. Muñoz, A. B. Gaspar, R. Ohtani, M. Ohba, K. Yoneda, Y. Hijikata, et al., *J. Am. Chem. Soc.* **2012**, *134*, 5083–5089; (c) Z. Arcís-Castillo, F. J. Muñoz-Lara, M. C. Muñoz, D. Aravena, A. B. Gaspar, J. F. Sánchez-Royo, E. Ruiz, M. Ohba, R. Matsuda, S. Kitagawa, et al., *Inorg. Chem.* **2013**, *52*, 12777–12783; (d) D. Aravena, Z. A. Castillo, M. C. Muñoz, A. B. Gaspar, K. Yoneda, R. Ohtani, A. Mishima, S. Kitagawa, M. Ohba, J. A. Real, et al., *Chem. - A Eur. J.* **2014**, *20*, 12864–12873; (e) A. Mishima, T. Koshiyama, J. A. Real, M. Ohba, *J. Mater. Chem. C* **2017**, *5*, 3706–3713.
5. (a) T. D. Keene, M. J. Murphy, J. R. Price, D. J. Price, C. J. Kepert, *Dalton Trans.* **2011**, *40*, 11621–11628; (b) R. Ohtani, S. Kitagawa, M. Ohba, *Polyhedron* **2013**, *52*, 591–597.
6. H. Ikeda, A. Ito, E. Sakuda, N. Kitamura, T. Takayama, T. Sekine, A. Shinohara, T. Yoshimura, *Inorg. Chem.* **2013**, *52*, 6319–6327.
7. A. L. Spek, *Acta Crystallogr. Sect. C, Struct. Chem.* **2015**, *71*, 9–18.
8. (a) K. Nakamoto, in *Infrared Raman Spectra Inorg. Coord. Compd. Part B Appl. Coord. Organometallic, Bioinorg. Chem.*, John Wiley & Sons, **2009**, pp. 110–117; (b) Y. Yamada, *Bull. Chem. Soc. Jpn.* **2016**, *68*, 16–28.

9. (a) Z. F. Chen, R. G. Xiong, J. Zhang, X. T. Chen, Z. L. Xue, X. Z. You, *Inorg. Chem.* **2001**, *40*, 4075–4077; (b) Z. Wei, Z.-Y. Gu, R. K. Arvapally, Y.-P. Chen, R. N. McDougald, J. F. Ivy, A. A. Yakovenko, D. Feng, M. A. Omary, H.-C. Zhou, *J. Am. Chem. Soc.* **2014**, *136*, 8269–8276.

Chapter 3

Guest-Selective Responce and Luminescence Properties of One-Dimensional Coordination Polymers

Abstract

Low-dimension CPs constructed by cyanide-linkages of tetracyanometallate analogue unit are expected to show unique guest responsivity including formation and cleavage of cyanide-linkage. Here novel luminescent 1D-CPs $\{[M^{I}(PPh_3)_2]_2[Re^{V}N(CN)_4(MeCN)]\cdot n\text{sol}\}$ (M^{I} = Cu, Ag; PPh_3 = triphenylphosphine; MeCN = acetonitrile) were prepared by reaction of $[ReN(CN)_4]^{2-}$ unit as guest-responsive luminescent building unit with $[M^{I}(PPh_3)_4]^{+}$ precursor complex. Their frameworks formed 1D-ladder-type structure elongated in a direction by cyano-linkages in the ratio of one $[ReN(CN)_4]^{2-}$ unit to two $[M(PPh_3)_2]^{+}$ units. The open-metal site of $[ReN(CN)_4]^{2-}$ unit was occupied by MeCN. The bulk sample, named as **MRe_as-syn** (**M** = Cu and Ag), showed lime-green emission originating from d-d transition of $[ReN(CN)_4]^{2-}$ units around 545 and 539 nm with high quantum yield of 68.6 and 82.1%, respectively. The emission band of **MRe_as-syn** did not shift so large by exposure of guest molecules. The crystals of **MRe**, however, were dissolved by dichloromethane, which was confirmed to be in complete solution because of no tyndal effect. The resulting solution showed red-orange color emission although $[Re^{V}N(CN)_4]^{2-}$ does not emit light in solution normally. Amorphous solids obtained by evaporation of the solution also showed the red-orange emission. After exposing the solids to various organic vapors, the initial structure and emission color of **MRe** were recovered only in response to acetonitrile. This result suggested that the template space of initial structure having MeCN as coordination solvent and bulky PPh_3 ligand related to selective responsivity and reversibility by MeCN. Moreover, the unique phase transition with large emission band shift was investigated.

Introduction

Over the past decades, there has been extensive interest in porous coordination polymers (PCPs) is defined as supramolecular materials fabricated by infinitely linking metal ions and organic/inorganic ligands through coordination bonds.[1] The greatly regular framework structure, and chemical and physical properties of PCPs are highly designed by selecting appropriate building components. Hofmann-type PCP family is one of the major series investigated extensively.[2] The basic framework structure is constructed by two-dimensional square reticular layers which expanded in four directions by cyano-linkages between square planar tetracyanometallate(II) units and transition metal(II) ions. In addition to 2D square plane structure, tetracyanometallate units can act as a connected linker with various bridging modes, and build a broad variety of framework structures depending on metal ions and/or complementary ligands functioned as cap or linker moiety for unoccupied coordination sites of metal cations.[3,4] Lanthanide(IIII) ions usually make two or three coordination with tetracyanometallate units, which gives low dimensional frameworks such as 1D chain and ladder structures.[4] On the other hand, in our previous work, we have attempted to reduce dimensions of 3D-Hofmann-type PCPs $\{M^{II}(pz)[M'^{II}(CN)_4]\}$ (pz = pyrazine) with remaining the pillar ligand of pz due to obtain a flexible structure and a unique adsorption properties. By using $[Au^{III}(CN)_4]^-$ unit instead of $[M^{II}(CN)_4]^{2-}$ unit, 2D hollow sheet-type PCPs $\{M^{II}(pz)[Au^{III}(CN)_4]_2\}$ was synthesized. Their structure showed lengthwise frameworks cut cyano-linkages in a direction parallelly and possessed pore space surrounding two $[Au^{III}(CN)_4]^-$ unit and two pillar pyrazine. The compounds exhibited unique reversible structure conversion between 2D-hollow sheets and 1D-chain structure accompanying with adsorption and desorption cycles of water molecules.

In this study, we attempted to synthesize low-dimensional flexible frameworks to obtain unique guest responsive luminescence with coupled with structure conversion. Low dimension frameworks as described above were consisted of combinations of Ln^{3+} and $[M^{II}(CN)_4]^{2-}$ unit, and M^{2+} and $[Au^{III}(CN)_4]^-$ unit, respectively. In these both cases, the electric charge of metal cation and tetracyanometallate anion is disagreement. Considering these results, it is expected that novel low dimensional framework is prepared by using a combination of M^+ and $[M^{II}(CN)_4]^{2-}$ unit, and obtain unique guest responsive property. In this chapter,

$[ReN(CN)_4]^{2-}$ unit is used as tetracyanometallate-based guest responsive luminescent building unit,[5] and monovalent precursor complex $[M^I(PPh_3)_4]^+$ (M^I = Cu and Ag, PPh_3 = triphenylphosphine) was used as cation nodes. In addition, monovalent coinage metal complexes have been well researched about its luminescent properties.[6] So, we also hope a new luminescent PCP show dual color emission from both of nitridotetracyanorhenate ion and M(I)-based unit. Here, we prepared new luminescent 1D-ladder type PCPs $\{[M^I(PPh_3)_2]_2[Re^VN(CN)_4(MeCN)\cdot n\text{sol}]\}$ (**MRe**, MeCN = acetonitrile) by reaction of $[ReN(CN)_4]^{2-}$ with M^I-based unit having PPh_3 as capping ligand. **MRe** exhibited the unique phase transition and selective guest responsivity. In addition, we investigated the chemical and physical properties based on guest responsivity and emission mechanism in each phase.

Experiments

Physical Measurements

Single-crystal X-ray diffraction data were collected on a Bulker SMART APEX II ULTRA CCD-detector Diffractometer, a rotating-anode (Bruker Tourbo X-ray source) with graphite-monochromated $Mo_{K\alpha}$ radiation (λ = 0.71073 Å) was used. Computations were carried out on a APEX2 crystallographic software package and OLEX2 software.[8] A single crystal was mounted on a polymer film with liquid paraffin and the temperature kept constant under flowing N_2. All of the structures were solved by a standard direct method (XSHELL V6.3.1 crystallographic software package of the Bruker AXS) and expanded using Fourier techniques. Fullmatrixleast-squares refinements were carried out with anisotropic thermal parameters for all non-hydrogen atoms. All of the hydrogen atoms were placed in the measured positions and refined using a riding model. X-ray powder diffraction (XRPD) was carried out on a Rigaku Ultima IV diffractrometer with graphite-monochromated $Cu_{K\alpha}$ radiation. X-ray fluorescence analysis was carried out on a Rigaku ZSX-100S. Infrared spectra were measured with a JASCO FT/IR-4200 using ATR method. Thermogravimetry analysis (TGA) was carried out on a Perkin Elmer STA6000. Elemental analysis of carbon, hydrogen and nitrogen was carried out by the staff of technical support division graduate school of science, Kyushu University. The emission spectra and emission quantum yields were measured by an absolute emission quantum yield measurement system C9920-02 (Hamamatsu Photonics K. K.) composed of an integrating sphere, a multi-channel photodetector PMA-12 (Hamamatsu Photonics K. K.), and a xenon lamp as an excitation light source (excitation wavelength = 365 nm) at room temperature. PL quantum yield was calculated with the following equation:

$$\phi = \frac{\int I_{em} d\lambda}{\int \left(I_{ex}^{before} - I_{ex}^{after} \right) d\lambda}$$

I_{em} is the amount of photon from emission, $I^{before}{}_{em}$ is amount of photon from excitation light that nothing absorbed, and $I^{after}{}_{em}$ is amount of photon from excitation light that something absorbed. The emission decay curves were acquired at room temperature using a Quantaurus-Tau C11367-24 (Hamamatsu Photonics K. K.) with excitation via a xenon flash lamp with a band-path filter (λ_{ex} = 370 nm). Theoretical value of emission lifetime was calculated with the following equation.

$$\sum_i A_i \exp\left(-\frac{t}{\tau_i}\right)$$

A_i is a coefficient, t is current time, τ_i is emission lifetime. A_i and τ_i are given by fitting of luminescent lifetime measurement.

Preparation

All chemicals were purchased from commercial sources and used without further purification. Synthesis of $K_2[ReN(CN)_4]\cdot H_2O$ and $[PPh_4]_2[ReN(CN)_4(MeOH)]\cdot 3MeOH$ are described in Chapter 1.

$[Cu(MeCN)_4](ClO_4)$

$[Cu(MeCN)_4](ClO_4)$ was prepared according to the literature method.[9] A suspension of Cu_2O (574.4 mg, 4.0 mmol), in 60% perchloric acid (40 mL), 40mL water and 80 mL acetonitrile was heated under reflux overnight under an atmosphere of nitrogen. The obtained colorless solution was cooled to room temperature slowly. The solution with colorless crystals stood in the cooler and filtered. Then, the obtained solid was washed with ethanol to give colorless microcrystals. Yield : 1.17 g (89.1 %).

$[Cu(PPh_3)_4](ClO_4)$

$[Cu(PPh_3)_4](ClO_4)$ was prepared according to the literature method.[10] A suspension of $[Cu(MeCN)_4](ClO_4)$ (1.58 g, 6.0 mmol) and triphenylphosphine (7.89 g, 30.0 mmol) in methanol (120 mL) was heated under reflux for 6 hours. The obtained colorless solution was cooled to room temperature slowly. The suspension was filtered and washed with methanol to give colorless microcrystals. Yield : 4.35 g (859.8 %).

$[Ag(PPh_3)_4](NO_3)$

$[Ag(PPh_3)_4](ClO_4)$ was prepared according to the literature method.[10] A suspension of $AgNO_3$ (592.4 mg, 3.4 mmol) and triphenylphosphine (4 g, 15.3 mmol) in ethanol (80 mL) was heated under reflux for 6 hours. The obtained colorless solution was cooled to room temperature slowly. The suspension was filtered and washed with ethanol to give colorless microcrystals. Yield : 4.16 g (97.8 %)

Single crystals of {[Cu(PPh$_3$)$_2$]$_2$[ReN(CN)$_4$(MeCN)] 2MeCN H$_2$O} (CuRe_sc)

Single crystals of **CuRe_sc** was prepared by diffusion method used straight tubes. A mixed solvent of H_2O / MeCN (1 mL, water : acetonitrile = 1 : 1 v/v) was layered on a solution of $K_2[ReN(CN)_4]\cdot H_2O$ in H_2O (2.0 mmol/L, 1.0 mL). Then, a solution of $[Cu(PPh_3)_4](ClO_4)$ in MeCN (4.0 mmol/L, 1.0 mL) added slowly. After a few days, clear pale yellow single crystals were prepared.

Powder samples of {[Cu(PPh$_3$)$_2$]$_2$[ReN(CN)$_4$(MeCN)] MeCN H$_2$O} (CuRe_as-syn)

CuRe_as-syn was prepared by slow addition using dropping funnel. A solution of $[PPh_4]_2[ReN(CN)_4(MeOH)]\cdot 3MeOH$ (219.6 mg, 0.200 mmol) in acetonitrile (20 mL) was added to a solution of $[Cu(PPh_3)_4](ClO_4)$ (484.2 mg, 0.399 mmol) in acetonitrile (20 mL) with slowly stirring. After stirring overnight, yellow solid was separated by centrifugation. Pale yellow powder was obtained by dryness in desiccator without vacuum condition. Yield : 311.0 mg (98.3%) .

Elemental Analysis: Calculated for $C_{80}H_{68}Cu_2N_7OP_4Re$ (%); C 60.79, H 4.34, N6.20; Found (%); C 61.12, H 4.26, N 6.29

{[Ag(PPh$_3$)$_2$]$_2$[ReN(CN)$_4$(MeCN)] 2MeCN} (AgRe_as-syn)

An 80 mL acetonitrile solution of $[PPh_4]_2[ReN(CN)_4(MeOH)]\cdot 3MeOH$ (442.6 mg, 0.403 mmol) was mixed with $[Ag(PPh_3)_4](NO_3)$ (489.7 mg, 0.402 mmol) in acetonitrile (80 mL). Pale yellow microcrystals began to crystallize gradually after standing for several tens of minutes. The yellow solid was filtered and washed with acetonitrile. The pale yellow microcrystals of **AgRe_as-syn** was obtained by dryness in desiccator without vacuum condition. Yield : 252.5 mg (78.1 %).

Results and discussion

X-Ray Structural Characterization

X-ray crystallographic analysis reveals that the frameworks of **CuRe_sc** and **AgRe_as-syn** are isomorphic structure, respectively. Crystal parameters for complexes are summarized in Table 1. The selected bond lengths and angles for complexes are described in Table 2-5. **CuRe_sc** and **AgRe_as-syn** crystallize in triclinic system with space group $P\bar{1}$. The asymmetric unit consists of one $[ReN(CN)_4]^{2-}$ unit, two M^+ ion and four PPh3 ligands. (**Figure 1** and **3**). The geometry of $[ReN(CN)_4]^{2-}$ unit is distorted square pyramidal, where the average bending angles of the diagonal C-Re-C in **CuRe_sc** and **AgRe_as-syn** are 162.7 and 161.9 degree, respectivery. An acetonitrile coordinates to the open-metal site at trans position of nitride ligand of $[ReN(CN)_4]^{2-}$ unit. The geometry of M^+ ions are tetrahedral with each a cyanide nitrogen atom of two $[ReN(CN)_4]^{2-}$ units and two PPh_3. **CuRe_sc** and **AgRe_as-syn** formed 1D-ladder structure extended parallel to *b* axis by Re-CN-M^+ linkages in the ratio of one $[ReN(CN)_4]^{2-}$ unit to two $[M(PPh_3)_2]^+$ units (**Figure 2-3** and **4-5**). As noted above, the frameworks of **CuRe_sc** and **AgRe_as-syn** are same 1D-ladder structure but their solvents in crystallization were different. **CuRe_sc** has one water and one acetonitrile per unit between each 1D-ladder frameworks while **AgRe_as-syn** has two acetonitrile per unit.

Table 1. Crystallographic parameters of **CuRe_sc** and **AgRe_as-syn**

Name	**CuRe_sc**	**AgRe_as-syn**
Formula	$C_{80}H_{68}Cu_2N_7OP_4Re$	$C_{82}H_{69}Ag_2N_8P_4Re$
Crystal System	triclinic	triclinic
Space Group	$P\bar{1}$	$P\bar{1}$
a / Å	13.991(3)	14.081(5)
b / Å	16.029(4)	16.345(6)
c / Å	17.871(4)	18.339(7)
α / deg.	101.616(3)	102.085(5)
β / deg.	105.879(3)	106.935(6)
γ / deg.	108.159(3)	107.850(4)
Temperature / K	100(2)	100(2)
V / Å^3	3478.1(14)	3631.(2)
Z value	2	2
GOF	1.043	0.762
R1	0.0582	0.0377
wR	0.1559	0.1017

Table 2. Bond length (Å) of **CuRe_sc**

Re1–N1	1.691(4)	Cu1–N5$^{\#}$	2.022(6)
Re1-C1	2.107(6)	Cu1–P1	2.271(2)
Re1-C2	2.105(6)	Cu1–P2	2.288(2)
Re1-C3	2.108(5)	Cu2$^{\#}$–N3	2.012(5)
Re1-C4	2.111(6)	Cu2–N4	2.038(5)
Re1–N6	2.454(6)	Cu2–P3	2.280(2)
Cu1–N2	2.017(4)	Cu2–P4	2.305(2)

Symmetry operation: (#) 1-x, 1-y, 1-z

Table 3. Bond angles (º) of **CuRe_sc**

N1-Re1-C1	98.7(2)	N2-Cu1-P1	107.3(2)
N1-Re1-C2	100.4(2)	N2-Cu1-P2	104.9(2)
N1-Re1-C3	97.5(2)	N5$^{\#}$-Cu1-P1	116.0(2)
N1-Re1-C4	97.9(2)	N5$^{\#}$-Cu1-P2	104.6(2)
C1-Re-C2	91.7(2)	P1-Cu1-P2	116.72(6)
C2-Re-C3	84.2(2)	N3$^{\#}$-Cu2-N4	108.4(2)
C3-Re-C4	93.8(2)	N3$^{\#}$-Cu2-P3	118.1(1)
C4-Re-C1	85.1(2)	N3$^{\#}$-Cu2-P4	107.1(1)
C1-Re-C3	163.8(2)	N4-Cu2-P3	110.2(2)
C2-Re-C4	161.6(2)	N4-Cu2-P4	97.8(2)
N2-Cu1-N5$^{\#}$	106.4(2)	P3-Cu2-P4	113.31(6)

Symmetry operation: (#) 1-x, 1-y, 1-z

Table 4. Bond length (Å) of **AgRe_as-syn**

Re1–N1	1.644(6)	Ag1–N5$^{\#}$	2.316(7)
Re1-C1	2.109(8)	Ag1–P1	2.445(2)
Re1-C2	2.104(8)	Ag1–P2	2.465(2)
Re1-C3	2.103(7)	Ag2$^{\#}$–N3	2.261(6)
Re1-C4	2.108(8)	Ag2–N4	2.299(6)
Re1–N6	2.484(6)	Ag2–P3	2.438(2)
Ag1–N2	2.276(6)	Ag2–P4	2.493(2)

Symmetry operation: (#) 1-x, 1-y, 1-z

Table 5. Bond angles (º) of **AgRe_as-syn**

N1-Re1-C1	102.0(3)	N2-Cu1-P1	108.4(2)
N1-Re1-C2	97.9(3)	N2-Cu1-P2	104.3(2)
N1-Re1-C3	97.9(3)	N5$^{\#}$-Cu1-P1	112.1(2)
N1-Re1-C4	98.2(3)	N5$^{\#}$-Cu1-P2	104.4(2)
C1-Re1-C2	89.3(3)	P1-Cu1-P2	119.74(6)
C2-Re1-C3	88.1(3)	N3$^{\#}$-Cu2-N4	105.1(2)
C3-Re1-C4	91.7(3)	N3$^{\#}$-Cu2-P3	117.7(1)
C4-Re1-C1	85.4(3)	N3$^{\#}$-Cu2-P4	107.9(1)
C1-Re1-C3	160.1(3)	N4-Cu2-P3	109.6(2)
C2-Re1-C4	163.7(3)	N4-Cu2-P4	99.5(2)
N2-Cu1-N5$^{\#}$	107.2(2)	P3-Cu2-P4	114.99(6)

Symmetry operation: (#) 1-x, 1-y, 1-z

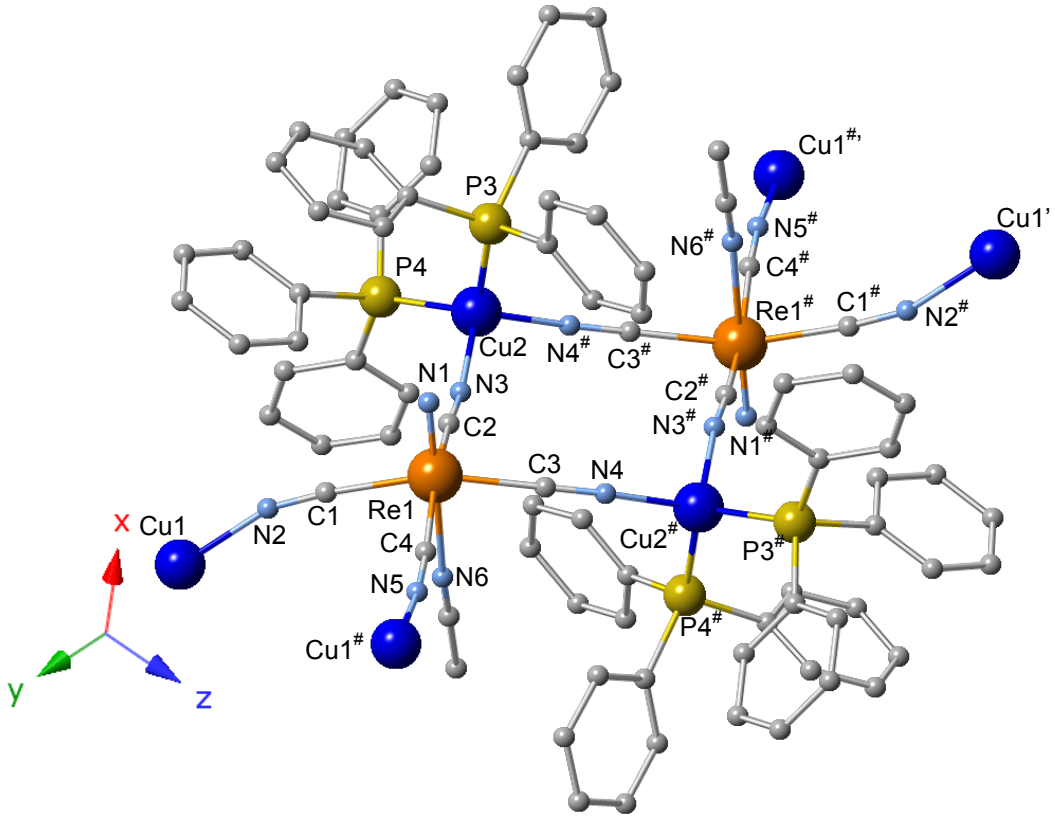

Figure 1. The drawing of the asymmetric unit for **CuRe_sc** with the atom numbering scheme. H atoms and crystal solvent molecules are omitted.

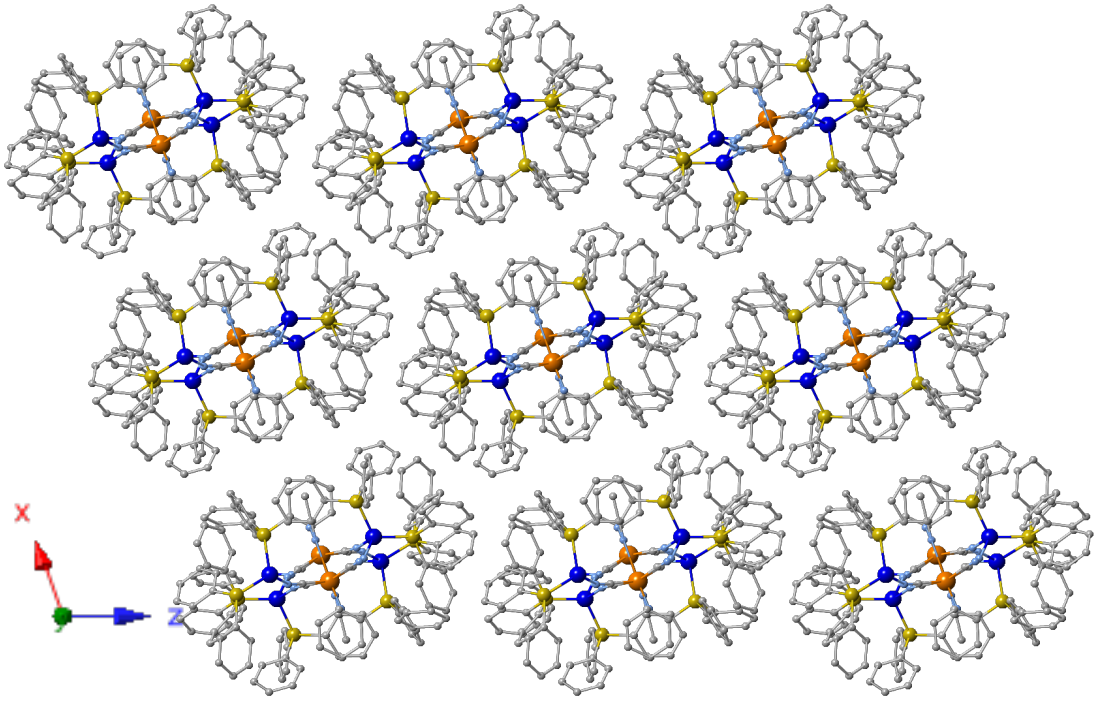

Figure 2. The projection of polymeric structure for **CuRe_sc** onto *ac* plane. H atoms and crystal solvent molecules are omitted.

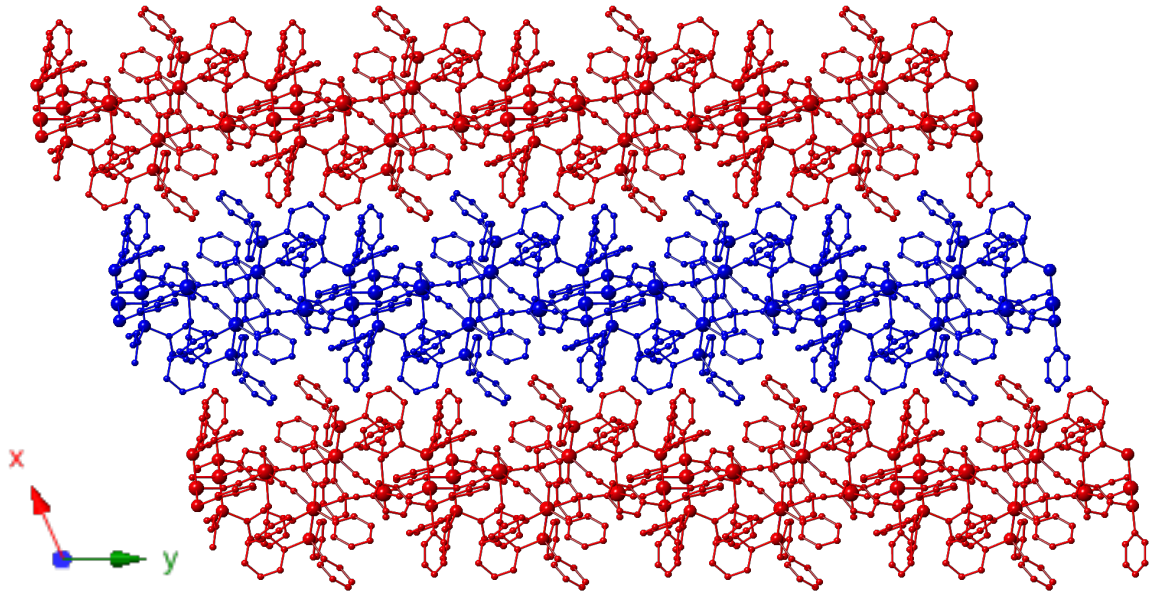

Figure 3. The projection of polymeric structure for **CuRe_sc** onto *ab* plane. Three neighboring ladder frameworks in the direction of *c* axis are represented by red, blue and red. H atoms and crystal solvent molecules are omitted.

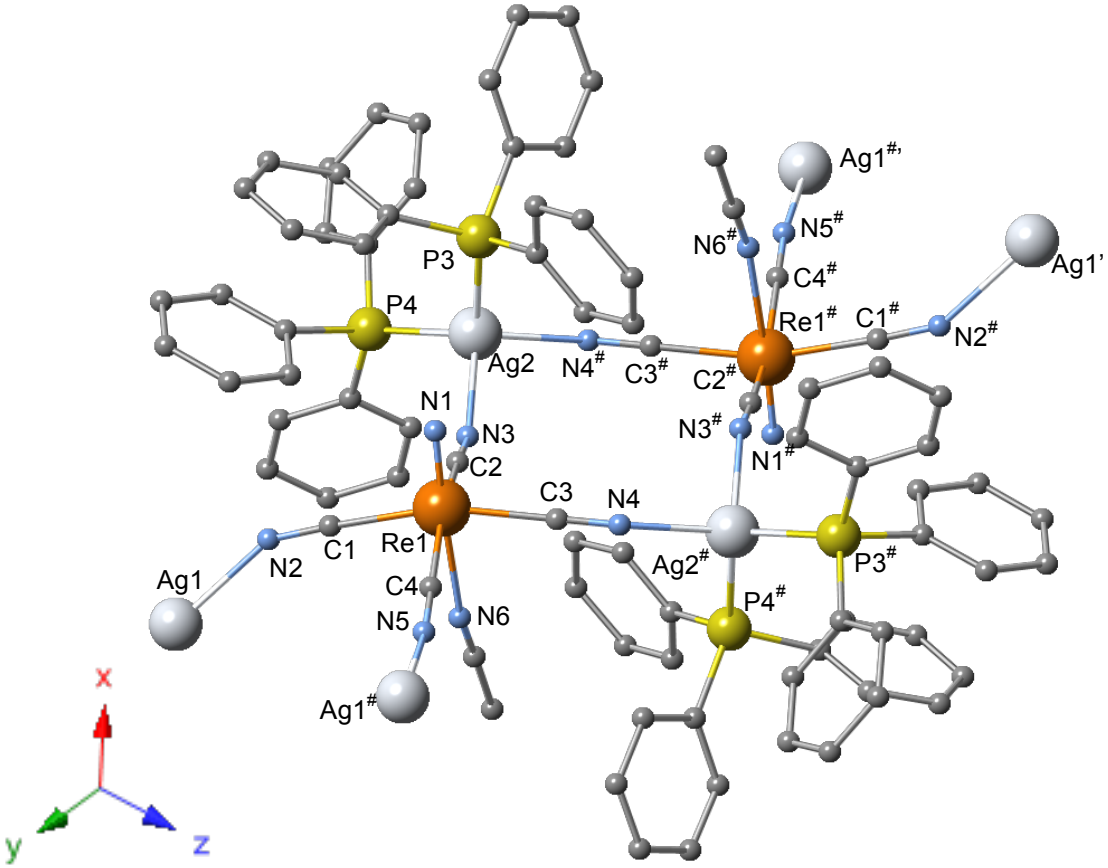

Figure 4. The drawing of the asymmetric unit for **AgRe_as-syn** with the atom numbering scheme. H atoms and crystal solvent molecules are omitted.

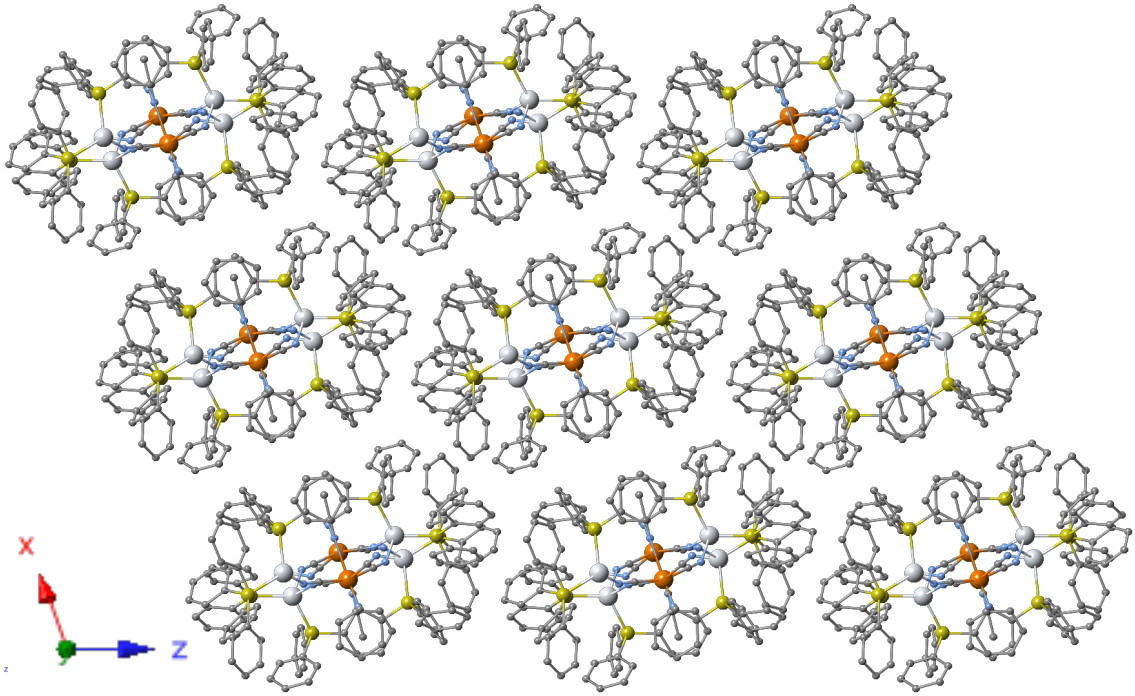

Figure 5. The projection of polymeric structure for **AgRe_as-syn** onto *ac* plane. H atoms and crystal solvent molecules are omitted.

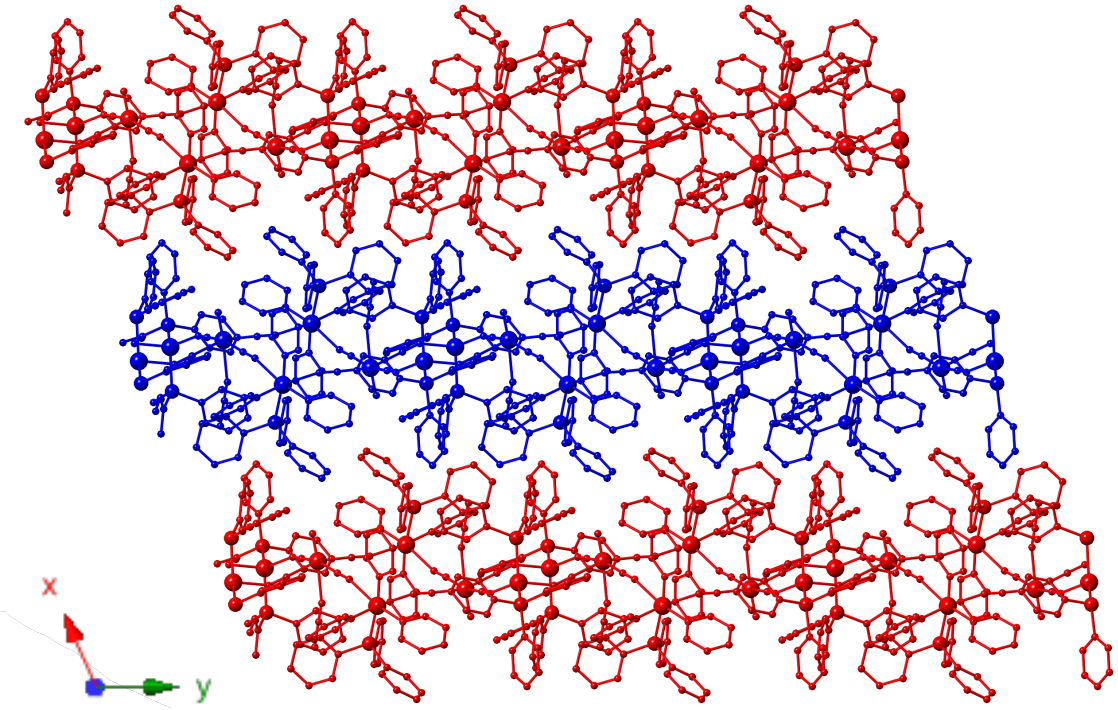

Figure 6. The projection of polymeric structure for **AgRe_as-syn** onto *ab* plane. Three neighboring ladder frameworks in the direction of *c* axis are represented by red, blue and red. H atoms and crystal solvent molecules are omitted.

Powder X-Ray Diffraction Patterns

The PXRD patterns of **CuRe_as-syn** and **AgRe_as-syn** were measured at room temperature under ambient atmosphere and the results show in **Figure 7**. The measured PXRD patterns of bulk samples compared to each simulated patterns of **CuRe_sc** and **AgRe_as-syn** and their structures were confirmed to be 1D-ladder structure.

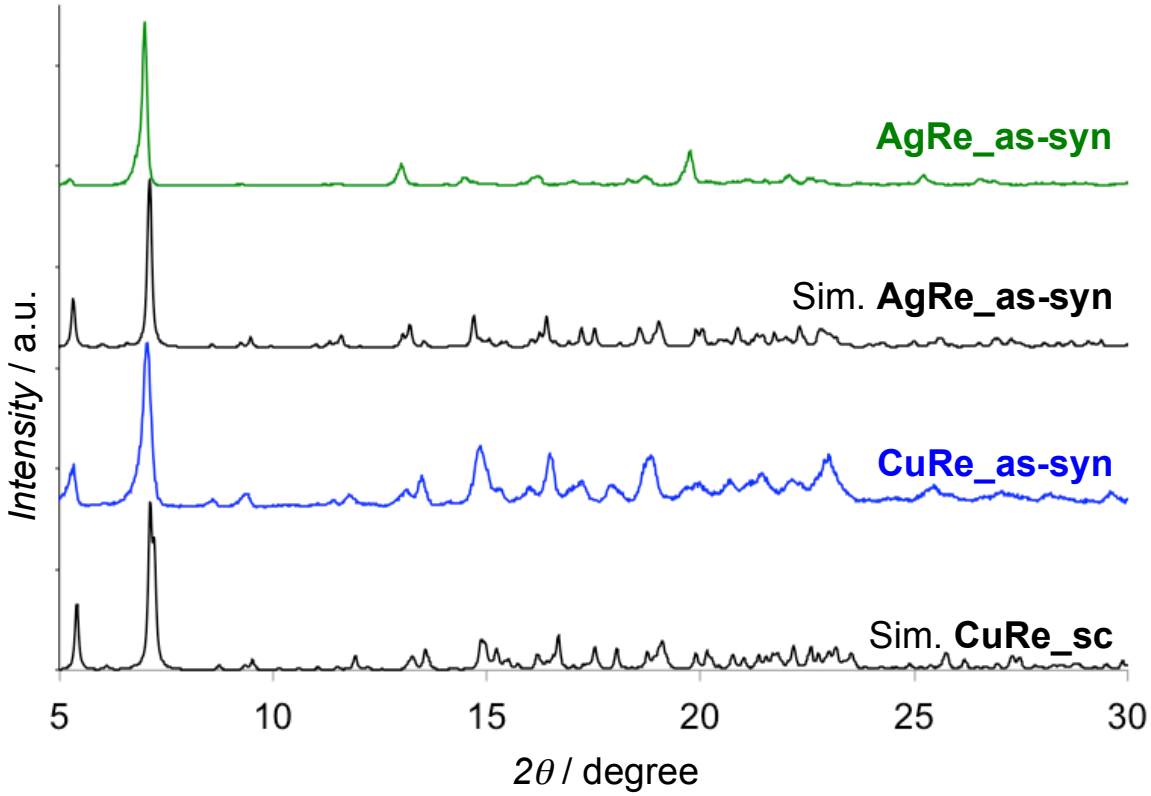

Figure 7. PXRD measured patterns of **CuRe_as-syn** and **AgRe_as-syn**, and simulated patterns of **CuRe_sc** and **AgRe_as-syn**.

IR spectra

FT-IR spectra of $[PPh_4]_2[ReN(CN)_4(MeOH)]\cdot 3MeOH$, **CuRe_as-syn** and **AgRe_as-syn** were shown in **Figure 8**. The strong absorption bands based on stretching vibration of cyano groups ($\nu_{C\equiv N}$) were observed at 2116 cm^{-1} in **CuRe_as-syn** and 2118 cm^{-1} in **AgRe_as-syn**. The formation of Re-C≡N-M bridges were confirmed by the upshift of the frequency of the $\nu_{C\equiv N}$ band from that of mono-nuclear complexes ($K_2[ReN(CN)_4]\cdot H_2O$; 2107 cm^{-1} and $[PPh_4]_2[ReN(CN)_4(MeOH)]\cdot 3MeOH$; 2105 cm^{-1}). The unique absorption bands of the $\nu_{C\equiv N}$ of acetonitrile were also observed at 2240 and 2270 cm^{-1} in both of **CuRe_as-syn** and **AgRe_as-syn**. In addition, the peaks derived from PPh^{4+} ion were disappeared and the peaks derived from PPh_3 were observed in IR spectra of **CuRe_as-syn** and **AgRe_as-syn**.

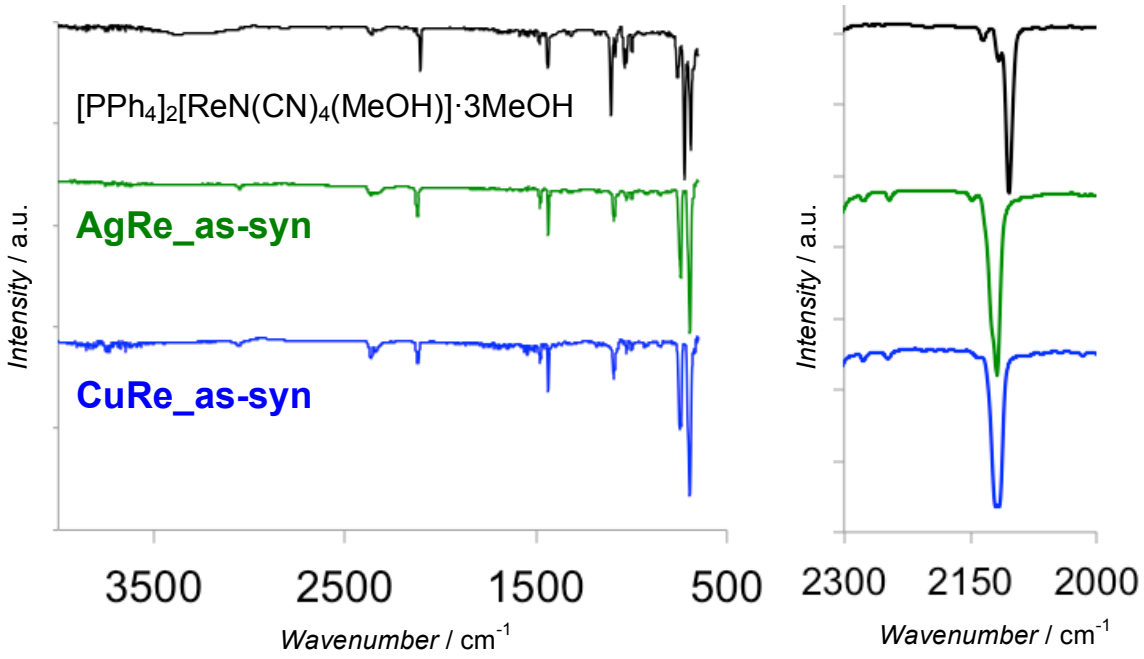

Figure 8. IR spectra of **CuRe_as-syn** (blue), **AgRe_as-syn** (green) and $[PPh_4]_2[ReN(CN)_4(MeOH)]\cdot 3MeOH$ (black).

Photophysical properties

Photoluminescence spectra of **CuRe_as-syn** and **AgRe_as-syn** show in **Figure 9** and the emission maximum wavelength (λ_{em}), the quantum yields and the life time summarize in **Table 6**. The emission maximum wavelength was observed at 545 and 539 nm in **CuRe_as-syn** and **AgRe_as-syn**, respectively. Their broaden emission spectra and emission color were typical luminescent features based on $[ReN(CN)_4]^{2-}$ unit. Photoluminescence quantum yields and emission lifetime of **MRe_as-syn** showed in **Table 6**. The quantum yields of **CuRe_as-syn** and **AgRe_as-syn** were very high efficiency with 68.60 and 82.07%. The quantum yield of luminescent components typically increased by rigidifying with attributed to construction of coordination frameworks. The quantum yield of $[ReN(CN)_4]^{2-}$ unit also increased by embedding in the frameworks because of restriction on the vibrational deactivation of terminal cyanide ligands of $[ReN(CN)_4]^{2-}$. The both life times were single component with sub-micro second at 27.4 μsec 18.9 μsec in **CuRe_as-syn** and **AgRe_as-syn**, respectively. In addition, from UV-vis reflectance spectra, the unique adsorption band based on MLCT did not observed in **Figure 10**. These results suggested that photoluminescence of **MRe_as-syn** originated from $^3[(d_{xy})^1(d_{\pi*})^1]$ excited state.

Table 6. Emission maximum wavelength, PL quantum yields and life times of **MRe_as-syn**.

Compound	λ_{em} [nm]	ϕ [%]	τ [μsec]
CuRe_as-syn	545	68.60	27.4
AgRe_as-syn	539	82.07	18.9

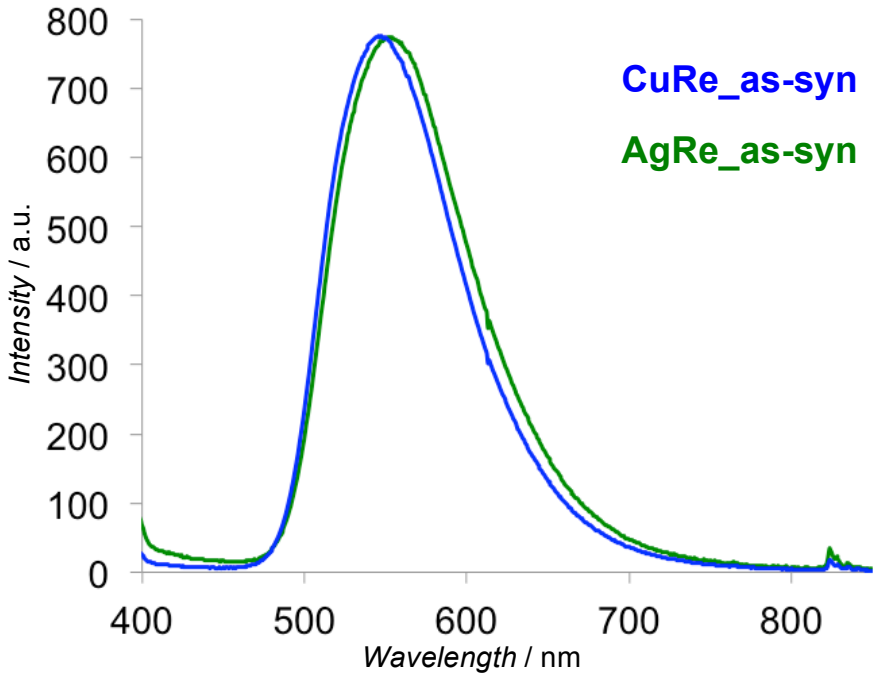

Figure 9. Emission spectra of **MRe_as-syn** in solid state at room temperature upon excitation at 365 nm.

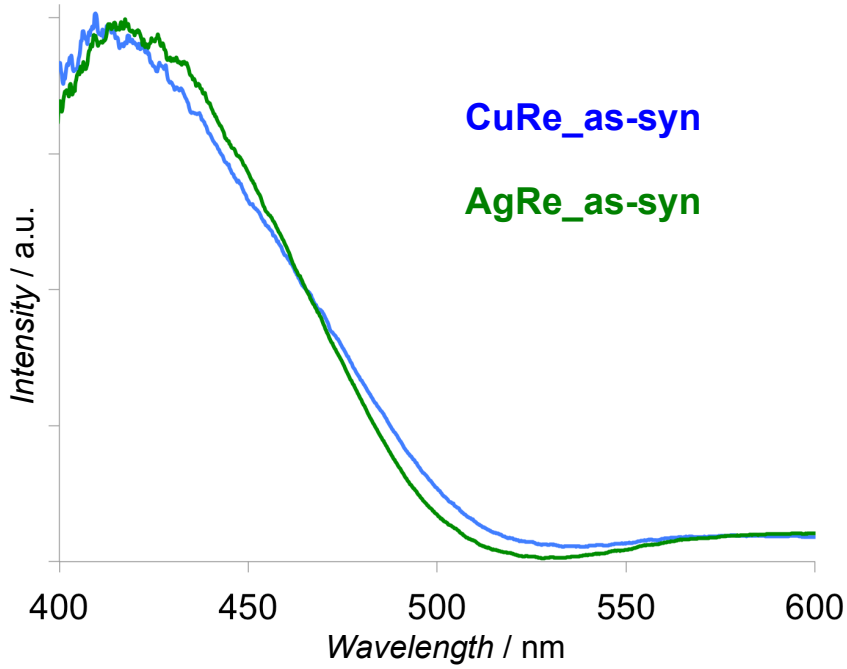

Figure 10. UV-Vis reflectance spectra of **MRe_as-syn** in solid state at room temperature.

Physical properties of activated sample of CuRe

Guest free sample **CuRe_GF** was obtained by activation of **CuRe_as-syn** at 120ºC with vacuum overnight. No coordination and crystal solvent in **CuRe_GF** was confirmed from TGA and IR spectra. TGA of **CuRe_as-syn** showed gradual weight loss of 7.5 wt% based on one water and two acetonitrile molecules but it of **CuRe_GF** was not observed (**Figure 11**). This result suggests that **CuRe_GF** has no guest molecule. Moreover, in IR spectra, the disappearance of unique absorption bands of the $\nu_{C\equiv N}$ of acetonitrile in **CuRe_GF** was also observed (**Figure 12**).

Photoluminescence spectra of **CuRe_as-syn** and **CuRe_GF** are shown in **Figure 13** and the emission maximum wavelength and the quantum yields are summarized in **Table 7**. The emission maximum wavelength of **CuRe_GF** shifted to higher wavelength at 630 nm although the emission spectrum of **CuRe_GF** has a shoulder around 545 nm that is the similar peak of the emission maximum wavelength of **CuRe_as-syn**. At that time, the emission color changed from lime green to yellow orange after desorption process (**Figure 14**). However, **CuRe_GF** showed no change when exposed to several organic vapors. When focusing on their structural difference, **CuRe_GF** maintained their framework structure and (1 0 0) and (1 0 $\bar{1}$) planes shifted to higher angle (**Figure 15**). In this case, according to Bragg's law, the distance between each 1D-ladder frameworks decreased (**Figure 16**). Therefore, the access space for guest molecules in frameworks of **CuRe_GF** appears to be insufficient although the crystallinity was maintained.

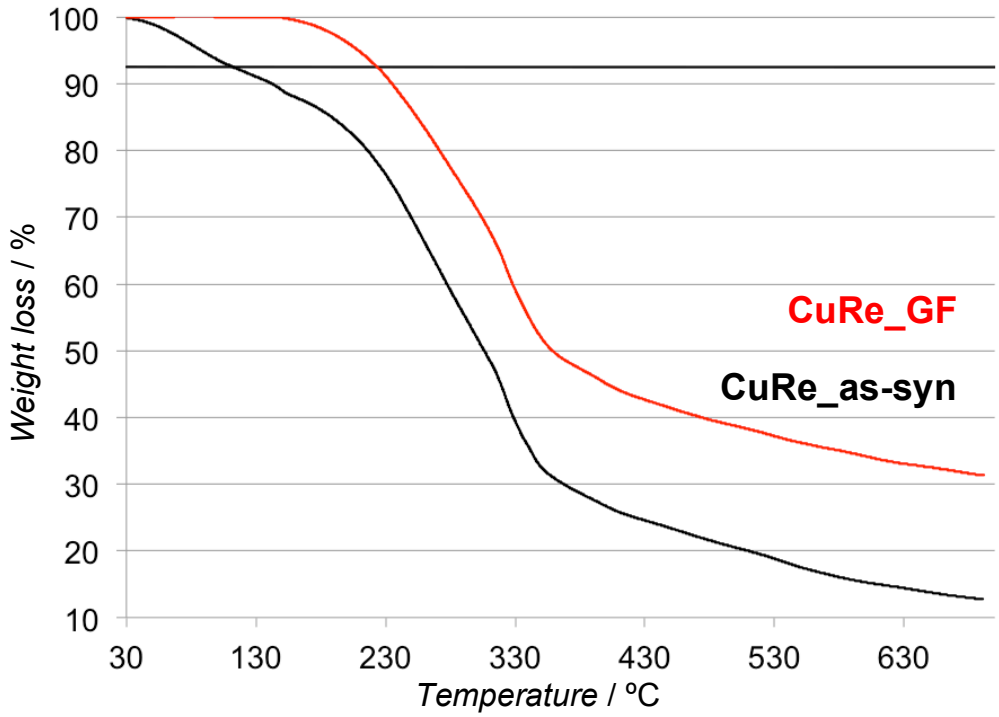

Figure 11. TGA curves of **CuRe_as-syn** (black) and **CuRe_GF** (red).

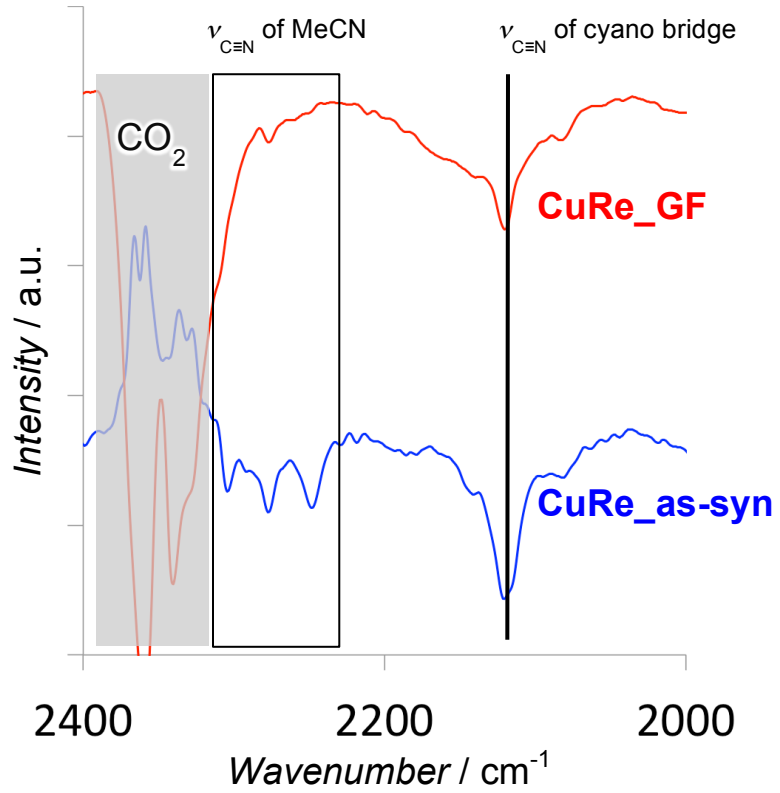

Figure 12. IR spectra of **CuRe_as-syn** (blue) and **CuRe_GF** (red).

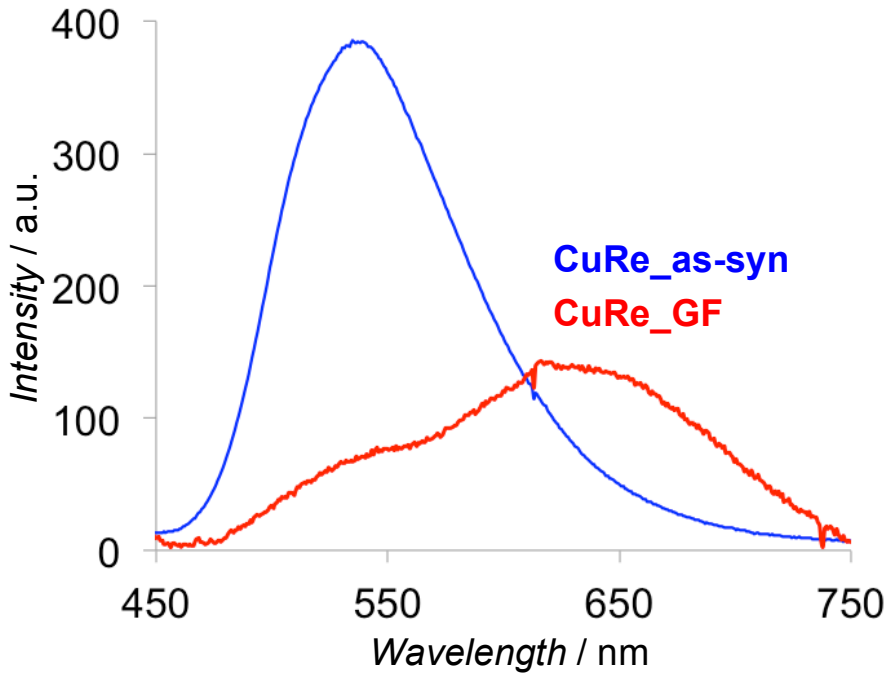

Figure 13. Emission spectra of **CuRe_as-syn** (blue) and **CuRe_GF** (red) in solid state at room temperature upon excitation at 365 nm.

Table 7. Emission maximum wavelength and PL quantum yields of **CuRe_as-syn** and **CuRe_GF**.

Compound	λ_{em} [nm]	ϕ [%]
CuRe_as-syn	545	68.60
CuRe_GF	630	46.46

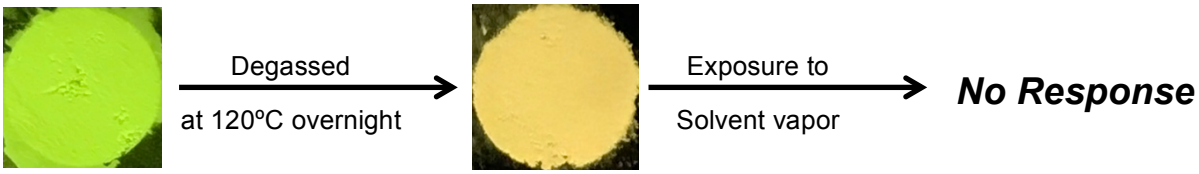

Figure 14. Emission color change of **CuRe_as-syn**.

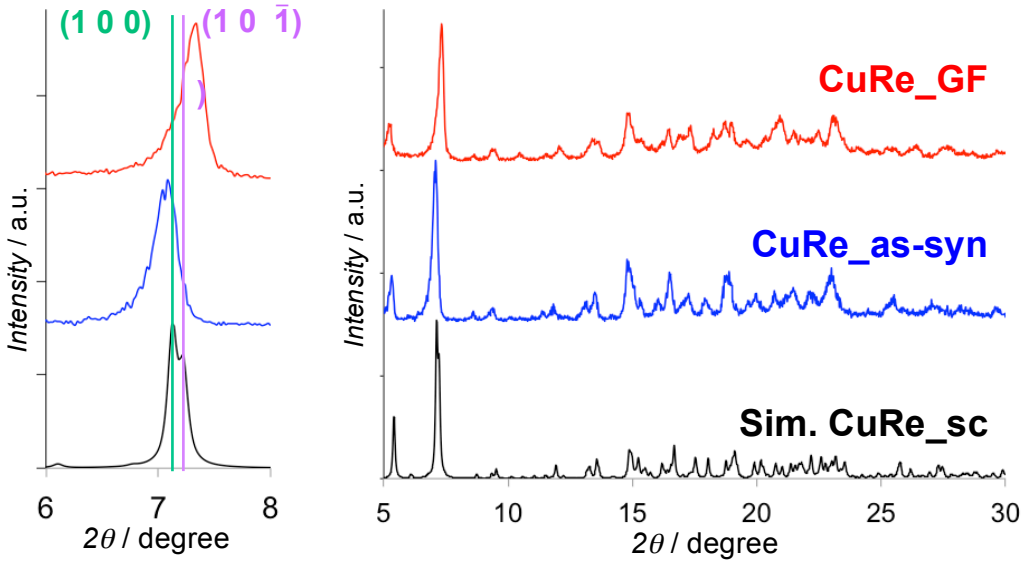

Figure 15. PXRD measured patterns of **CuRe_as-syn** and **CuRe_GF**, and simulated patterns of **CuRe_sc**.

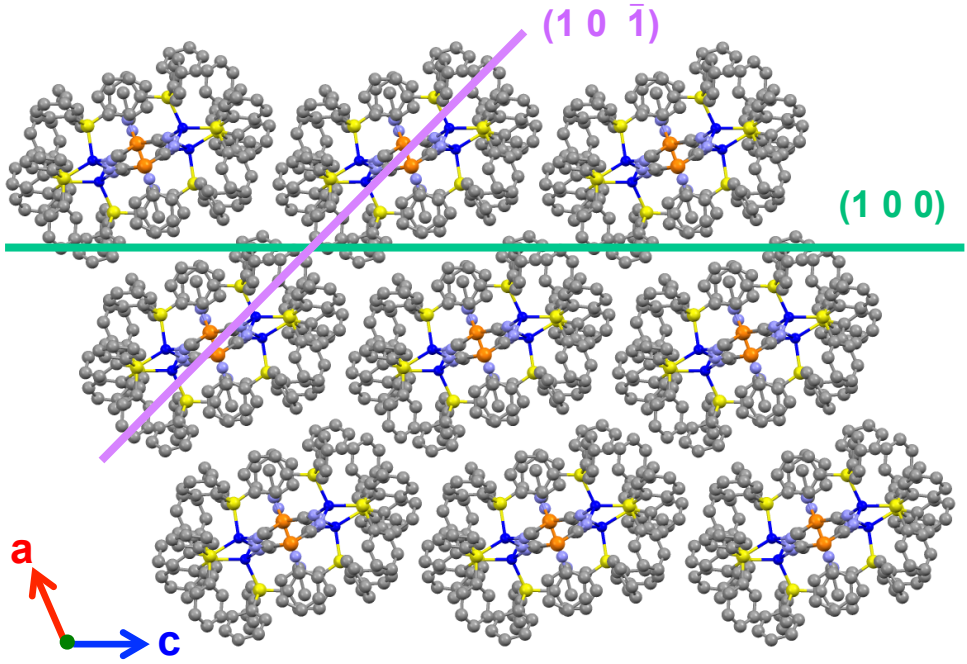

Figure 16. The projection of polymeric structure for **CuRe_as-syn** onto *ac* plane, and the lattice planes of (100) and (10$\bar{1}$).

Guest vapor exposure to CuRe_as-syn

We tried to expose **CuRe_as-syn** directly to several guest vapors such as acetone, acetonitrile, dichloromethane, dimethyl sulfoxide, ethanol, methanol, and water because the guest free sample **CuRe_GF** does not show guest responsivity. Then, PXRD pattern and emission spectra of **CuRe_as-syn** after exposing to guest vapor were measured (**Figure 16-17** and **Table 8**). Unfortunately, the PXRD patterns did not show any changes, and their emission maximum wavelength also little changed.

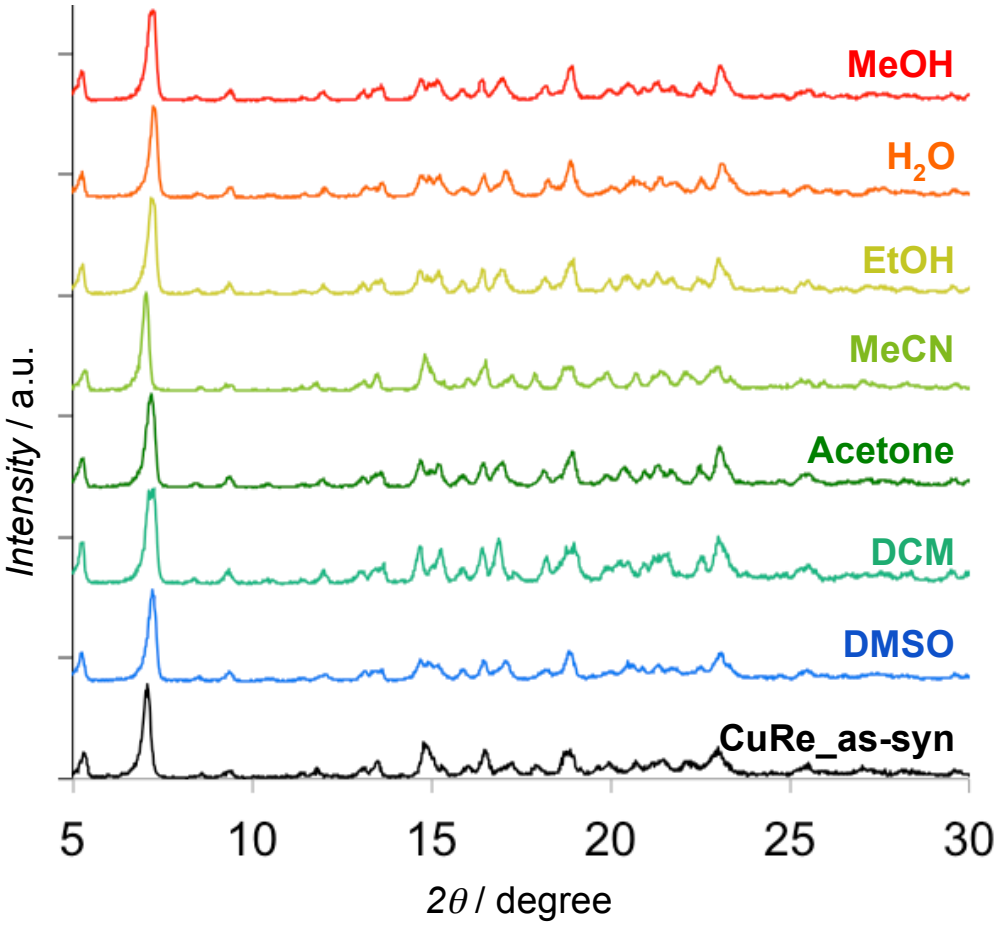

Figure 16. PXRD patterns of **CuRe_as-syn** obtained by exposure of various solvents vapor.

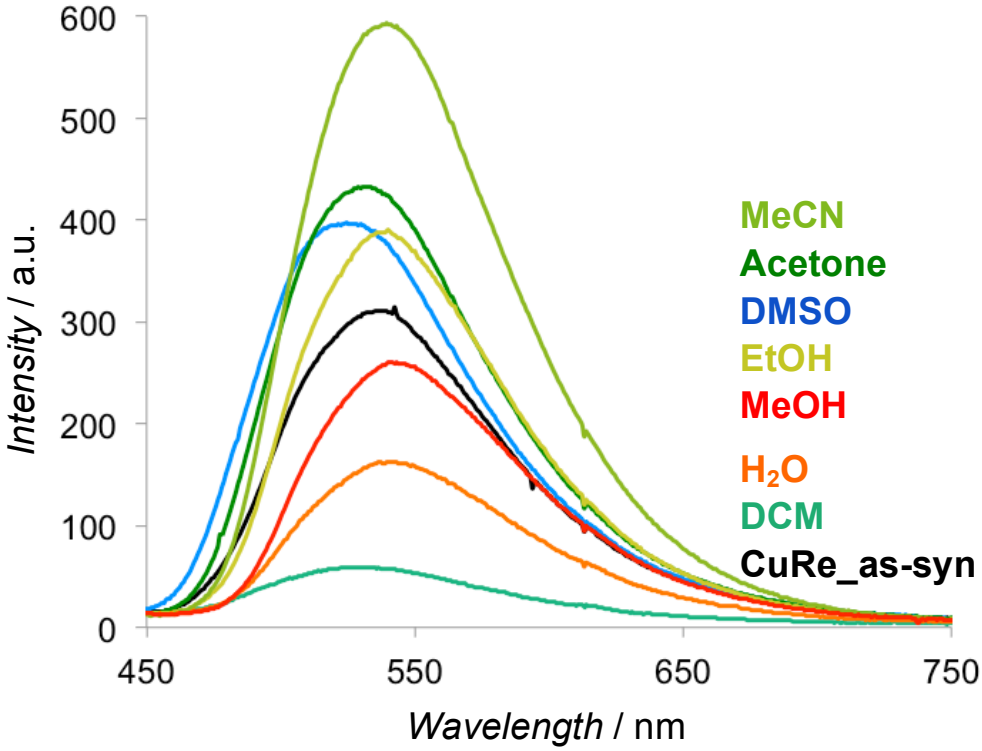

Figure 17. Emission spectra of **CuRe_as-syn** obtained by exposure of various solvents vapor, in solid state at room temperature upon excitation at 365 nm.

Table 8. Emission maximum wavelength and PL quantum yields of **CuRe_as-syn** obtained by exposure of various solvents vapor.

Guest	λ_{em} [nm]	ϕ [%]	Guest	λ_{em} [nm]	ϕ [%]
CuRe_as-syn	545	68.60	MeCN	539	86.6
DMSO	525	84.8	EtOH	540	81.4
DCM	529	28.9	MeOH	543	44.5
Acetone	533	72.4	H_2O	540	70.9

Physical properties of CuRe in solution phase

The crystals of **CuRe_as-syn** were dissolved by dichloromethane interestingly. The orange solution, **CuRe_DCM**, was prepared to dissolve 79.0 mg of **CuRe_as-syn** in 10 mL of dichloromethane (5.0 mmol/L) and confirmed to be in complete solution because of no tyndal effect (**Figure 18**). **CuRe_DCM** showed red-orange color emission around 650 nm (ϕ = 42.27%) (**Figure 19** and **Table 9**). The photoluminescence decay profile of **CuRe_DCM** was shoun in **Figure 20**. The origin of red-orange emission was assumed to be d-d excited state of $[Re^{V}N(CN)_4]^{2-}$ unit because the emission life time was 17.1 μsec as single component and an emission life of $[Re^{V}N(CN)_4]^{2-}$ system is the typical sub-nanosecond life time. In addition, ESI measurement of 100 μmol/L **CuRe_DCM** solution showed a peak at m/z 893.33 and the value can be assigned as a dinuclear fragment $\{[Cu(PPh_3)_2][ReN(CN)_4]\}^{-}$ (m/z 892.40, calculated) (**Figure 21**). In practice, the condition of ESI-MS measurement was at a lower concentration than the condition for emission spectra measurement. So, we assumed bigger fragments exist in higher concentration solution. To investigate concentration dependence of photophysical properties of **CuRe_DCM**, UV-vis absorption spectra and emission spectra were measured at every 10 from 10 to 100 μmol/L of dichloromethane solutions (**Figures 22-23**). The absorption intensity increased and the absorption maximum wavelength exhibited red-shift accompanying with higher concentration. The red-shift suggested that an assembly state of Cu–Re composite unit transit with higher concentration. On the other hand, in the emission spectra of **CuRe_DCM**, the emission maximum wavelength did not almost shift independing on molar concentrations although the emission intensity increased with higher concentration. These results suggested that, in the different concentration of **CuRe_DCM** solution, the first excited state (S_1) changed but the triplet state (T_1; $^3[(d_{xy})^1(d_{\pi*})^1]$) involved in phosphorescence emission was retained. Thus, in the solution phase, the final structure of $[Re^{V}N(CN)_4]^{2-}$ unit at the excited state was expected to be a similar structure independently of on molar concentrations. This hypothesis is supplemented with what the curve of emission lifetime was a good single component decay. However, $[Re^{V}N(CN)_4]^{2-}$ does not emit light in solution normally because of vibrational deactivation of terminal cyanide ligands. From results of ESI-MS and UV-vis absorption spectra, the existence of Re-CN-Cu(I) cyanide linkages even in solution phase and the restriction of vibrational deactivation by the linkages were

expected. This red-orange emission of **CuRe_DCM** was the first case of luminescent $[ReN(CN)_4]^{2-}$ system in solution phase.

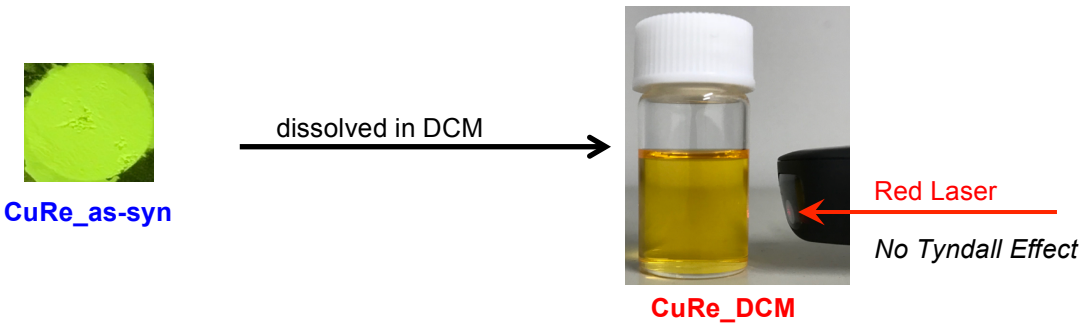

Figure 18. Image of **CuRe_DCM** completely dissolved in dichloromethane.

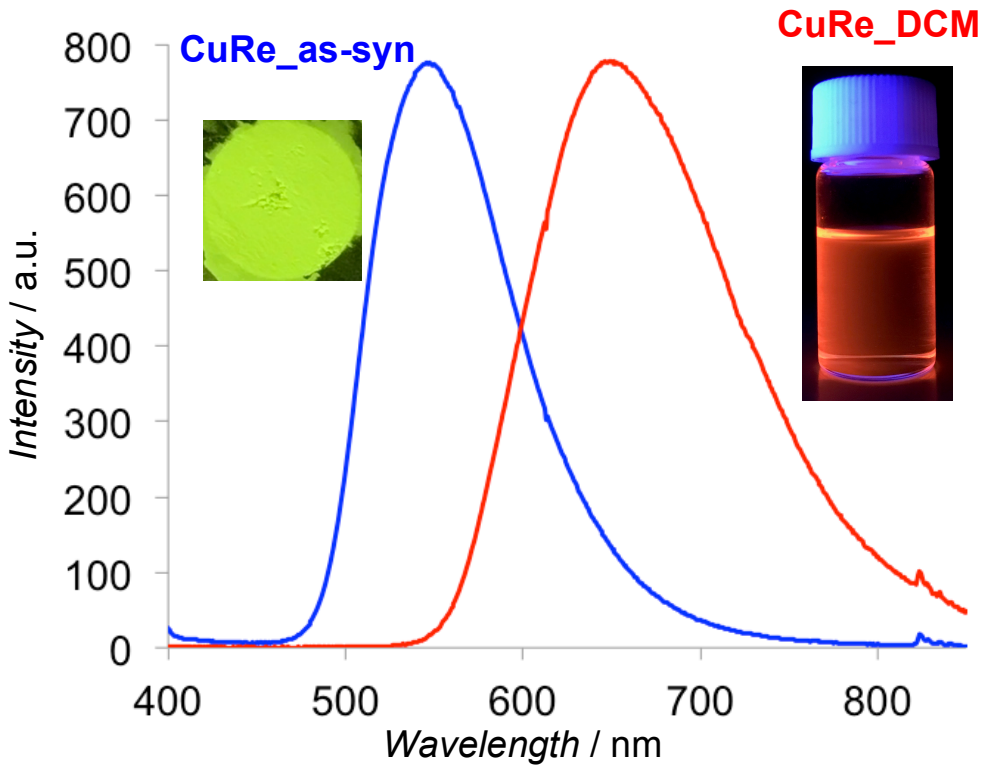

Figure 19. Emission spectra of **CuRe_as-syn** in solid state and **CuRe_DCM** in DCM solution at room temperature upon excitation at 365 nm.

Table 9. Emission maximum wavelength, PL quantum yields and life times of **CuRe_as-syn** and **CuRe_DCM**.

Compound	λ_{em} [nm]	ϕ [%]	τ [μs]
CuRe_as-syn	545	68.60	27.4
CuRe_DCM	650	42.27	17.1

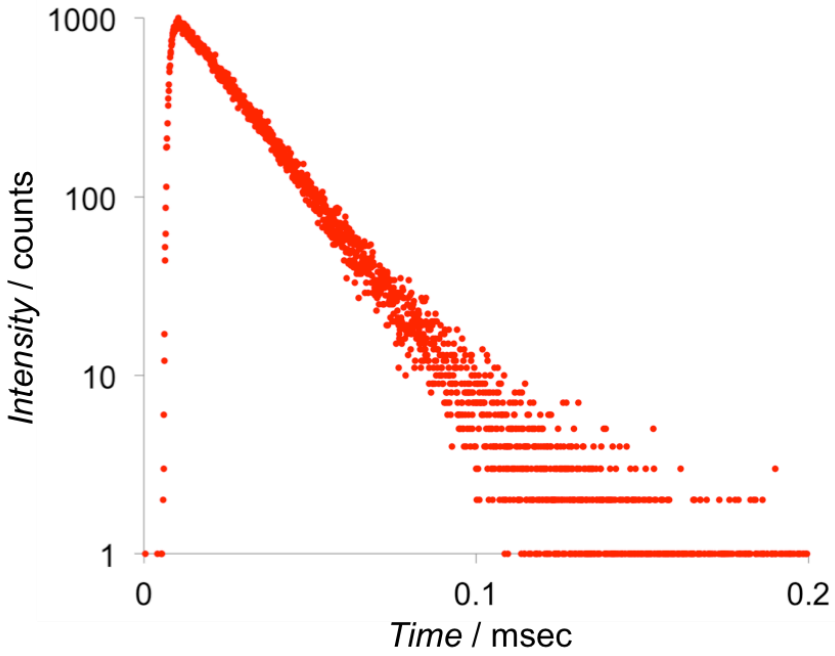

Figure 20. Photoluminescence decay profile of **CuRe_DCM** solution at room temperature upon excitation at 370 nm.

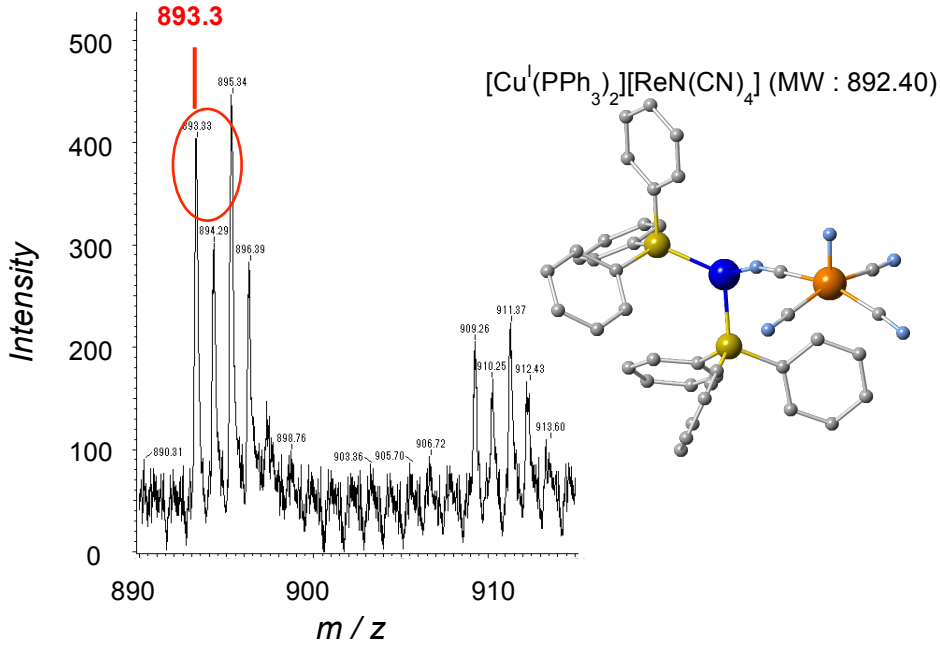

Figure 21. ESI-MS spectrum of **CuRe_DCM** and dinuclear model of $\{[Cu(PPh_3)_2][ReN(CN)_4]\}^-$.

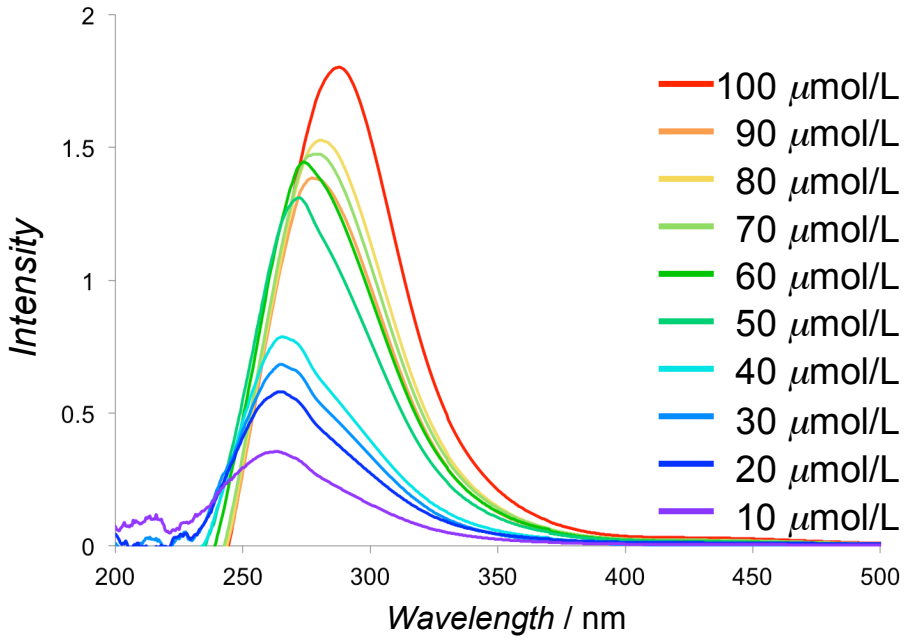

Figure 22. UV-vis absorption spectra of **CuRe_DCM** in the different concentration at every 10 from 10 to 100 μmol/L at room temperature.

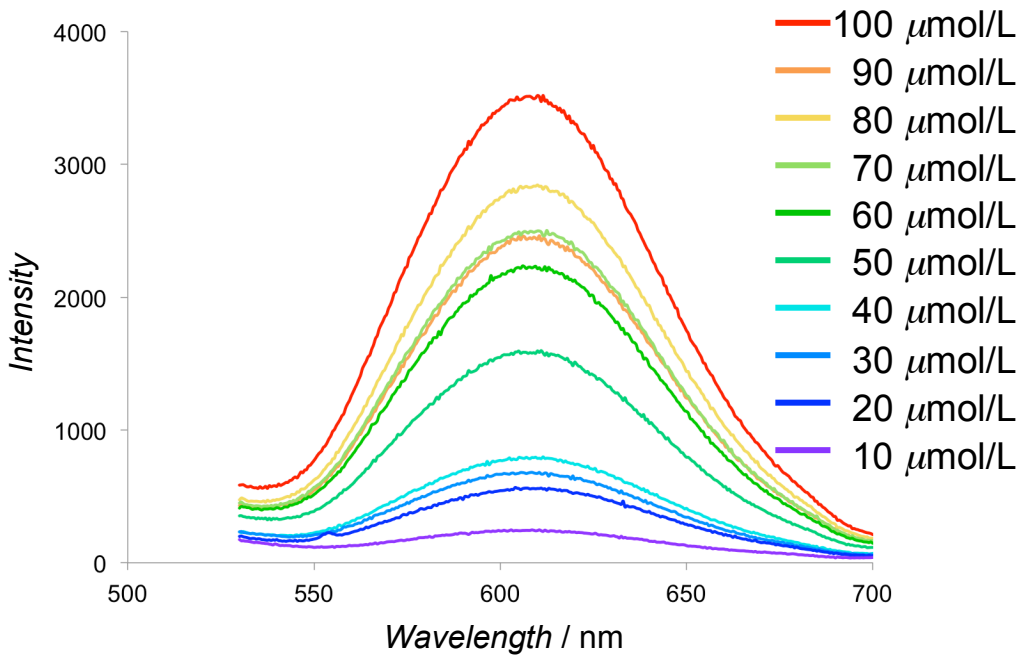

Figure 23. Emission spectra of **CuRe_DCM** in the different concentration at every 10 from 10 to 100 μmol/L at room temperature upon excitation at 365 nm.

Photophysical properties and guest responsivity of CuRe_am

An orange solid **CuRe_am** was obtained after evaporation of the solution **CuRe_DCM**. The PXRD pattern and emission spectra of **CuRe_am** were measured at room temperature under ambient atmosphere. From PXRD pattern of **CuRe_am**, their structure formed amorphous phase (**Figure 24**). The emission maximum wavelength of **CuRe_am** was at 647 nm similar to orange emission of **CuRe_DCM** (**Figures 25-26**). Then, the photoluminecent quantum yield of **CuRe_am** increased to 58.35% in comparison to 42.27% of **CuRe_DCM** (**Table 10**). In the case of solution phase, emission efficiency is quenched by molecular vibration of surrounding solvent molecules. As a result, the quantum yield of amorphous **CuRe_am** is higher than the quantum yield of **CuRe_DCM** solution.

To investigate the guest responsivity of **CuRe_am**, **CuRe_am** was exposed to guest solvent vapor; acetonitrile, ethanol and methanol were picked up as representative guest molecules. Each guest adsorbed **CuRe** (**CuRe_Guest**) was prepared by guest solvent vapor diffusion to amorphous **CuRe_am**, because desolvated framework of **CuRe_GF** and as-synthesized **CuRe_as-syn** exhibited little changes. In detail procedure, and powder **CuRe_am** in a sample tube (1.5 mL) and a few mL of guest solvents were putted in a sample tube (50 mL). All of the **CuRe_Guest** showed photoluminescence by excitation of 365 nm UV light in the solid state at room temperature. **Figure 27** shows photoluminescence image of **CuRe_as-syn, CuRe_am** and **CuRe_Guest** under UV light at 365 nm. **Figure 28** shows the emission spectra of the **CuRe_Guest** in the solid state at room temperature. **Table 10** summarizes the photoluminescent maximum peak wavelength and emission quantum yield. When **CuRe_am** was exposed to methanol vapor, the emission color was no change. In the case of exposure to ethanol, the photoluminescence spectra exhibited two broaden peaks based on similar **CuRe_as-syn** and **CuRe_am**, and the part of lime color emission and orange color emission mixed inhomogeneously in visual. Finaly, by uptake of acetonitrile vapor, the photoluminescent spectrum of **CuRe_MeCN** almost completely recovered to the initial state and the emission maximum wavelength shifted to 548 nm.

To clarify the difference responsivity depending on guest molecules in terms of structural property, the PXRD patterns and IR spectra were measured at room temperature under ambient atmosphere and the results show in **Figure 29**. The structures of **CuRe_MeOH** and **CuRe_EtOH** retained amorphous phase. On the other

hand, the measured PXRD pattern of **CuRe_MeCN** exhibited the similar pattern of **CuRe_as-syn**, and proved the reconstruction of initial 1D-ladder structure. Moreover, in IR spectra from **CuRe_am** to **CuRe_MeCN**, the absorption band of $\nu_{C\equiv N}$ based on cyano-linkages became sharp peak again, and the absorption band of $\nu_{C\equiv N}$ based on acetonitrile also reappeared. When focusing on an acetonitrile coordinating to the open-metal site of $[ReN(CN)_4]^{2-}$ unit in initial 1D-ladder structure, the coordinating acetonitrile fell into place surrounded by four phenyl group of PPh_3 and obtained high affinity with CH/π interactions (**Figure 30**). The space cannot allow even an introduction of chloroacetonitrile. These results suggested the spatial and chemical affinities contributed to structure recovery by acetonitrile selectively.

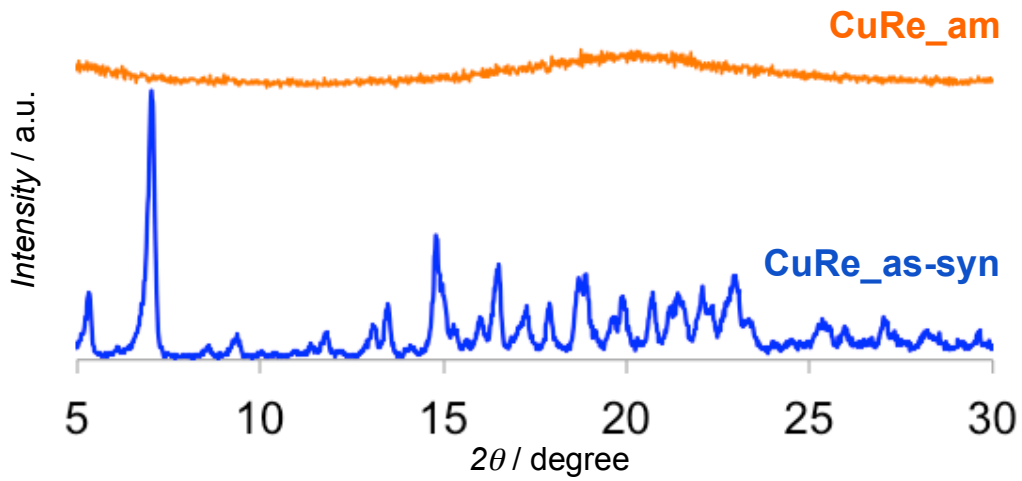

Figure 24. PXRD patterns of **CuRe_as-syn** and **CuRe_am**

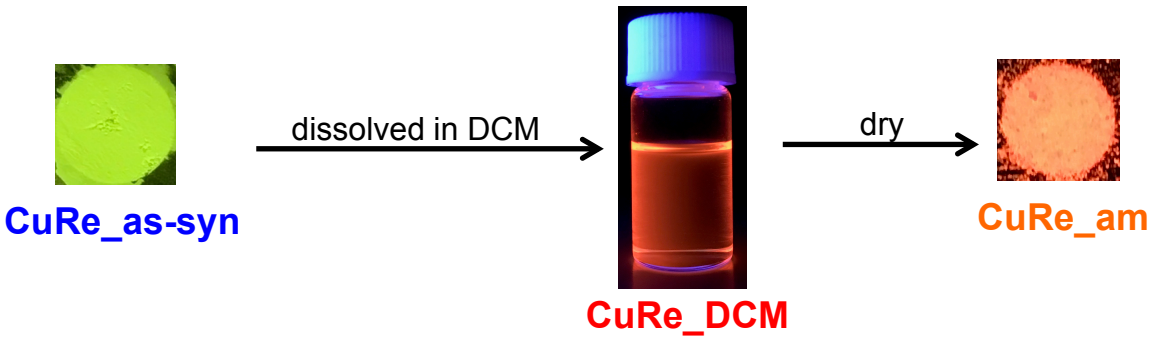

Figure 25. Photoluminescence image of as-synthesized, solution phase and amorphous phase **CuRe**.

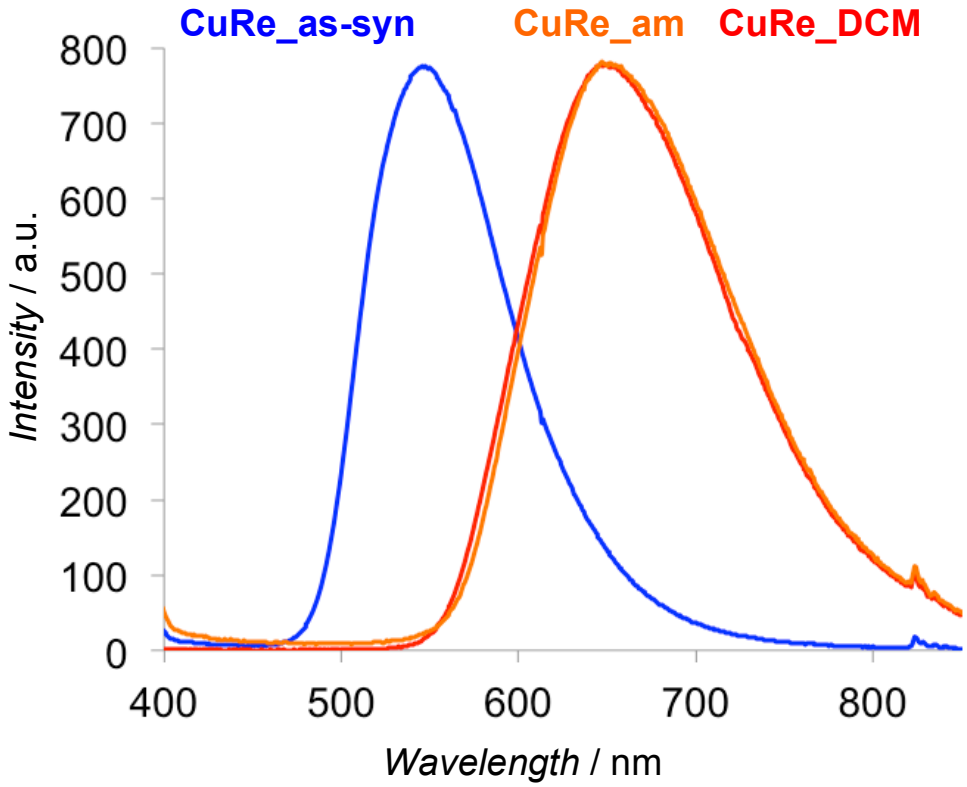

Figure 26. Emission spectra of **CuRe_as-syn** in solid state and **CuRe_DCM** in DCM solution at room temperature upon excitation at 365 nm.

Table 10. Emission maximum wavelength, PL quantum yields and life times of **CuRe_as-syn**, **CuRe_DCM**, **CuRe_am** and **CuRe_Guest**.

Compound	λ_{em} [nm]	ϕ [%]	τ [μs]
CuRe_as-syn	545	68.60	27.4
CuRe_am	647	58.35	16.
CuRe_MeCN	549	30.94	25.3
CuRe_MeOH	637	27.81	21.3
	532		25.2 (78), 50.7 (22)
CuRe_EtOH	623	36.99	24.6

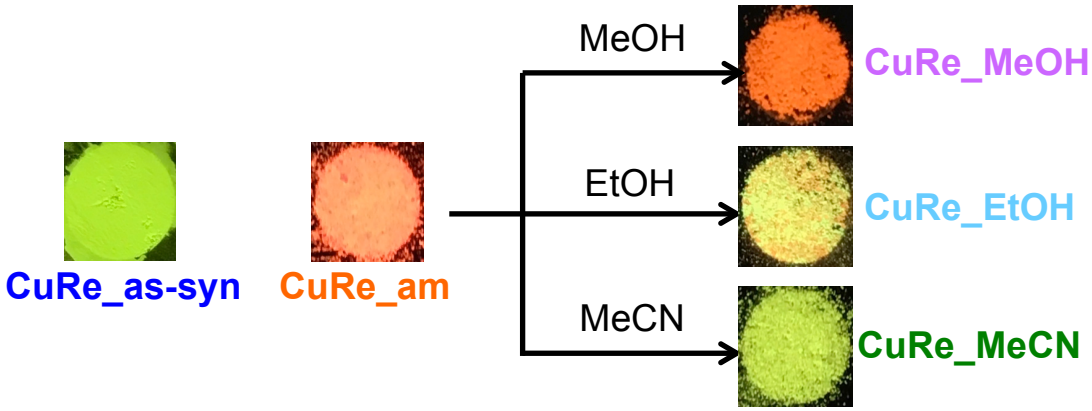

Figure 27. Photoluminescence images of **CuRe_as-syn, CuRe_am** and **CuRe_Guest**.

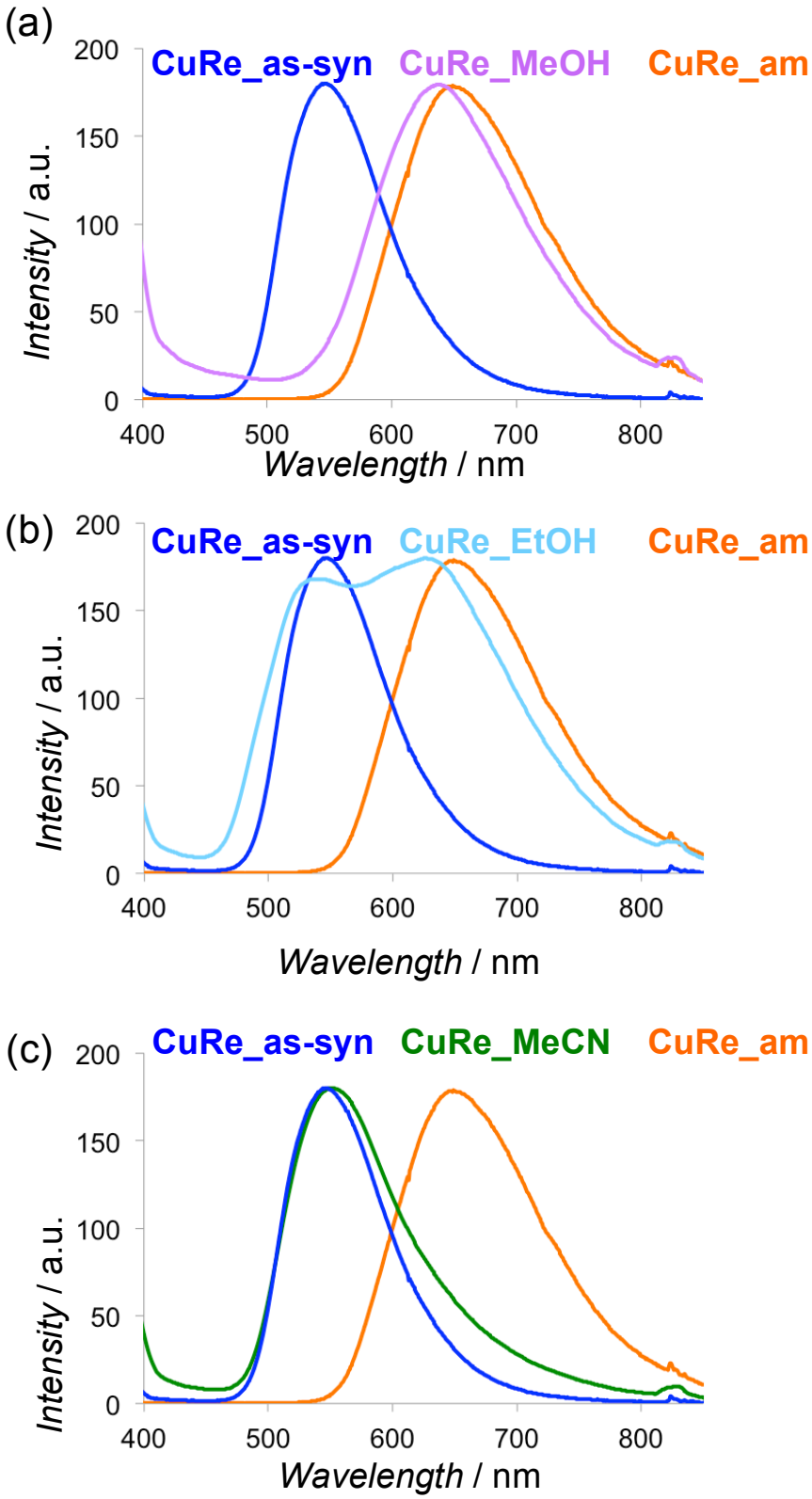

Figure 28. Emission spectra of **CuRe_as-syn** and **CuRe_am** with (a) **CuRe_MeOH**, (b) **CuRe_EtOH** and (c) **CuRe_MeCN** in solid state at room temperature upon excitation at 365 nm.

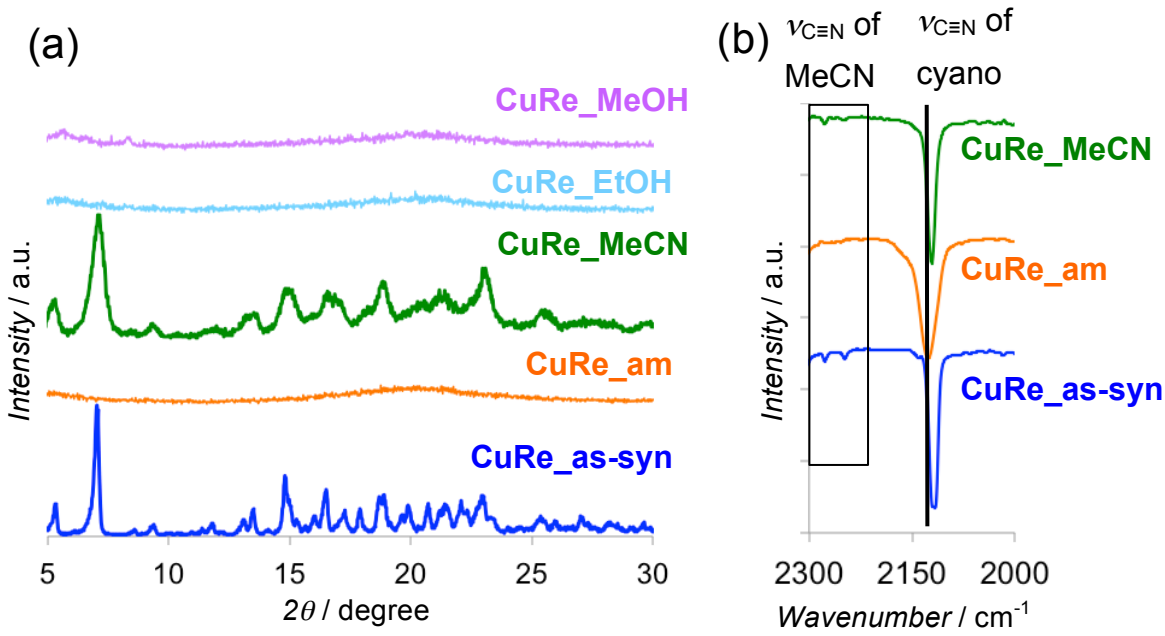

Figure 29. (a) PXRD patterns and (b) IR spectra of **CuRe_as-syn**, **CuRe_am** and **CuRe_Guest**

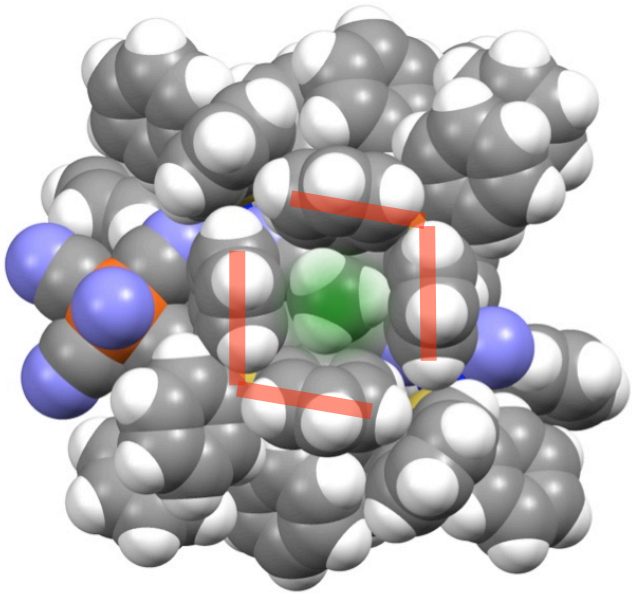

Figure 30. Space-filling model of a part of **CuRe** in the direction of the coordination bond of an acetonitrile (semitransparent green sphere). Four red bars indicate four phenyl groups surrounding the coordinating acetonitrile.

Phase transition and guest responsivity of AgRe

Phase transition of **AgRe** from crystalline to amorphous through solution state was investigated because the crystals of **AgRe_as-syn** were also dissolved by dichloromethane. The orange solution, **AgRe_DCM**, was prepared to dissolve 67.7 mg of **AgRe_as-syn** in 10 mL of dichloromethane (4.0 mmol/L) and confirmed to be in complete solution because of no tyndal effect. **AgRe_DCM** showed red-orange color emission around 655 nm (ϕ = 4.17%) (**Figures 31-32** and **Table 11**). The origin of red-orange emission was assumed to be d-d excited state of $[Re^{V}N(CN)_4]^{2-}$ unit because The origin of red-orange emission was assumed to be d-d excited state of $[Re^{V}N(CN)_4]^{2-}$ unit because the emission life time was 10.4 μsec as with a typical sub-nanosecond life time of $[Re^{V}N(CN)_4]^{2-}$ system. An orange solid **AgRe_am** was obtained after evaporation of the solution **AgRe_DCM**. The PXRD pattern and emission spectra of **AgRe_am** were measured at room temperature under ambient atmosphere. From PXRD pattern of **AgRe_am**, their structure formed amorphous phase (**Figure 33**). The emission maximum wavelength of **AgRe_am** was at 619 nm and the photoluminecent quantum yield of **AgRe_am** increased to 29.64% in comparison to 4.17% of **AgRe_DCM** (**Table 11**). In the case of solution phase, emission efficiency is quenched by molecular vibration of surrounding solvent molecules. As a result, the quantum yield of amorphous **AgRe_am** is higher than the quantum yield of **AgRe_DCM** solution.

The guest responsivity of **AgRe_am** to guest solvents vapor was also investigated similar to **CuRe_am**. Each guest adsorbed **AgRe** (**AgRe_Guest**, Guest = acetonitrile, ethanol and methanol) was prepared by guest solvent vapor diffusion to amorphous **AgRe_am**. All of the **AgRe_Guest** showed photoluminescence by excitation of 365 nm UV light in the solid state at room temperature. **Figure 32** shows photoluminescence image of **AgRe_as-syn, AgRe_am** and **AgRe_Guest** under UV light at 365 nm. The PXRD patterns, IR spectra and emission spectra of the **AgRe_Guest** were measured in the solid state at room temperature (**Figure 33-34**). **Table 13** summarizes the photoluminescent maximum peak wavelength and emission quantum yield. When **AgRe_am** was exposed to acetonitrile vapor, the emission color and almost completely recovered to the initial state. In other words, **AgRe_MeCN** showed lime-green color emission and formed 1D-ladder structure. In the case of **AgRe_am** exposed to methanol (**AgRe_MeOH**), the orange color emission and

amorphous phase were still maintained. On the other hand, the PXRD patterns of **AgRe_EtOH** showed somewhat incomplete recovery of crystallinity because of appearance of some peaks, although the emission maximum wavelength did not almost shift. In the case of d10 metal ion, a coordination bond length with a ligand is longer and looser with heavier main group elements because d10 metal ions are lack ligand field stabilization energy. Actually, the bond length of Ag–N (ave. 2.288(6) Å) and Ag–P (ave. 2.460(5) Å) in **AgRe** frameworks is longer than Cu–N (ave. 2.022(8) Å) and Cu–P (ave. 2.286(2) Å) in **CuRe** frameworks according to the results of the crystallographic data. In addition, **AgRe_am** was dissolved more easily than **CuRe_am**. Based on the above, a coordination bond of Ag^+ ion can associate and dissociate more flexibly than Cu^+ ion. Thus, the framework structure of **AgRe** was able to regenerate to some crystalline structure.

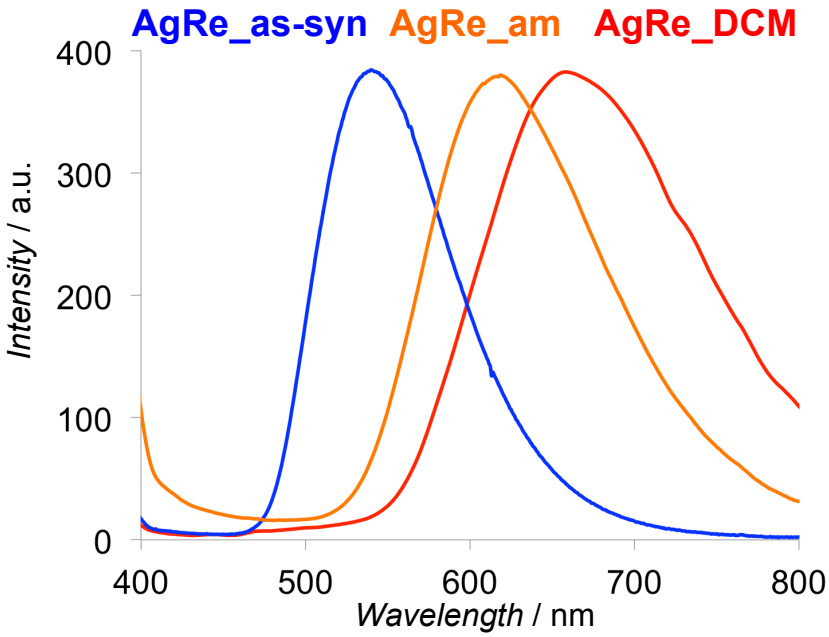

Figure 31. Emission spectra of **AgRe_as-syn** and **AgRe_am** in solid state and **AgRe_DCM** in DCM solution at room temperature upon excitation at 365 nm.

Table 11. Emission maximum wavelength, PL quantum yields and life times of **AgRe_as-syn**, **AgRe_DCM**, **AgRe_am** and **AgRe_Guest**.

Compound	λ_{em} [nm]	ϕ [%]	τ [μs]
AgRe_as-syn	539	82.07	18.9
AgRe_DCM	655	4.2	10.4
AgRe_am	619	31.7	28.5
AgRe_MeCN	539	46.22	17.0
AgRe_MeOH	606	10.81	27.0
AgRe_EtOH	617	6.85	24.3

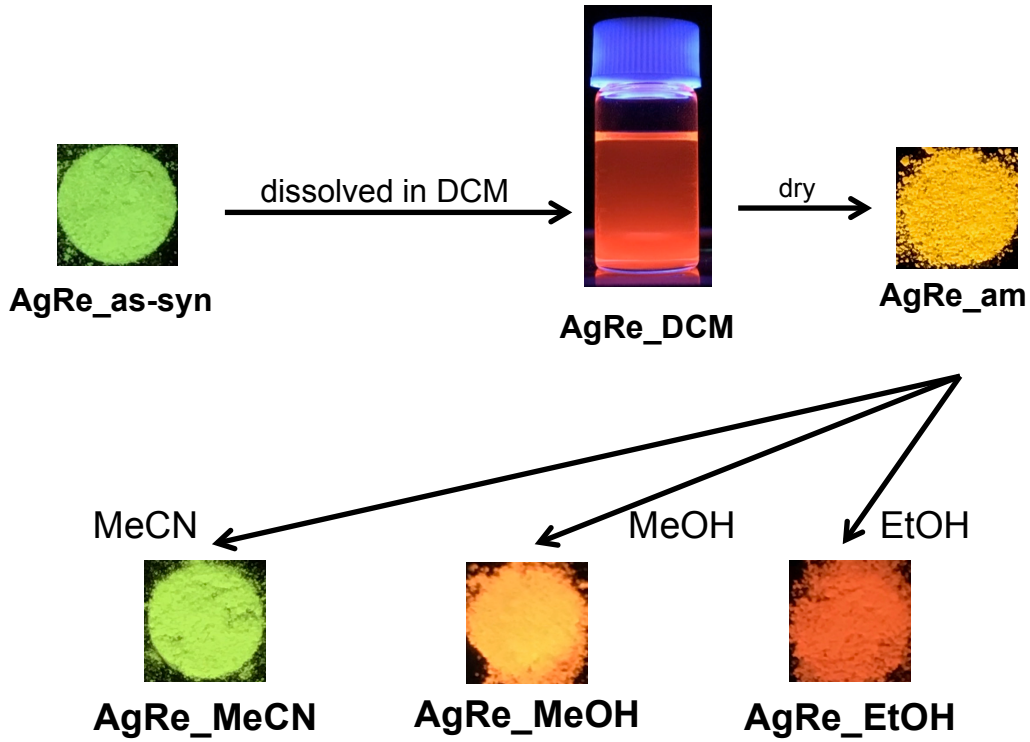

Figure 32. Photoluminescence image of as-synthesized, solution phase and amorphous phase of **AgRe** and **AgRe_Guest**.

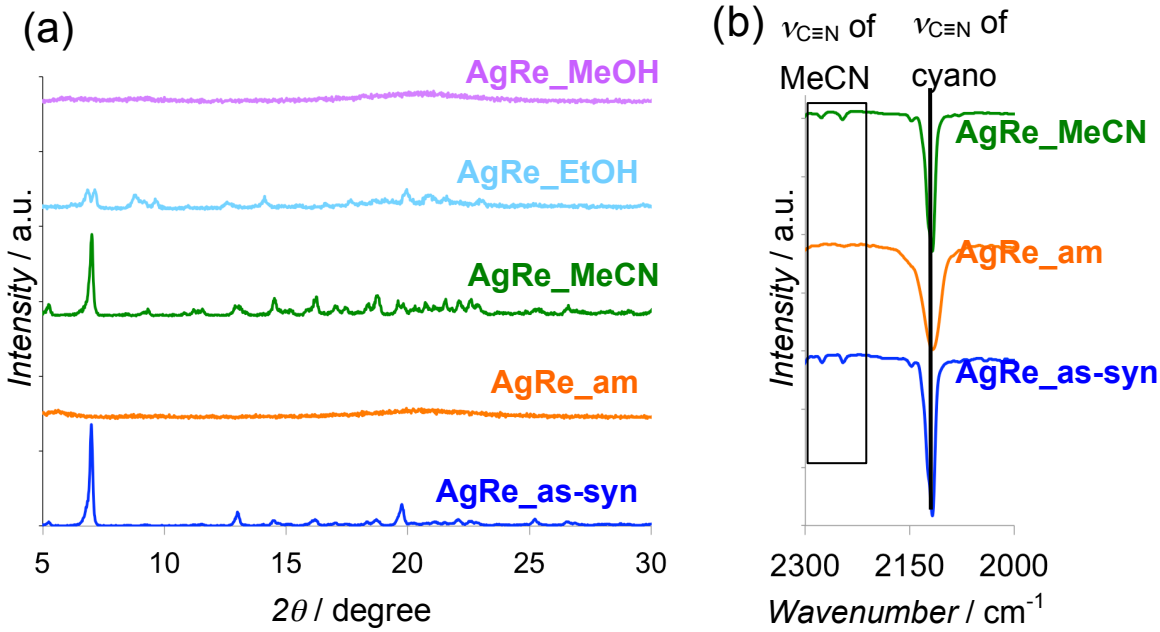

Figure 33. (a) PXRD patterns and (b) IR spectra of **AgRe_as-syn**, **AgRe_am** and **AgRe_Guest**

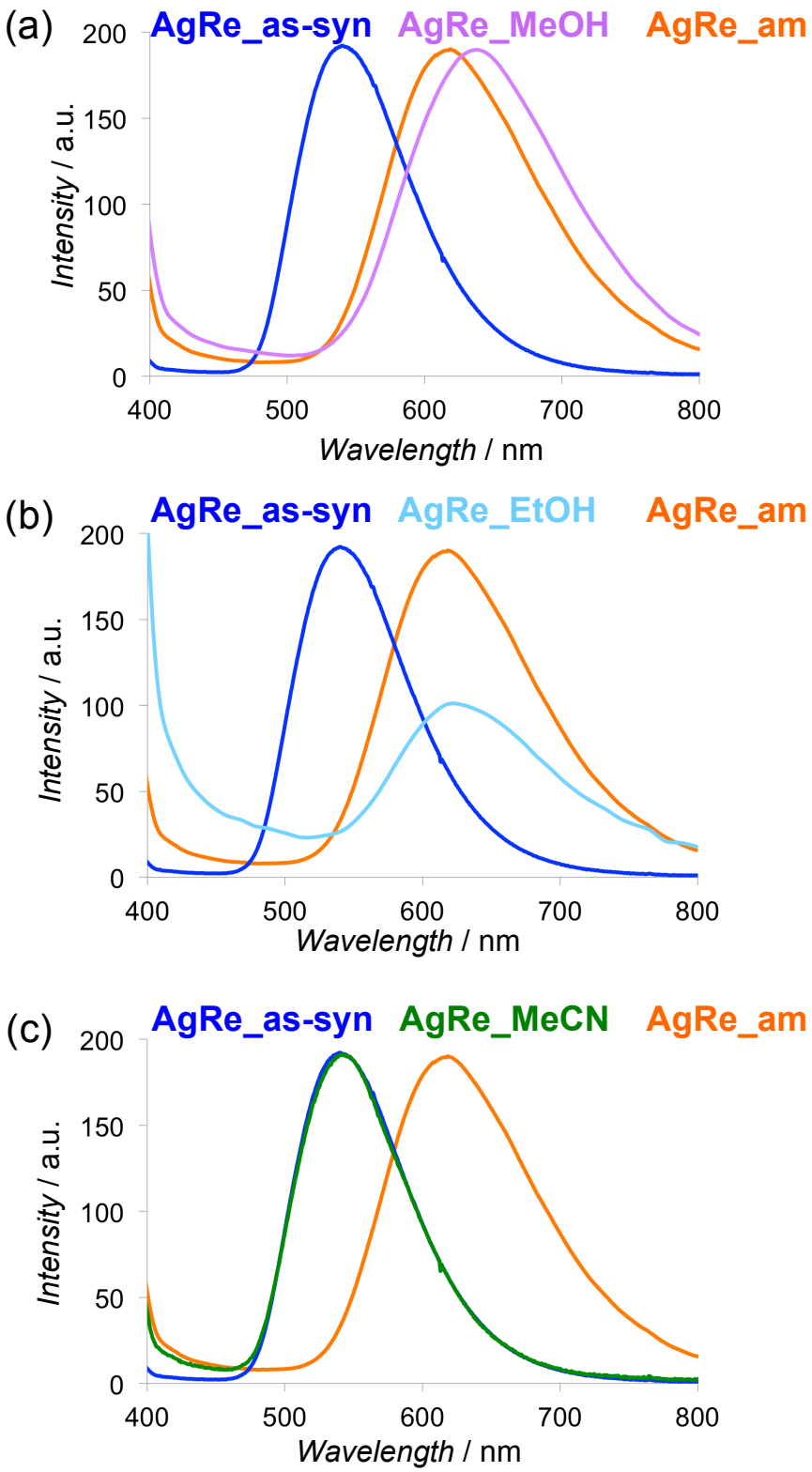

Figure 34. Emission spectra of **AgRe_as-syn** and **AgRe_am** with (a) **AgRe_MeOH**, (b) **AgRe_EtOH** and (c) **AgRe_MeCN** in solid state at room temperature upon excitation at 365 nm.

Conclusion

We successfully prepared novel luminescent one-dimensional coordination polymers $\{[M^{I}(PPh_3)_2]_2[Re^{V}N(CN)_4(MeCN)]\cdot n\text{sol}\}$ (M^{I} = Cu, Ag; PPh_3 = triphenylphosphine; MeCN = acetonitrile), and reduced the dimension of the cyano-bridged frameworks with strategic synthesis. Their frameworks formed infinite –M_2–Re–M_2–Re– ladder chain having a MeCN at each open-metal site of $[ReN(CN)_4]^{2-}$ units. Bulk sample **MRe_as-syn** (**M** = Cu and Ag), showed lime-green emission originating from d-d excited state of $[ReN(CN)_4]^{2-}$ units around 545 and 539 nm with high quantum yield of 68.6 and 82.1%, respectively. The crystals of **MRe** dissolves in dichloromethane, and shows orange emission. This is the first report demonstrating the emission by $[ReN(CN)_4]^{2-}$ in solution. For ESI-MS measurement, the formation of Re–CN–M linkage in solution state induced the restriction on the vibrational deactivation of terminal cyanide ligands of $[ReN(CN)_4]^{2-}$. Amorphous solids obtained by evaporation of the solution also show orange emission. By the investigation of the guest responsivity of amorphous solids, the initial structure and emission color of **MRe** recovers in response to acetonitrile selectively. The result suggests that the template space of initial structure having MeCN as coordination solvent and bulky PPh_3 ligand related to selective responsivity and reversibility by MeCN. Reduction of dimension of cyano-bridged frameworks provides flexible frameworks and unique physical properties, such as phase transition and structure transformation. Development of sophisticated molecular design especially for framework structure, framework arrangement and guest interactive site is expected to enable more sensitive and selective sensing.

References

1. (a) M. O'Keeffe, M. Eddaoudi, H. Li, T. Reineke, O. M. Yaghi, *J. Solid State Chem.* **2000**, *152*, 3–20; (b) O. M. Yaghi, M. O'Keeffe, N. W. Ockwig, H. K. Chae, M. Eddaoudi, J. Kim, *Nature* **2003**, *423*, 705–714; (c) J. L. C. Rowsell, O. M. Yaghi, *Microporous Mesoporous Mater.* **2004**, *73*, 3–14; (d) S. Kitagawa, R. Kitaura, S. I. Noro, *Angew. Chem. Int. Ed.* **2004**, *43*, 2334–2375; (e) S. Kitagawa, K. Uemura, *Chem. Soc. Rev.* **2005**, *34*, 109–119; (f) S. Kitagawa, S. I. Noro, T. Nakamura, *Chem. Commun.* **2006**, 701–707; (g) G. Férey, *Chem. Soc. Rev.* **2008**, *37*, 191–214; (h) G. Férey, C. Serre, *Chem. Soc. Rev.* **2009**, *38*, 1380–1399.
2. (a) K. A. Hofmann, F. Küspert, *Zeitschrift für Anorg. Chem.* **1897**, *15*, 204–207; (b) H. M. Powell, *J. Chem. Soc.* **1948**, 61–73; (c) J. H. Rayner, H. M. Powell, *J. Chem. Soc.* **1952**, 319–328; (d) M. Kondo, M. Kubo, *J. Phys. Chem.* **1957**, *61*, 1648–1651; (e) T. Kitazawa, Y. Gomi, M. Takahashi, M. Takeda, M. Enomoto, A. Miyazaki, T. Enoki, *J. Mater. Chem.* **1996**, *6*, 119–121; (f) V. Niel, J. M. Martinez-Agudo, M. C. Muñoz, A. B. Gaspar, J. A. Real, *Inorg. Chem.* **2001**, *40*, 3838–3839; (g) J. A. Rodríguez-Velamazán, M. A. González, J. A. Real, M. Castro, M. C. Muñoz, A. B. Gaspar, R. Ohtani, M. Ohba, K. Yoneda, Y. Hijikata, et al., *J. Am. Chem. Soc.* **2012**, *134*, 5083–5089; (h) Z. Arcís-Castillo, F. J. Muñoz-Lara, M. C. Muñoz, D. Aravena, A. B. Gaspar, J. F. Sánchez-Royo, E. Ruiz, M. Ohba, R. Matsuda, S. Kitagawa, et al., *Inorg. Chem.* **2013**, *52*, 12777–12783; (i) D. Aravena, Z. A. Castillo, M. C. Muñoz, A. B. Gaspar, K. Yoneda, R. Ohtani, A. Mishima, S. Kitagawa, M. Ohba, J. A. Real, et al., *Chem. - A Eur. J.* **2014**, *20*, 12864–12873; (j) A. Mishima, T. Koshiyama, J. A. Real, M. Ohba, *J. Mater. Chem. C* **2017**, *5*, 3706–3713; (f) Z. P. Ni, J. L. Liu, M. N. Hoque, W. Liu, J. Y. Li, Y. C. Chen, M. L. Tong, *Coord. Chem. Rev.* **2017**, *335*, 28–43.
3. I. Muga, J. M. Gutiérrez-Zorrilla, P. Vitoria, P. Román, L. Lezama, J. I. Beitia, *Eur. J. Inorg. Chem.* **2004**, 1886–1893.
4. (a) D. W. Knoeppel, J. Liu, E. A. Meyers, S. G. Shore, *Inorg. Chem.* **1998**, *37*, 4828–4837; (b) B. A. Maynard, P. A. Smith, L. Ladner, A. Jaleel, N. Beedoe, C. Crawford, Z. Assefa, R. E. Sykora, *Inorg. Chem.* **2009**, *48*, 6425–6435.
5. H. Ikeda, A. Ito, E. Sakuda, N. Kitamura, T. Takayama, T. Sekine, A. Shinohara, T. Yoshimura, *Inorg. Chem.* **2013**, *52*, 6319–6327.

6. (a) R. A. Rader, D. R. McMillin, M. T. Buckner, T. G. Matthews, D. J. Casadonte, R. K. Lengel, S. B. Whittaker, L. M. Darmon, F. E. Lytle, *J. Am. Chem. Soc.* **1981**, *103*, 5906–5912; (b) J. A. Simon, W. E. Palke, P. C. Ford, *Inorg. Chem.* **1996**, *35*, 6413–6421; (c) R. Czerwieniec, J. Yu, H. Yersin, *Inorg. Chem.* **2011**, *50*, 8293–8301; (d) H. Suh, D. J. Casadonte, L. Hope-Weeks, H. J. Kim, B. Kim, T. Chang, *Inorganica Chim. Acta* **2013**, *394*, 710–714; (e) A. Kobayashi, M. Kato, *Chem. Lett.* **2017**, *46*, 154–162; (f) T. Hasegawa, A. Kobayashi, H. Ohara, M. Yoshida, M. Kato, *Inorg. Chem.* **2017**, *56*, 4928–4936; (g) A. Kobayashi, R. Arata, T. Ogawa, M. Yoshida, M. Kato, *Inorg. Chem.* **2017**, *56*, 4280–4288.
7. (a) K. Matsumoto, T. Shindo, N. Mukasa, T. Tsukuda, T. Tsubomura, *Inorg. Chem.* **2010**, *49*, 805–814; (b) D. Kakizoe, M. Nishikawa, T. Degawa, T. Tsubomura, *Inorg. Chem. Front.* **2016**, *3*, 1381–1387; (c) M. Z. Shafikov, R. Czerwieniec, H. Yersin, *Dalton Trans.* **2019**, *48*, 2802–2806.
8. A. L. Spek, *Acta Crystallogr. Sect. C, Struct. Chem.* **2015**, *71*, 9–18.
9. (a) I. Csöregh, P. Kierkegaard, R. Norrestam, *Acta Crystallogr. Sect. B Struct. Sci. Cryst. Eng. Mater.* **1975**, *31*, 314–317; (b) D. F. Shriver, *Inorg. Synth.*, **1979**, *9*, 90–92.
10. L. M. Engelhardt, C. Pakawatchai, A. H. White, P. C. Healy, *J. Chem. Soc. Dalton Trans.* **1985**, *599*, 125–133.

Concluding Remarks

In this thesis, the author systematically studied on the synthesis and the photophysical properties of luminescent coordination polymers (CPs) using nitridotetracyanorhenate(V) ion as d-d transition-based luminescent building unit. Although only a few reports regarding d-d transition-based luminescent CPs are available in the literature, we extended the series of d-d luminescent CPs and investigated the guest-responsivity with elucidating the mechanism.

In chapter 1, 3D poorous coordination polymer $\{Zn^{II}[Re^{V}N(CN)_4]\cdot n\text{sol}\}$ (**ZnRe**) was successfully prepared by reaction of nitridotetracyanometalate(V) ion $[Re^{V}N(CN)_4]^{2-}$ with Zn^{2+}. **ZnRe** formed a PtS-type porous structure extended by Re-CN-Zn linkages between square plane of $[Re^{V}N(CN)_4]^{2-}$ and tetrahedral of Zn^{2+}. **ZnRe_Guest**, which adsorbed various guest molecules including acetone, acetonitrile, ethanol, methanol and water, showed remarkable guest responsive emission band shift with high quantum yields depending on the guest molecules rather than that of mononuclear complex $[Re^{V}N(CN)_4]^{2-}$. The guest-dependent emission band shifts were good correration with changeing C–Re–C bond angles in the $[Re^{V}N(CN)_4]^{2-}$ unit because the energy levels of the d-orbitals are susceptible to surrounding coordination environment. In addition, high sensitive response to acetone is confirmed. Luminescent PCPs embedded $[Re^{V}N(CN)_4]^{2-}$ unit wood be a good sensing materials.

In chapter 2, two-dimensional nitridotetracyanorhenate(V)-based PCPs $\{[Zn(co\text{-}L)_2][ReN(CN)_4(co\text{-}L)]\}$ (**ZnReco-L**; co-L = pyridine (py) and 3-chloropyridine (Clpy)) by incorporation of pyridine derivatives as co-ligands (co-L) were successfully prepared. Their framework consisted of cyanide-bridged layers extended by Re-CN-Zn linkages between $[Re^{V}N(CN)_4(co\text{-}L)]^{2-}$ and Zn^{2+} which having co-L at unoccupied coordination sites at axial position. Although **ZnRepy** and **ZnReClpy** showed lime green emission originating from d-d transition, guest responsivity was not shown because the frameworks had strong intra- and inter-layer π-π interactions. **ZnRepy** showed mechanochromic luminescence shift and amorphousization. The emission color and crystallinity were recovered partially by exposing the ground sample to volatile organic compounds, which suggested that the emission property changed by the coordination structure due to the change of the pyridine arrangement in the frameworks.

ZnReco-L does not have guest responsivity due to the strong and rich π-π interaction in the frameworks providing rigid frameworks and insufficient void space. To achieve guest-responsive luminescence, a flexible framework and a sufficient void space is needed.

In chapter 3, novel luminescent one-dimensional coordination polymers $\{[M^{I}(PPh_3)_2]_2[Re^{V}N(CN)_4(MeCN)]\cdot n\text{sol}\}$ (M^{I} = Cu, Ag; PPh_3 = triphenylphosphine; MeCN = acetonitrile) were successfully prepared by reaction of $[Re^{V}N(CN)_4]^{2-}$ ion with $[M^{I}(PPh_3)_4]^{+}$ precursor complexes. Bulk sample **MRe_as-syn** (**M** = Cu and Ag), showed lime-green emission originating from d-d transition of $[ReN(CN)_4]^{2-}$ units. The crystals of **MRe** exhibited phase transition to solution state and amorphous state by dissolution in DCM and evaporation, respectively. At the same time, the luminescence changed to orange emission. In addition, we found that the initial structure and emission color of **MRe** were recovered from amorphous sample in response to acetonitrile selectively among some volatile organic compounds. The template space constructed by the bulky PPh_3 ligand and the coordinated MeCN in the initial structure contributed to selective responsivity and reversibility by MeCN.

These works highlighted rational and systematic synthesis of coordination polymers exhibiting photoluminescence originating from d-d transition and investigation of their physical properties including guest-responsivity. As a next step, it is necessary to design sophisticatedly the frameworks of coordination polymers. Control of structure transformation accompanying with guest adsorption is expected to achieving more sensitive and selective guest-responsivity.

List of Publications

1. Guest-Responsive Luminescence Properties of Three-Dimensional Porous Coordination Polymer
   H. Miura, H. Yamate, A. Mishima, T. Koshiyama, M. Ohba
   submitted to Angewandte Chemie

2. Synthesis and Luminescence Properties of Two-Dimensional Hofmann-type Coordination Polymers with Complementary Ligands
   H. Miura, M. Ohba
   (*to be submitted*)

3. Construction of Low-Dimensional Coordination Polymers and Guest-Selective Luminescent Properties
   H. Miura, M. Ohba,
   (*to be submitted*)

Other Publications

1. Tuning the gate-opening pressure and particle size distribution of the switchable metal–organic framework DUT-8(Ni) by controlled nucleation in a micromixer
   H. Miura, V. Bon, I. Senkovska, S. Ehrling, S. Watanabe, M. Ohba, S. Kaskel
   Dalton Transactions, 2017, 46, 14002-14011., DOI: 10.1039/c7dt02809a

Acknowledgement

All the study in this thesis has been carried out under the direction of Professor Masaaki Ohba during April 2013- June 2019 at the Department of Chemistry, Graduate School of Science, Kyushu University.

The author expresses his deepest appreciation to Professor Masaaki Ohba for his guidance and encouragement. The author could research liberally in the study due to his generosity. The author could learn a lot of things not only science but also design and thinking faculty for him. The author thanks to Professor Ken Sakai, Professor Ken Onda, Associate Professor Ryo Ohtani and Associate Professor Tomomi Koshiyama for their guidance.

The author expresses his gratitude to Professor Stefan Kaskel (Dresden University of Technology) and Dr. Volodymyr Bon (Postdoctoral Researcher of Dresden University of Technology) for accepting me as visiting scholar and careful guidance, and valuable discussion.

The acknowlecgement is also given the Advanced Graduate Course on Molecular Systems for Devices for the financial surpports for the activities of the author, which enabled the author to attend various domestic and international conferences, together with his 9-months of oversea reserch in Germany.

Finally, the author gives special thanks to all members of Ohba group and Kaskel group for their kind support.

Hiroki Miura
Department of Chemistry
Graduate School of Science
Kyushu University
June 2019